# Biocatalytically And Photoelectrochemically Driven Active Motion of Liposomes

by

Hui Jin

A dissertation submitted to the Graduate Faculty of Auburn University
in partial fulfillment of the requirements for the
Degree of Doctor of Philosophy of Science

Auburn, Alabama,
May 6th 2023

Keywords: Lipid bilayer, Janus particle, liposomes, Janus liposomes, diffusion, active motion



Approved by

Wei Zhan, Chair, Professor of Chemistry and Biochemistry
Eduardus (Evert) Duin, Professor of Chemistry and Biochemistry
Pengyu Chen, Associate Professor of Mechanical Engineering
Ahmed Hamid, Assistant Professor of Chemistry and Biochemistry

# Abstract

Self-propelled artificial micro/nanomotors are currently attracting increased interest as not only mimics of biological motors but also potential components of nanomachinery, robotics, and sensing devices. In regards to studying such kinds of self-propelled micro/nanomotors, Janus particles have been an excellent candidate for researchers for a long time due to their special asymmetrical structure and decoration. As micro-/nanosized soft-matter bilayer vesicles with biocompatibility and broad utility, liposomes have been widely regarded as a potential platform for drug delivery, biosensor application, and mimic cell models. Sharing similar chemical properties and character, Janus liposomes have numerous advantages as an amphiphilic material on which different chemical entities, such as peptides, nucleotides and antibodies, can be attached. In this Dissertation, by taking full advantage of the phase separation of saturated lipids and unsaturated lipids on the liposome membrane surface, we generated high-quality Janus liposomes via PVA gel-assisted swelling hydration method reproducibly with the common ternary lipids system (DPPC/DOPC/cholesterol). With such reproducible and effective liposomes hydration and membrane extrusion for uniform size control methods in hand, we then explored the enzyme-based (horseradish peroxidase and catalase) biocatalytically-driven active motion behavior of well-prepared Janus liposomes. In addition, we further investigated the enzyme-free liposome active motion driven by asymmetrical lipid efflux in which the motion was induced by β-CD extraction of cholesterol from the membrane. Finally, we examined laser light-based photoelectrochemically-driven active motion behavior of $Ru(bpy)_3^{2+}$ labeled Janus liposomes under different mass transfer molecule fuel in bulk by replacing the inserted rhodamine- DOPE with $Ru(bpy)_3^{2+}$-DOPE (light-sensitive material) on the membrane of Janus liposomes.

**Acknowledgments**

The Ph.D. research process is a reliable path to explore the unknown and mysterious natural world which makes it a tough challenge for both the mind and physical body of whom want to undertake the Ph.D. degree. During my Ph.D. study life, a lot of kindhearted and generous people offered their great support and help to me to whom I want to express my sincere gratitude.

First and foremost, I would thank my advisor Dr. Wei Zhan for his wise instruction, guidance, consistent patience, and encouragement especially during the difficult period in my Ph.D. study after I joined his group. In my whole Ph.D. study career, he always helps me figure out the key issue of the experiment setup and possible challenges of each working project. Also, he always gives me a hand to conquer and accomplish these challenges in some hard times of my Ph.D. career. His one-on-one encouragement gives me enough confidence to explore the unknown science world in my Ph.D. study.

Then I wish to sincerely thank all my committee members, Dr. Pengyu Chen, Dr. Eduardus (Evert) Duin, Dr. Ahmed Hamid, and University outside reader, Dr. Kathleen Martin for their valuable suggestions, wise instruction, and patient assistance to my Ph.D. study career, especially for their warm encouragement in the annual report meeting when I encountered challenges in the experiment exploration and data expectation. I feel really appreciative of all your guidance during my oral examination which makes my projects work much more smoothly.

Furthermore, many thanks to my friends Mengzhou Wang, Nan Shi and lab mates Zening Liu, Jinyan Cui, and Mingming Wang in the Department of Chemistry and Biochemistry. They offered a lot of assistance to not only my research career but also my own life in Auburn.

At last but not least, I would give my special thanks to my family, my mother, my wife Hui Zhang, my daughter Ruitian Jin, and my son Ruichen Jin, especially my wife Hui Zhang. She offered unconditional support and reliability throughout my whole Ph.D. career.

# Contents for The Dissertation

## List of Figures

# List of Abbreviations

| | |
|---|---|
| GUVs | Giant unilamellar vesicles |
| LUVs | Large unilamellar vesicles |
| SUVs | Small unilamellar vesicles |
| DPPC | 1,2-dipalmitoyl-sn-glycero-3-phosphochline |
| DOPC | 1,2-dioleoyl-sn-glycero-3-phosphocholine |
| DOPE | 1,2-dioleoyl-sn-glycerol-3-phosphoethanolamine |
| Biotin-DOPE | 1,2-dioleoyl-sn-glycero-3-phosphoethanolamine-N-(biotinyl) (sodium salt) |
| Bodipy-chol | 23-(dipyrrometheneboron difluoride)-24-norcholesterol |
| Rho-DOPE | 1,2-sn-glycero-3-phosphoethanolamine-N-(Lissamine rhodamine B sulfonyl) (ammoniu salt) |
| $Ru(bpy)_3^{2+}$ | Tris(bipyridine)ruthenium(II) |
| DI | Deionized |
| PVA | Poly(vinyl alcohol) |
| PDMS | Poly(dimethylsiloxane) |
| $L_d$ | Liquid-disordered |
| $L_o$ | Liquid-ordered |
| NMR | Nuclear magnetic resonance |
| $T_m$ | Melting temperature |

# CHAPTER 1. Introduction

## 1.1 Colloidal Particles

Colloidal particles are a special type of material, which have been widely used in chemistry, biology, and pharmaceutical fields due to their small size (ranging from a few hundred nanometers to a few micrometers) and high surface area of the dispersed phase. [1] As building blocks for advanced materials, colloidal particles exhibit a wide variety of functionality including enhanced mechanical behavior, conductivity, and optical properties.[2] Most colloidal particles retain their monodispersed stability in an aqueous solution because they have more or less electric charges on the surface making each particle repel others before they come into actual contact and form clusters. Obvious applications of colloidal particles can be cited in drug delivery, special coatings, corrosion protection, and catalysis.[1] The reported polymer colloidal particles (latex) were the best example for such mentioned applications which led to the significant development of a variety of techniques for the production of other materials.[2] Currently, multifarious novel materials for colloidal particles' preparation such as inorganic metal oxides, pure metal components or mixed metal components and biological materials have been developed.

On the other hand, the majority of researchers' efforts have invested in generating finely and uniformly dispersed colloidal particles through both physical and chemical processes, including precipitation, phase transformation, and chemical reaction in the past few decades.[3] Recently, colloidal particles with different sizes, shapes (rods, cubes, tetrahedral, prim, half shells, striped particles, polyvalent sphere, stars), compositions (metals, metal oxides, polymers), and functionalities have been reported which have gathered a lot of attention by scientists.[3-4]

## 1.2 Janus Particles

As a subcategory of patchy particles, Janus particles (Figure 1), which were named after the two-faced god Janus, have played an important role in advanced nanomaterial application on account of their multifunctional character and properties on the two opposite faces such as amphiphilic (hydrophobic on one side and hydrophilic on the other side), dipolar (anionic on one side and cationic on the other) and active interfaces (antifouling or anti-icing).[4] Generally, Janus particles can be classified into the following three major groups: hard Janus particles (including inorganic and metal-based ones), soft Janus particles (including liposomes, organic, polymer-based), and hybrid organic/inorganic Janus particles.[2][5] Different groups of Janus particles have

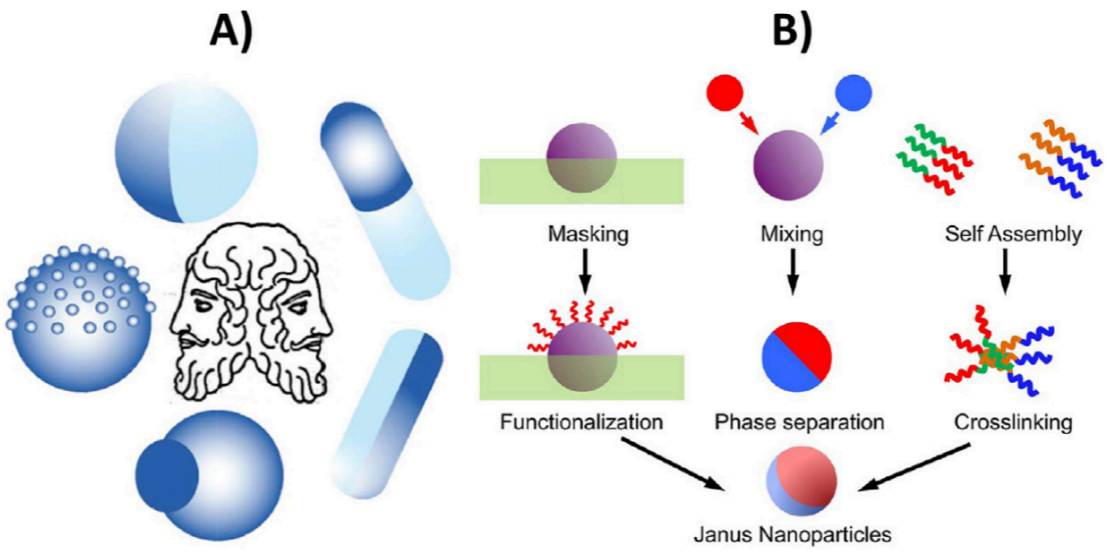


Figure 1.1 Different shapes of Janus particles [6] (Copyright by *Langmuir*, 2017)

different synthesis strategies and methods. For soft Janus particles (eg Janus liposomes), self-assembling through gentle hydration is the most common method, especially for Janus

liposomes[6] and Janus micelle formation.[7-8] Some other approaches include phase separation in confined volumes, [9] electrohydrodynamic jetting, [10] seeded emulsion polymerization [11], and microfluidic droplets.[12-13] For hard Janus particles (silica and titanium dioxide) generation, the most popular method is based on temporarily masking one side of these particles using an immobilization template and exposing the other side's surface for modification (metal or NP deposition).[14] For example, Dr. Jurriaan Huskens and his group fabricated Janus particles with a variety of chemical functionality through the masking and unmasking technique.[11] In this process, controllable anisotropic particle structures are generated by covalent coupling and solution-based supramolecular recognition. For hybrid Janus particles, most of them are composed of organic/inorganic materials; for example, stimuli-responsive polymers as shells combined with inorganic cores. The controlled and living radical polymerization technique was also utilized to fabricate hybrid Janus particles by grafting polymer brushes onto the opposite sides of core particles [2][15]. This is true except for the common synthetic approaches aforementioned for hard Janus particles and soft Janus particles including phase separation, selective modification, and microfluidic droplets. As early as 2008, Manfred and his group fabricated hybrid hairy Janus particles of different sizes through a combination of "grafting from" and "grafting to" approaches. (Figure 2) [15]

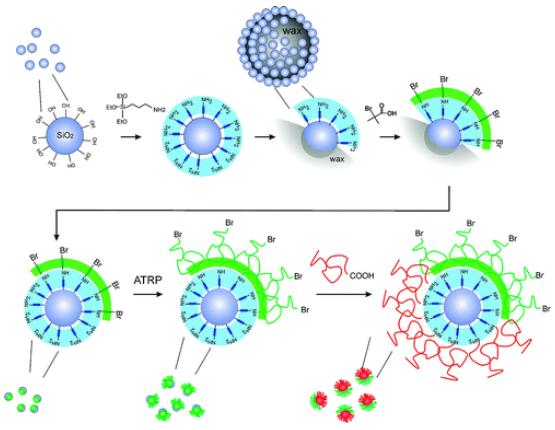


Figure 1.2 Schematic illustration of the fabrication generation hybrid Janus particles with "grafting from" and "grafting to" techniques. [15] (Copyright by *Macromolecules*, 2008)

Compared with traditional homogenous particles, Janus particles demonstrated a growing number of contributions and possibilities in developing brand-new smart materials in the past few years. [5] The most important application for Janus particles is taking full advantage of the active interface of the particle. In 2003, Michael J. Sailor and his group synthesized and generated smart-dust Si-based Janus particles containing an alkylated hydrophobic green mirror on one side and an oxidized hydrophilic red mirror on the other side. (Figure 1.3) [16]

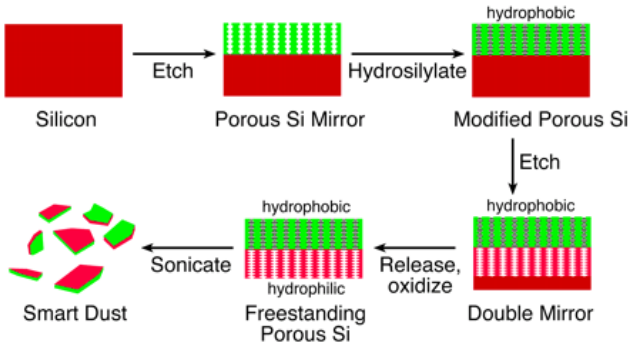


Figure 1.3 The synthesis process of the biofunctional smart-dust particles [16] (Copyright by *Proc. Natl*. 2003)

These chemically modified small-dust particles could be applied in high-throughput screening, optical switching, and biological sensors. [16] Later in 2010, Seung-man Yang and his group developed a Janus microsphere composed of superhydrophobic and hydrophilic surfaces through a photocurable Pickering emulsion droplet.[17] These Janus microspheres could be used as highly flexible superhydrophobic barriers in which the hydrophilic surfaces were held and aligned along the interface. When the membrane formed with these Janus microspheres, it still maintained integrity under a dynamic disturbance induced by a hydrophilic glass stick.[17] Other applications of Janus particles for active interface were also widely used, including electrical actuation[18], magnetic actuation[19], dual photonic band gap[20], stabilization of foams for catalysis[21], and interfacial catalysis.[22] On the other hand, several applications were attracting increased attention from researchers by taking full advantage of the active surface of Janus particles including biofunctional substrates,[23]targeted therapy, [24] imaging, [25] photocatalytic substrates,[26]optically active substrates, [27]superhydrophobic coatings,[28] anti-icing coatings[29] and antifouling coatings.[30]

### 1. 3 Lipid self-assembled particles—liposomes

As a major class of small biomolecules, which generally have a hydrophilic head and a hydrophobic tail and are soluble in nonpolar solvents but typically insoluble in water, lipids are widely existing like cell membranes.[31] The main functions of lipids in the cells are including signaling, storing energy, and structural components of the normal cell membrane. Currently, there more than 10,000 lipid molecules are discovered so far and are available in the Lipid Data Base.

Based on their well-defined chemical and biochemical principles, they were classified into the following categories: facyls, glycerolipids, glycerophospholipids, sphingolipids, sterol lipids, prenol lipids, saccharolipids, and polyketides. The main two types of lipids employed in our active motion experiments are including cholesterol and glycerophospholipid such as DPPC and DOPC. The structure of these aforementioned lipids was displayed in Figure 4 below.[32]

In the meanwhile, the most widely class of lipids in lipid-based nanoparticle formulations are phospholipids, which are also the major class of biomembrane lipids in human cells. Since lipid nanoparticles (LNP) have emerged across the pharmaceutical industry as a promising vehicle, the selection of lipids for the preparation of these lipid nanoparticles has become crucial. Several aspects need to be taken into consideration when preparing such lipid nanoparticles employed with phospholipids, including phase state, biocompatibility, fluidity, electric charge, toxicity, size controlling, circulation time, cargo release, stability, and encapsulation efficiency.

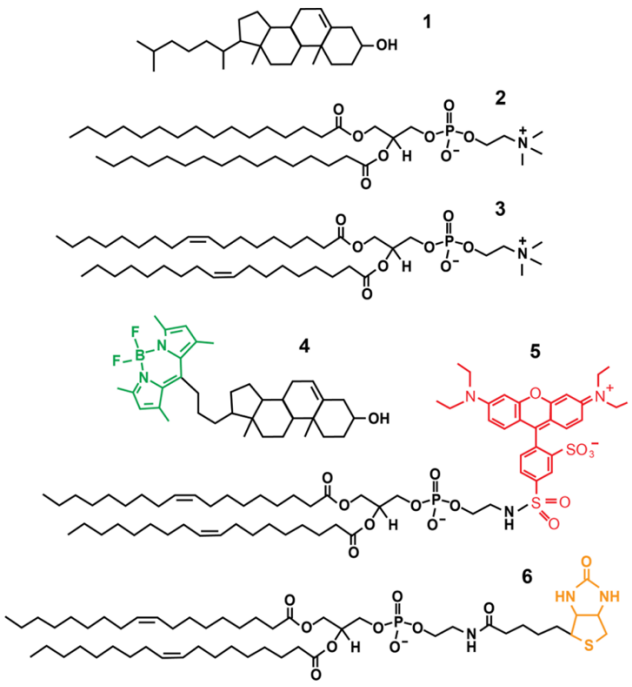


Figure 1.4 Main lipids molecules employed in this Dissertation (1-6) :1. cholesterol; 2. DPPC; 3. DOPC; 4. Bodipy-cholesterol; 5. rho-DOPE; 6. biotin-DOPE. Printed with permission from *Langmuir* 2018, 34, 7509-7518. (Copyright by *Langmuir*, 2018).[32]

Liposomes are a classic soft particle and cell membrane model, which is composed of phospholipids self-enclosed to form spheres in the shape of lipid bilayers and an aqueous core within bilayers and have attracted significant attention from researchers.[31][32] Most of the work has been focused on these cell-membrane-like vesicles in the past decades. The phospholipids present polar shells in aqueous solutions due to the hydrophobic acyl chain in phospholipids producing a hydrophobic effect with the surrounding aqueous medium.[33] This thermodynamically favorable formation could be further enhanced by hydrogen bonding, Van der Waals forces, and other electrostatic interactions. Lipid bilayers self-assembled from different lipid species are often used as drug delivery tools on account of them having similar properties and structures to cell membranes. There are a lot of advantages for liposomes as drug delivery tools

with these specific structures including: improved solubility of the encapsulated drugs, versatility when chemically modified with attached specific surface ligands for targeting, prevention of chemical and biological degradation under storage conditions and during patient administration and compatibility with biodegradable and nontoxic material. Based on their size, compositions and number of bilayers, liposomes can be classified into the following groups: Small unilamellar vesicles (SUV) (20-100nm); Large unilamellar vesicles (LUV) (100nm-1000nm); Giant unilamellar vesicles (GUV) (>1000nm) and Multilamellar vesicles (MLV) (>500nm).[33] (Figure 1.5) These generated liposomes could be a gel state or fluidic state at room temperature, mainly dependent on the phase transition temperatures (Tm) of composited lipids.

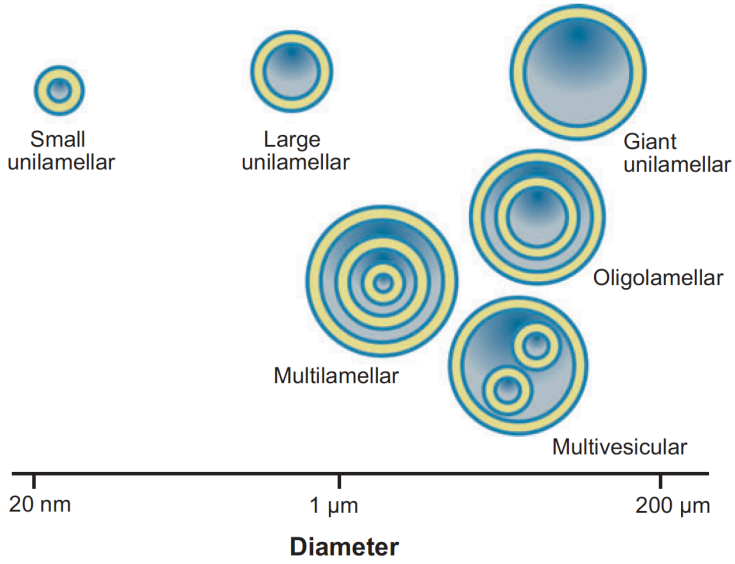


Figure 1.5 Classification of liposomes (Copyright by *Anal. Chem.,* 2008) [33]

GUV plays a prominent role in studying the biomembrane due to their large dimensions in the range of typical cell size, which can be easily observed and manipulated under an optical microscope. New preparation methods, which can provide a fast and easy route to generate vesicles

from different lipids compositions and under different buffer conditions, have been sought and developed because of the unique property of GUVs. [32-33]

### 1.4 Liposomes applied in drug and vaccine delivery

Liposomes are useful drug delivery systems for carrying hydrophilic (in the aqueous core), lipophilic (in the lipid bilayer), and amphiphilic (partitioned at the surface of the bilayers) drugs. Different kinds of drug reagents such as peptides, enzymes, antibodies, and DNA/RNA sequences can be encapsulated in the aqueous core or attached to the surface of the membrane bilayer. A great number of liposome-based drug delivery formulations have been approved and used in practice. The latest single application of liposomes in drug delivery is in cancer treatment, because of the improved bioavailability and selectivity of liposomes-encapsulated antitumor agents over free drugs.[34] Lipid-based nanocarriers reduce the toxicity of anticancer drugs to normal tissue, increase the water solubilities of hydrophobic drugs, extend the drug residence time, and improve control over drug release.[35] Lipid-based nanoparticles also improve the efficacy of cancer therapies through the enhanced permeability and retention effect (EPR). Additionally, the accumulation of lipid-based nanoparticles in tumors as a result of the EPR effect allows the nanoparticles to release the antitumor agents selectively in the vicinity of tumor cells. As we know, the latest and most successful use of lipid-based nanoparticles as the delivery vehicle is the two recently approved COVID-19 messenger RNA (mRNA) vaccines by Pfizer and Moderna, which have been developed with unparalleled speed and have shown notable effusiveness in disease prevention.[36] mRNA vaccines have revolutionary vaccine development be use of their high efficacies, accelerated development cycles, and potential for low-cost manufacture. The

advancement in lipid-based nanoparticle technology makes it possible for the rapid development of mRNA vaccines. [35] The use of mRNA for the expression of therapeutic proteins bears promise in treating a wide range of diseases.

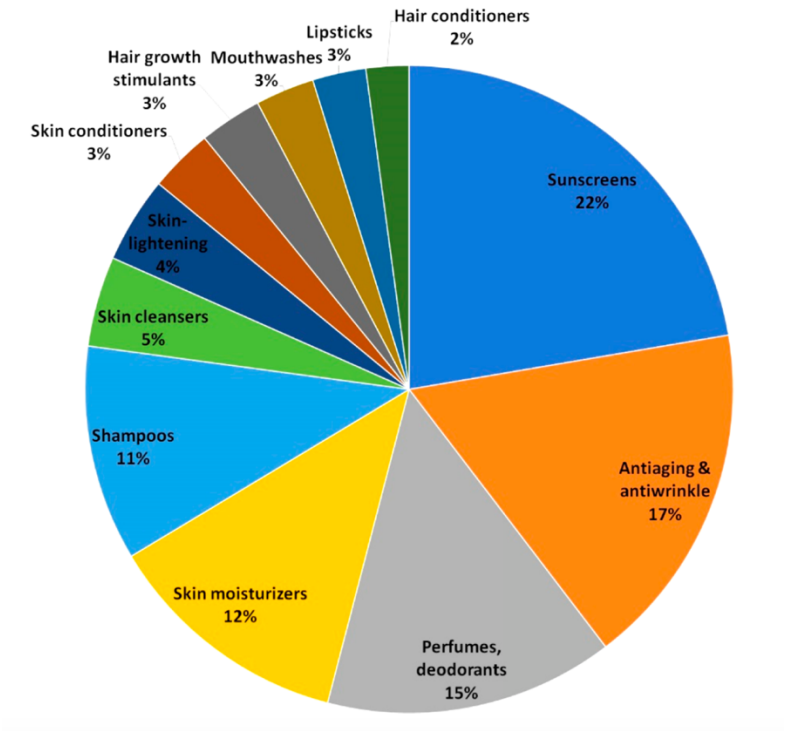


Figure 1.6 Distribution of liposomes based on different cosmetic product types. *(Copyright by ACS Nano)* [36]

## 1.5 Liposomes applied in cosmetics

Nanoparticles, especially for nanosized-liposomes, has employed in various cosmetic products for a long time since the technology and materials were developed. There are several anticipated advantages of liposomal cosmetic formulations, including enhanced stability, the efficacy of these formulations, and successful penetration of the ingredients into the skin. Additionally, liposomes could be also formulated with various extracts, moisturizers, antibiotics,

and proteins for uses such as wound healing, sunburn relief, hair conditioners, antiaging products, and long-lasting perfumes. The most famous product containing hyaluronic acid in a liposomal delivery preparation is the Advanced Night Repair Protective Complex introduced by Estee Lauder.[36] As Figure 1.6 displays, there were many cosmetic products that contained the nanosized liposome, including shampoos, perfume, skin cleaners and sunscreens, and so on.

### 1.6 Liposomes applied as nanoreactors

Recently, with the rapid development of nanotechnology and nanobiotechnology, liposomes could be employed as nanoscale chemical reactors in which the size-controlled synthesis of metal nanoparticles could be accomplished. The size of nanoparticles plays an important role in determining their chemical and physical properties and suitability for use. The classic example of preparing metal nanoparticles belongs to the application of nanosized liposomes encapsulating tetracholoroauric acid to fabricate 2-5nm gold nanoparticles.[37] In this case, the controlled diffusion of the reduced agent-sodium borohydride-through the liposomal membrane regulated the particle formation kinetics and resulted in ultrasmall nanoparticles with a narrow size distribution. Additionally, liposome-based nanoreactors have also been proposed as tools for the treatment of disease and for eliminating harmful substances by allowing the production of therapeutic agents in situ. Here the classic example is, the antioxidant enzyme catalase has been encapsulated inside liposomes comprising a cisplatin prodrug-conjugated phospholipid, for enhanced chemo-radiotherapy of cancer.[38]

## 1.7 General Methods for Liposomes Preparation

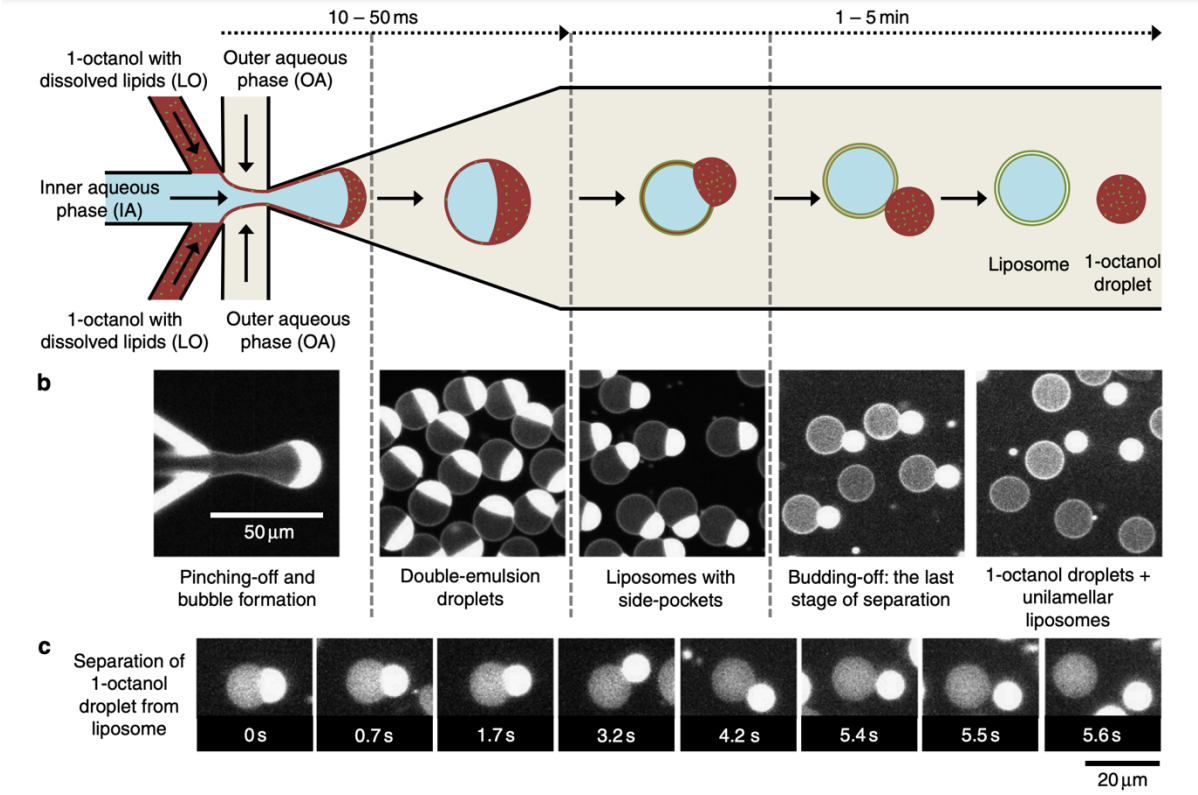


Figure 1.7 Octanol-assisted liposomes generation process. [48] *(Copyright by 2016 Nature Communication)*

Theoretically, GUV formation normally involves a lipid bilayer preassembly step through the evaporation of organic solvent from the lipids at the solid-liquid interface. There were four main approaches generating GUVs in the past few years including gentle hydration, [39] solid hydration, [40] electroformation, [41-44] emulsion-based methods [45-47], and gel-assisted swelling formation. [40][41][49] For the gentle hydration method, the main disadvantage is that vesicle formation requires long timescales on the order of several days. Besides, it only works with restricted lipids compositions and ionic conditions. To solve the time-consuming problem,

electroformation has been one of the most widely used vesicle formation methods in which an electrical field was applied across a buffer-filled chamber bound by conductive slides. Even though this method shortens the vesicle growing time to several hours, generating vesicles in physiological buffers or from charged lipids mixtures is still challenging. [38][49] Recently, microfluidic methods

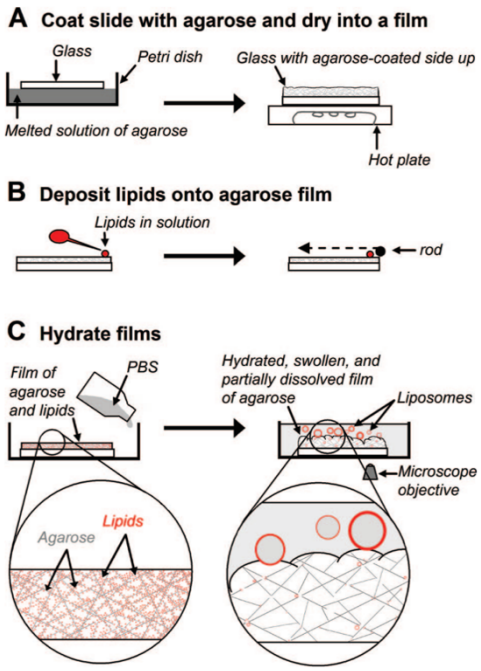


Figure 1.8 Giant liposomes generation process through agarose gel film [39] (Copyright by *J. Am. Chem. Soc*, 2009)

have been introduced to generate liposomes due to their highly controlled and reproducible environment. (Figure 1.7) By forming a water-in-organic solvent-in-water double emulsion droplet and then slowly extracting the organic solvent in the microfluidic channels, the dissolved lipids could form bilayer liposomes. [48] The fast solvent-extraction mechanism plays a key role in these microfluidic methods. The lipids-carrying phases could be rather flexible including oil-based, alkane-based, or alcohol-based. A large number of uniform, monodisperse, unilamellar, cell-sized liposomes could be generated efficiently through microfluidics.[48] However, designing,

fabricating, and controlling microfluidic chips need a lot of expertise and could be labor-intensive. Moreover, most microfluidic fabrication materials including PDMS or PMMA are toxic to liposomes and these monomers could influence the liposomes' generation. As an updated hydration method, gel-assisted swelling formation provides a facile and fast way to generate liposomes with a wide range of lipids compositions.[47-48] In the year of 2009, Dr. Mayer and his group first found that films of agarose (Figure 1.8) could enable the lipid formation of giant liposomes in solutions of physiologic ionic strength. [40] Through this specific method, they not only generated giant liposomes in high yield without specialized equipment but also made it possible to form giant liposomes  a wide range of lipids composition.[41]To optimize the lipid distribution of the interface and decrease the gel dissolution, different gels have been attempted from agarose to polyvinyl alcohol (PVA) gel. There are obvious advantages in the liposome formation process with PVA gel including 1) offering more water channels in the liposome hydration process; 2) PVA swelling helps the generated liposome separation; 3) PVA gels are less prone to dissolution upon swelling at low temperatures; 4) PVA gel deficits are good for liposomes leaving the gel surface. [40][49]

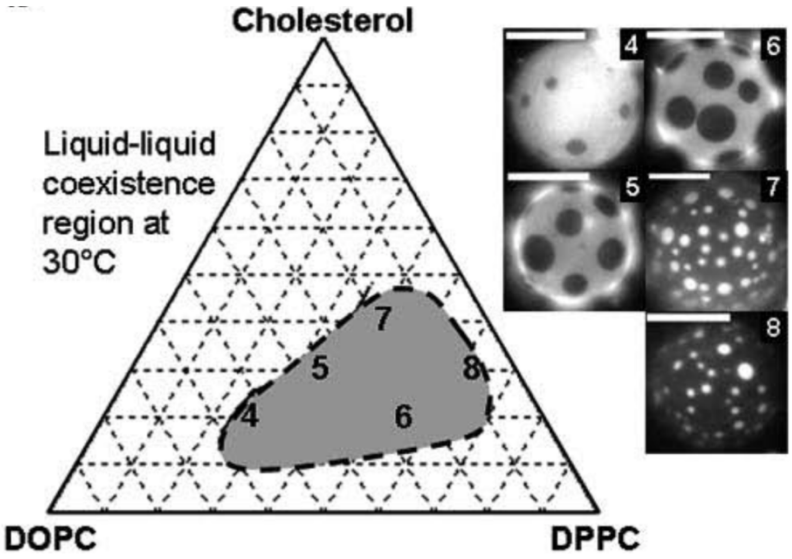


Figure 1.9 Phase diagram of micron-scale liquid immiscibility region on GUV.[50] (Copyright by *Biophysical* 2003)

**1.8 Janus liposomes (special kind of liposomes due to phase separation)**

Phase separation is a common phenomenon in cell membranes and it has already become an attractive field in recent years. A large number of research focusing on cholesterol-induced liquid-liquid immiscibility and forming liquid domains in the surface of the liposome when cholesterol is mixed with saturated/unsaturated hydrocarbon chains lipids (DPPC/DOPC) have been reported.[49-52] In the DPPC/DOPC/Cholesterol membrane system, the cholesterol molecules have strong interaction with DPPC and DOPC, in which cholesterol inserts normal to the plane of the bilayer, with its hydroxyl group in close vicinity to the ester carbonyl of phospholipids and its alkyl side-chain extending towards the bilayer center. In this specific situation, cholesterol is intercalated in the membrane parallel to the phospholipid hydrocarbon chains, and the carbons in positions 2-10 from the phospholipid molecule are estimated to lie in close to proximity to the sterol tetracyclic ring which will order the hydrocarbon chains and diminish trans-gauche isomerization about their

carbon-carbon bonds. It has been estimated that the effective length of cholesterol can correspond to a 17-carbon all-trans hydrocarbon chain because the sterol sidechain is flexible the regions in the methyl end of the phospholipid are not as ordered by cholesterol molecules as upper part. Upon the cholesterol/phospholipid interactions, van der Waals forces and hydrophobic forces were formed in the process. Moreover, the interactions of cholesterol with phospholipid can be strengthened by hydrogen bonding of the cholesterol hydroxyl group to the polar head group and interfacial regions in phospholipids. Since as early as 2000, Dr. Sarah Keller and her group systematically studied the separation of liquid phases in giant vesicles which formed patchy particles of ternary mixtures of DPPC/DOPC/Chol with different ratios. [50][51] They mapped phase boundaries for these full ternary systems through studying this particular model mixture. (Figure 1.9) The phase separation (domain formation) on liposome membrane in ternary mixtures of DPPC/DOPC/Chol is mainly on account of immiscibility between saturated lipids (DPPC) and unsaturated lipids (DOPC), as well as cholesterols that promote tight packing of saturated lipids (DPPC) while inhibiting tight packing of unsaturated lipids (DOPC).[53] This immiscibility property was mainly affected by the transition temperature of composed lipids and the ratio of different components.

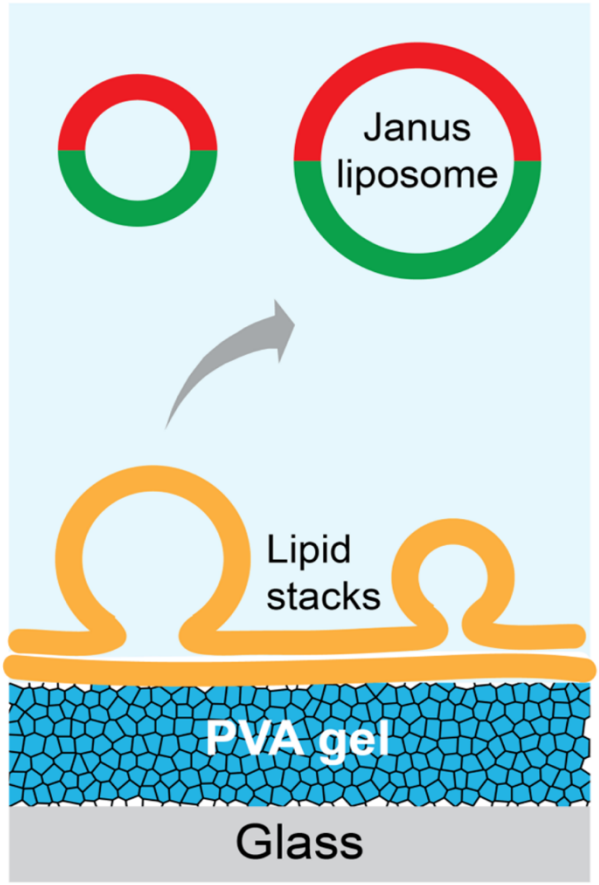


Figure 1.10. Formation of Janus liposomes via gel-assisted lipid swelling. [32] (Copyright by *Langmuir*, ACS,2018)

Here giant Janus liposomes take up a large portion of patch particles in such surface immiscibility due to hydrophobic mismatch between DOPC and DPPC and cholesterols' preferential association with DPPC rather than DOPC. [51] In such structures, rigid cholesterol inserted into enriched DPPC produces a liquid-ordered phase ($L_O$) while cholesterol inserted into enriched DOPC produces a liquid-disordered phase ($L_d$).[50] Taking advantage of the phase separation mechanism of liposomes, our lab developed a high-yield procedure for generating microsized Janus liposomes via a gel-assisted swelling method with DPPC/DOPC/Cholesterol

system. (Figure 1.10) [49] Those prepared giant Janus liposomes hold apparent strength with their broken surface symmetry and heterogeneous surface property which make them a novel carrier in the specific application. Our research mainly focuses on different characters, properties, and behavior such as the active motion of Janus liposomes compared with homogeneous liposomes which will be covered in more detail in the following part of this dissertation.

### 1.9 Liposome Size Control

Most traditional liposome generation methods including electroformation, [50-54] emulsion-based methods [55-57], and gentle hydration can only prepare nonuniform giant liposomes with large size distribution. Acquiring well-fined, uniform, size-controlled liposomes has been a great challenge for researchers. To this end, there is an increasing need to generate uniform size-controlled giant liposomes for further research. Double-emulsion with octanol assisted through multiphase laminar flow in microfluidic in which the oil phase needs to be removed in the subsequent process was applied to generate size controllable liposomes. [64-65] Even though high throughput and high-yielding production of liposomes in which size distribution ranged from tens to hundreds of microns, this method requires complicated microfluidic device design and sensitive operation of the instrument, as well as some residual oil phase could remain in the lipid membrane.[63] Later, Dr. Han and his group reported that the microcontact stripping technique could be combined with the classic electroformation method to generate size-controlled giant liposomes. [66] (Figure 1.11) Based on their experiment, patterned lipids film microarrays on ITO glass slides were required to be prepared first, followed by the fabrication of giant unilamellar

vesicle microarrays. The homemade polytetrafluoroethylene (PTFE) frame was the key factor for their result. However, the size distribution of fabricated giant liposomes was not narrowed down to a few microns.

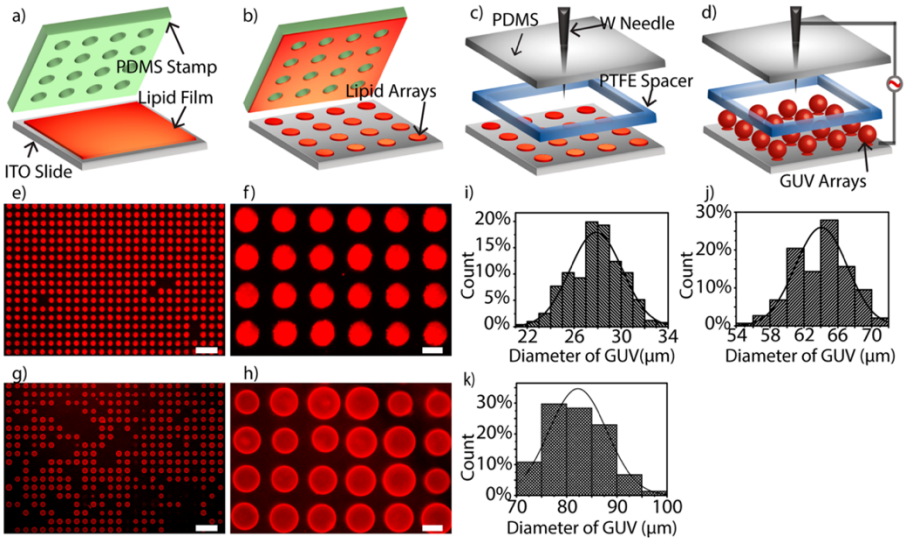


Figure 1.11 Diagram of GUV microarray formation by combining microcontact stripping and electroporation and liposomes size distribution graph.[59] (Copyright by *Anal. Chem*. 2018)

Previous work by Zening Liu in our lab has demonstrated a novel approach to generating size-controlled giant liposomes via combining gel-assisted swelling lipid hydration with membrane-based liposome extrusion. [67] According to this special featured design, planar lipid stacks were deposited on poly(vinyl alcohol) gel, which was further laminated atop microporous polycarbonate membranes. With the fixed size of pores ranges from 3 microns to 10 microns on the polycarbonate membrane, which defined the upper size limit of liposomes passing through. Low distribution of size-controlled liposomes was produced after this hydration process. (Figure 1.12) [67] At the while, Janus liposomes can still keep an even phase separation state under this

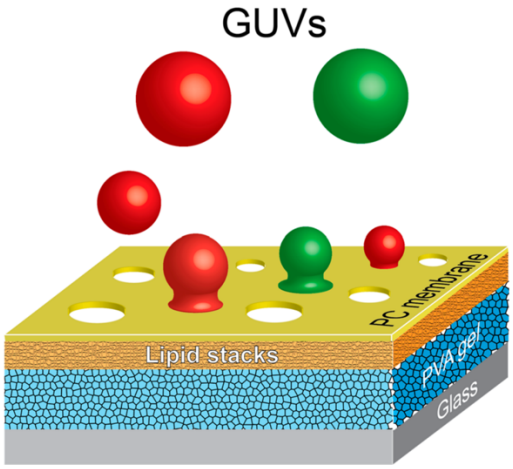


Figure 12. Schematic of multilayered design of the membrane-gated, gel-assisted lipid hydration method. [67] (Copyright by *ACS, Langmuir* 2020)

size-controlled hydration process which made it a reliable operation method compared to other approaches. Nevertheless, the low yield production of liposomes for each batch of hydration made it not a preferred method if a large quantity of uniform size-controlled liposome samples were needed for further study. Except for the prementioned protocols, more post-process steps were applied for controlling the size of liposomes after the hydration step, including membrane extrusion (Figure 1.13), size exclusion column separation (Figure1.14), freeze-thaw, and sonication. Among these

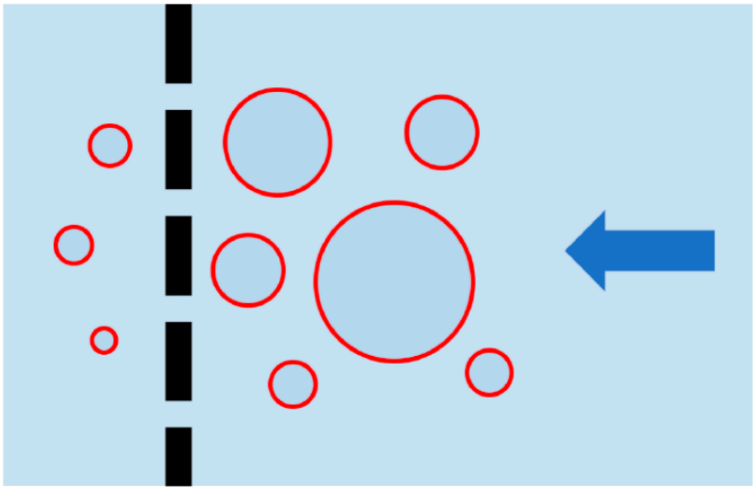

Figure 13 Schematic presentation of liposomes extrusion. [67] *(Copyright by ACS, Langmuir 2020)*

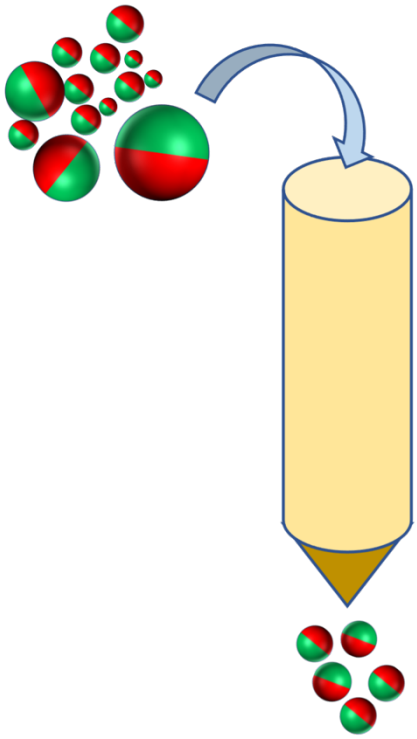

Figure 1.14. Diagram of size exclusion column for preparing size-controlled liposomes purification

post-processing methods, sonication is mainly focused on nano-sized liposomes preparation especially for some protein or drug encapsulation experiments while membrane extrusion can be applied to both micro-sized and nano-sized liposomes preparation depending on the pore size of the membrane chosen which will be discussed in detail in the following chapters. For quite a long time, size exclusion chromatography purification was an effective and powerful technique for separating free, unencapsulated molecules from encapsulated liposomes which make full use of the different mobile speeds of small molecules and liposomes in the gel-packed column.[68] To prevent the significant loss of liposomes retained, the column has to be saturated with the same type as the liposomes component. The gel selection for packing the exclusion column in which liposomes are excluded and small molecules are included became the main factor that will affect

the effectivity of separation. [69] Most conventional gels were made of soft agarose (such as Sepharose 2B or CL-2B, Sepharose 4B or CL-4B), cross-linked dextrans(such as Sephadex G-25,G-100), and some bisacrylamide copolymer (Sephacryl S-1000) By the use of suitable gel material, different sizes of liposomes separation ranging from tens of nanometers to a few micrometers liposomes could be achieved.[68-69] Taking full advantage of the powerful separation technique of the size exclusion column, we tested the efficiency of liposome size control carefully, which will be discussed in detail in the following chapters.

### 1.10 Diffusion and Active Motion of Janus particles

Brownian motion, also known as diffusion, is caused by random collisions between a nanosized or microsized dispersed particle and the molecules of the surrounding fluid. Based on Einstein's famous finding on Brownian motion [58] for a spherical particle larger than the solvent molecules, the diffusion of the particle in a low-viscosity medium can be predicted by the Stokes-Einstein equation:

$$D=\frac{kBT}{6\pi\eta r} \qquad [58]$$

Where D is the diffusion constant, $k_B$ is Boltzmann's constant, T is the absolute temperature, η is the viscosity of the fluid, and r is the particle's radius.

In comparison with diffusion, active motion [70-74], in which self-propelled Janus particles additionally take up energy from their surrounding environment and convert it into directed motion[70], has drawn increased attention by researchers since the pioneering report by Whitesides'

group in which the surround hydrogen peroxides were decomposed by the platinum catalysis on the surface of Janus particle in past decades.[71] To achieve such self-propelled directional motion

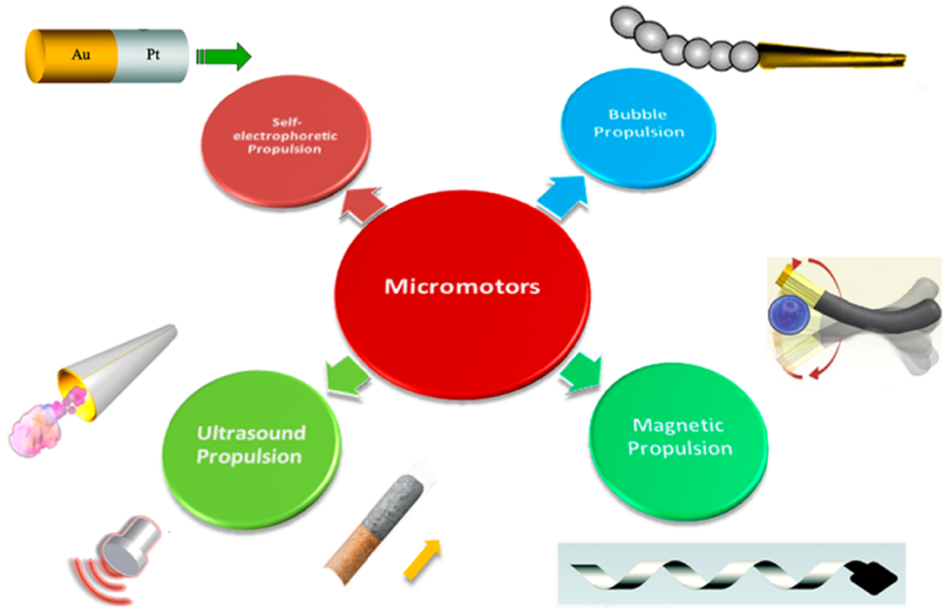


Figure 1.15. Janus micromotors by deferent mechanism.[74] (Copyright by *ACS Nano* 2012)

behavior (Figure 1.15) [74] of this artificial microscale or nanoscale swimmers, several significant strategies motivate and steer the motion in the environment of low Reynold number as well as overcome the ubiquity of Brownian motion.[72] According to the mechanism of self-propelled motion of Janus particles, the strategies applied to the active motion were mainly grouped into two separate directions: chemically powered systems and externally actuated systems (chemical fuel free).[73-75] For the former case, there are Bubble propulsion micromotors,[76-78] Self-electrophoretic micromotors, [79] Self-diffusiophoretic[80-81](Chemical gradient different based) propulsion micromotors, and Thermophoretic micromotors[82] while the latter case is including

Magnetic propulsion micromotors[83-86], Electrical propulsion micromotors[87-88], Ultrasound propulsion micromotors[89-90]and Light-driven propulsion micromotors.[91-93] (Figure 1.16)[94]

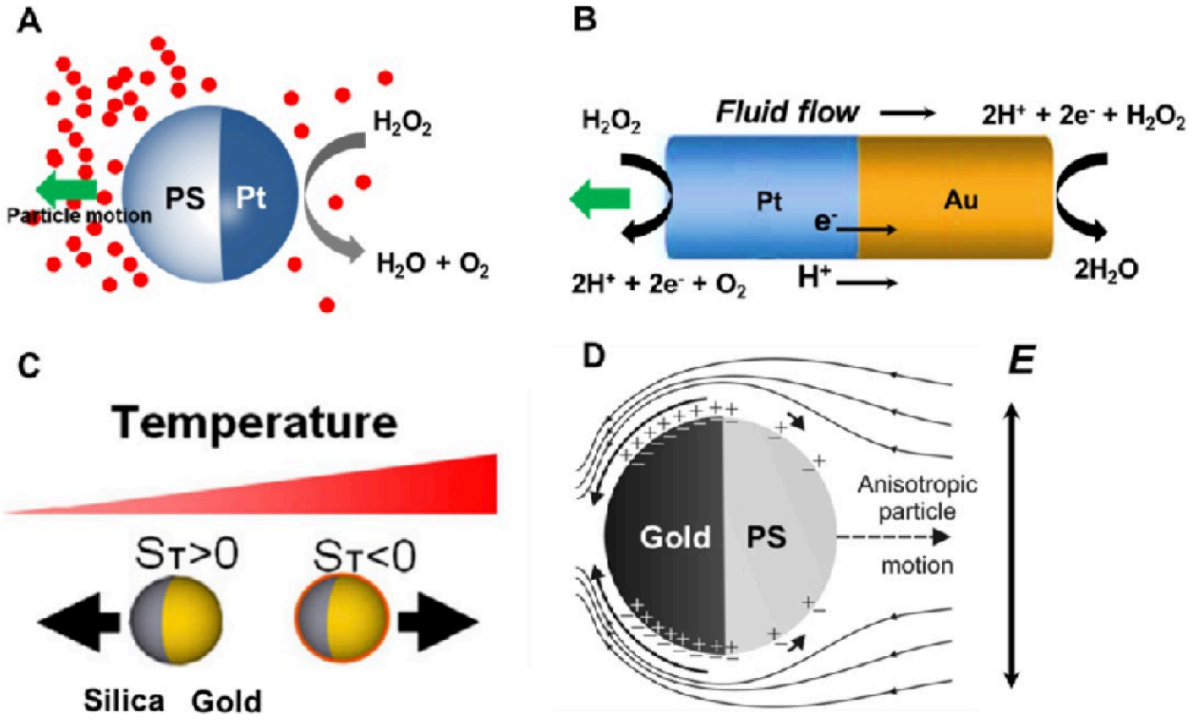


Figure 1.16. Different Janus Micromotors [94] (Copyright by *ACS, Langmuir* 2017)

Such efficient conversion of other energy into mechanical work makes these micro- and nanomotors become excellent drug delivery carriers with numerous functions ranging from nanomedicine therapy to chemical sensing and intracellular transport.[95] Due to the remarkable performance of these biological micro- and nanomotors, extensive efforts are currently developing low-cost, nontoxic, modified, and transformable materials that can be generated and fabricated for active motors.[96-97] Considering all the biological advantages and requirements such as biocompatibility with the human body, soft and abundant drug-loading positions for being certificated active motors, Janus liposomes become a preferential achievable candidate for deep

research. Inspired by the production of enzyme-based biological motors,[98] we completed the formation of enzymatic Janus liposomes by immobilizing horseradish peroxidase on the half-face of our Janus liposomes and investigated the motion behaviors of these Janus liposomes through single particle tracking methods which will be discussed in detail in following chapters.

### 1.11 Single Particle Tracking (SPT) Technique for Nano/Microparticle Motion Analysis

Measurement of trajectory for single nanosized or microsized particles has remained a great challenge for the motion behavior study of particles for a long time. Both time resolution and spatial resolution accounted for this challenge, especially in the dynamic environment solution. Single Particle Tracking (SPT) technique (Figure 1.17) [99] provides a reliable approach to

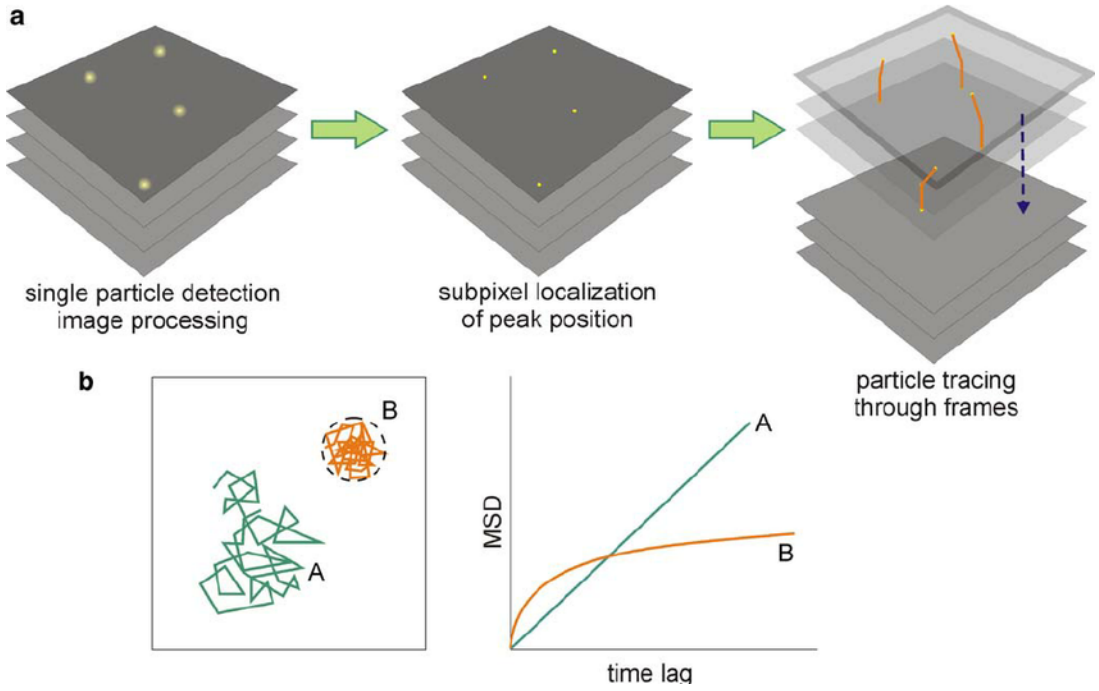


Figure 1.17 Scheme of single particle tracking ($MSD=4Dt+V^2t^2$) [99] (Copyright by *Applied Microbiology and Biotechnology*, 2007)

collecting dynamic information about both two-dimensional (2D) and three-dimensional (3D) motion behavior of micro-particles under Fluorescence Microscopy or Confocal Laser Scanning Microscopy (CLSM).[100-101] Generally, the SPT method can be grouped into several independent Modules, including signal-to-noise ratio enhancement, particle identification and localization, particle tracking, and post-dynamic/kinetic analysis.[101] The crucial goal of SPT is understanding and investigating the motion behavior of single particles or molecules in various solution environments and extracting mechanistic descriptions of their dynamics. In the meanwhile, modern advanced SPT achieved temporal resolution as high as tens of microseconds with spatial resolution down to 1nm. In our experiments of liposomes motion study, all the motion videos were recorded through the CCD camera from Confocal Laser Scanning Microscopy and analyzed in tracking software Image J with SPT technique.

### 1.12 Janus Liposomes Characterization - Confocal Laser Scanning Microscopy (CLSM)

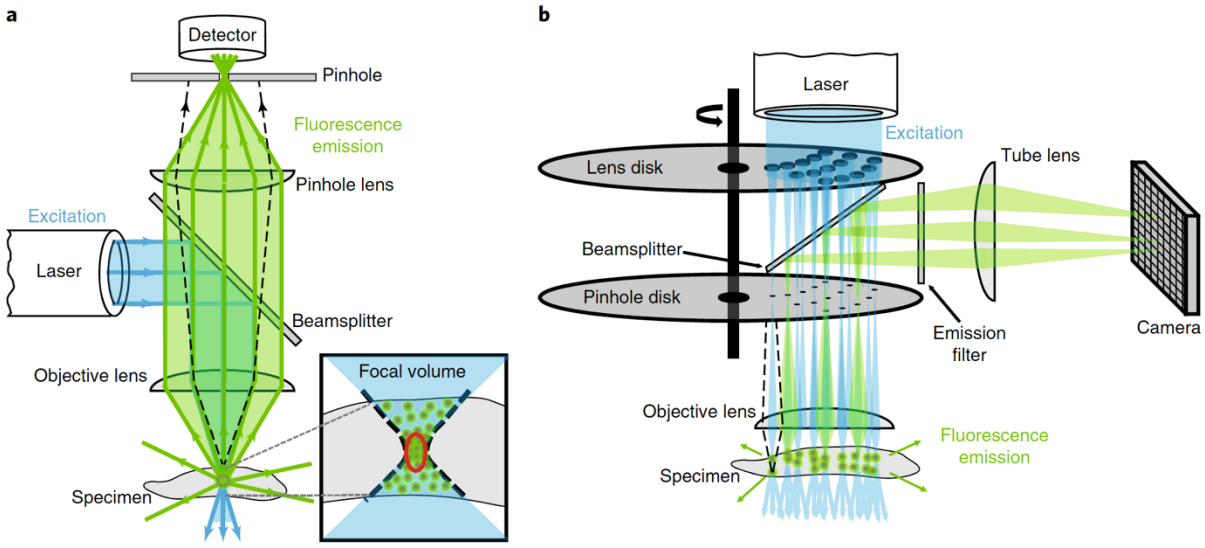


Figure 1.18 Schematic of a classic Confocal Laser Scanning Microscopy.[102] (Copyright by *Nature Protocols*)

To generate optical sections thinner than 1 μm without having to physically slice samples, normally a high-resolution objective lens is equipped on a confocal microscope. Therefore these kinds of confocal microscopes are applied to quantify the intensities and explore the spatial arrangement of fluorescent molecules with high precision.[102] When placing an essential component-pinhole aperture on the conventional confocal microscope with a laser beam as a scanning light source, a confocal laser scanning microscope is assembled and achieved. The specific pinhole ensures only fluorescence that originates at the focal point is captured by detectors, while fluorescence emission from above or below the focal plane will be blocked, which offers high axial resolution, sharp image quality, ty and construction of structural three-dimensional images.[103] Figure 1.18 shows a general scheme of most main components and the lightpath in classic CLSM. Compared with a conventional microscope, CLSM holds many apparent advantages as follows: increased effective resolution (500nm); improved signal-to-noise ratio, reduced blurring of an image from light scattering, XY-scanning ova er wide area of the specimen, tunable Z-scanning and providing complex contrast effects with simple equipment. So far, all the Janus liposomes or homogeneous liposomes samples were characterized under our CLSM instrument, as well as the active motion behaviors study of Janus liposomes, which will be introduced in the following charter.

### 1.13 Permeation of solutes to the bilayer membrane on liposomes

In biology, membrane permeability is an essential property of cells and plays a key role in regulating the passage of solutes and solvents into and out of cells. [104-105] This membrane permeation is either mediated by membrane transport proteins or specific channels or passive

diffusion. Recently, passive diffusion for small solutes permeating through the bilayer membrane of cell mimic model, liposomes, has drawn increased attention from researchers. Most reported literature[106-109] focuses on investigating the properties of the permeants, namely size, shape, and polarity while relatively fewer studies explored the impact of liposome membrane lipid composition on passive diffusion. Based on the developed solubility-diffusion model, the permeability coefficient (P) of a molecule is predicted to be inversely proportional to the thickness of the membrane and proportional to the product of the partition coefficient and diffusion coefficient in the membrane.[111] Bert Poolman and his group investigated the permeability coefficient of synthetic membranes and the plasma membrane of living cells for small molecules such as weak acids, bases, water, and neutral solutes. They tested liposomes of different lipid compositions including DOPC and DPPC, then observed a relationship between acyl chain saturation and membrane permeability for both water, formic acid, and lactic acid. On account of the difference between liquid-ordered membranes (Lo) and liquid-disordered membranes, the permeability of water molecules through the Lo membrane is much lower than through the model Ld membrane.[105] What's more, the difference becomes increasingly important in membranes with more complicated compositions and rich phase behavior, like the plasma membrane of yeast, which contains not only patches of highly ordered lipids in the Lo phase, but also regions in the gel ($L_\beta$) phase.[110-111]

Phase separation in lipid bilayers is of fundamental importance to our understanding of the organization and functions of cell membranes. As a special Janus particle, Janus liposomes hold several advantages, including two opposing halves with distinct makeup/functionality, in which one hemisphere membrane of the liposomes displays a liquid disordered (Ld) domain and the other hemisphere shows a liquid-ordered (Lo) domain. [110] This particular structure of Janus liposomes

makes them an excellent candidate to study the passive diffusion of most small solutes to the bilayer membrane in one vesicle. There was seldom literature reporting the passive diffusion coefficient difference on bilayer membranes of Janus liposome to take full advantage of the unique phase structure of Janus liposomes, we herein explored the passive diffusion and permeation effect of small classic solutes to the Janus liposome membrane, including hydrogen peroxide ($H_2O_2$), glucose, ascorbate acid, formic acid, and sucrose. For those solutes (for example, $H_2O_2$ and formic acid) that could permeate through both sides of the bilayer membranes of Janus liposomes, the osmotic pressure outside and inside of the bilayer membrane was almost maintained and besides, the morphology of Janus liposomes also maintained even the different passive diffusion speed for the solutes permeating through the two hemisphere membrane. However, the other kind of solutes (glucose and sucrose) which could not permeate through the bilayer membrane of Janus liposomes would squeeze the membrane, resulting in the burst of these liposomes. These findings offered some guidance for the enzyme-based active motion research of Janus liposomes under a chemical fuel environment. The osmotic pressure limit for liposome bilayer membrane needs to be taken into consideration before investigating the fuel-existing active motion of Janus liposomes. Much more detail will be introduced in the following parts.

### 1.14 The Scope of This Dissertation

The main body of my Ph.D. study is devoted to the development and implementation of mechanisms to drive directional liposome motion in aqueous media. Toward this goal, I have explored three mechanisms: 1) enzymatic gas generation, 2) lipid extraction and 3) photoelectrochemical gas generation, during the study. According, the rest of this Dissertation is organized as follows.

In **Chapter 2**, we first generated biotinylated Janus liposomes reproducibly via PVA-gel assisted swelling hydration method as reported in our lab before. [49] Biotin-DOPE localization on the surface of these prepared Janus liposomes was investigated through conjugating avidin-Alexa Fluor. The HRP-bound biotinylated Janus liposomes were achieved when incubating these liposomes in solution with avidin conjugated-HRP following the fixed biotin to avidin ratio. Later on, uniform size-controlled Janus liposomes were prepared through pore membrane extrusion and these size-controlled liposomes were employed to study the active motion behavior with hydrogen peroxide mixed solution, which will be introduced in chapter 2. In meanwhile, the extra enzyme was removed through size exclusion column purification.

In **Chapter 3**, we demonstrate liposome active motion taking advantage of mainly a pair of intrinsic material properties associated with these assemblies: lipid phase separation and extraction. We show that global phase separation of ternary lipid systems (such as DPPC/DOPC/Cholesterol) within individual liposomes yields stable Janus particles with two distinctive liquid domains. While these anisotropic liposomes undergo pure Brownian diffusion in water, similar to their homogeneous analogs, adding extracting agents (cyclodextrins), to the system triggers asymmetrical cholesterol efflux about the liposomes, setting the latter into active motion. We present detailed analyses of liposome movement and cholesterol extraction kinetics to establish their correlation. We explore various experimental parameters, as well as mechanical details responsible for such motion. Our results highlight the rich possibility of hierarchically designed lipid-based artificial motors, from individual lipids, to their organization, surface chemistry, and interfacial mechanics.

In **Chapter 4**, inspired by light-driven micromotors reports, we placed the Rhodamine/Bodipy labeled Janus liposomes in the reduced reagents existing solution to

investigate the active motion behavior compared with a controlled experiment. Later on, we synthesized $Ru(bpy)_3^{2+}$-DOPE to replace Rhodamine-DOPE inserting it into an original $L_d$ phase of Janus liposomes ourselves on account that $Ru(bpy)_3^{2+}$-DOPE is not commercially available. As a more efficient and active photosensitizer, $Ru(bpy)_3^{2+}$ holds excellent and stable electrochemical properties which could be employed as both oxidized reagent and reduced reagent and make it a suitable electron transfer or mass transfer product in light-driven micromotors research. Herein, we generated $Ru(bpy)_3^{2+}$-labeled Janus liposomes and further studied the active motion behavior of these special liposomes in variable oxidized reagents solution.

In **Chapter 5**, the conclusions of this Dissertation were drawn and future work that may be developed from this work suggested.

## 1.15 References


1. Matijevic E. Production of monodispersed colloidal particles. *Annual Review of Materials Science*, **1985**, *15(1)*: 483-516.

2. Kirillova A, Marschelke C, Synytska A. Hybrid Janus particles: challenges and opportunities for the design of active functional interfaces and surfaces. *ACS Applied Materials & Interfaces*, **2019**, *11(10)*: 9643-96715.

3. Hu J, Zhou S, Sun Y, et al. Fabrication, properties and applications of Janus particles. *Chemical Society Reviews*, **2012**, *41(11)*: 4356-4378.

4. Walther A, Muller A H E. Janus particles: synthesis, self-assembly, physical properties, and applications. *Chemical Reviews*, **2013**, *113(7)*: 5194-5261.

5. Jiang S, Chen Q, Tripathy M, et al. Janus particle synthesis and assembly. *Advanced Materials*, **2010**, *22(10)*: 1060-1071.

6. Zhang J, Grzybowski B A, Granick S. Janus particle synthesis, assembly, and application. *Langmuir*, **2017**, *33(28)*: 6964-6977

7. Voets I K, De Keizer A, De Waard P, et al. Double-Faced Micelles from Water-Soluble Polymers. *Angewandte Chemie International Edition*, **2006**, *45(40)*: 6673-6676.

8. Voets I K, Fokkink R, Hellweg T, et al. Spontaneous symmetry breaking: formation of Janus micelles. *Soft Matter*, **2009**, *5(5)*: 999-1005

9. Higuchi T, Tajima A, Yabu H, et al. Spontaneous formation of polymer nanoparticles with inner micro-phase separation structures. *Soft Matter*, **2008**, *4(6)*: 1302-1305.

10. Roh K H, Martin DC, Lahann J. Biphasic Janus particles with nanoscale anisotropy. *Nature Materials*, **2005**, *4(10)*: 759

11. Kang C, Honciuc A. Influence of geometries on the assembly of snowman-shaped Janus nanoparticles. *ACS Nano*, **2018**, *12(4)*: 3741-3750

12. Nie Z, Li W, Seo M, et al. Janus and ternary particles generated by microfluidic synthesis: design, synthesis, and self-assembly. *Journal of the American Chemical Society*, **2006**, *128(29):* 9408-9412.

13. Hessberger T, Braun L B, Henrich F, et al. Co-flow microfluidic synthesis of liquid crystalline actuating Janus particles. *Journal of Materials Chemistry C*, **2016**, *4(37)*: 8778-8786.

14. Ling X Y, Phang I Y, Acikgoz C, et al. Janus particles with controllable patchiness and their chemical functionalization and supramolecular assembly. *Angewandte Chemie International Edition*, **2009**, *48(41)*: 7677-7682.

15. Berger S, Synytska A, Ionov L, et al. Stimuli-responsive bicomponent polymer Janus particles by "grafting from"/"grafting to" approaches. *Macromolecules*, **2008**, *41(24)*: 9669-9676.

16. Link J R, Sailor M J. Smart dust: Self-assembling, self-orienting photonic crystals of porous Si. *Proceedings of the National Academy of Sciences*, **2003**, *100(19)*: 10607-10610.

17. Kim S H, Lee S Y, Yang S M. Janus Microspheres for a Highly Flexible and Impregnable Water-Repelling Interface. *Angewandte Chemie International Edition*, **2010**, *49(14)*: 2535-2538.

18. Komazaki Y, Hirama H, Torii T. Electrically and magnetically dual-driven Janus particles for handwriting-enabled electronic paper. *Journal of Applied Physics*, **2015**, *117(15)*: 154506.

19. Lee S Y, Choi J, Jeong J R, et al. Magnetoresponsive photonic microspheres with a structural color gradient. *Advanced Materials*, **2017**, *29(13)*: 1605450.

20. Liu S S, Wang C F, Wang X Q, et al. Tunable Janus colloidal photonic crystal superballs with dual photonic band gaps. *Journal of Materials Chemistry C*, **2014**, *2(44)*: 9431-9438.

21. Yi F, Xu F, Gao Y, et al. Macrocellular polymer foams from water in oil high internal phase emulsion stabilized solely by polymer Janus nanoparticles: Preparation and their application as support for Pd catalyst. *RSC Advances*, **2015**, *5(50)*: 40227-40235.

22. Crossley S, Faria J, Shen M, et al. Solid nanoparticles that catalyze biofuel upgrade reactions at the water/oil interface. *Science*, **2010**, *327(5961)*: 68-72.

23. Yoshida M, Roh K H, Mandal S, et al. Structurally controlled bio-hybrid materials based on unidirectional association of anisotropic microparticles with human endothelial cells. *Advanced Materials*, **2009**, *21(48)*: 4920-4925.

24. Zhang L, Chen Y, Li Z, et al. Tailored Synthesis of Octopus-type Janus Nanoparticles for Synergistic Actively-Targeted and Chemo-Photothermal Therapy. *Angewandte Chemie International Edition*, **2016**, *55(6)*: 2118-2121.

25. Hu S H, Gao X. Nanocomposites with spatially separated functionalities for combined imaging and magnetoelastic therapy. *Journal of the American Chemical Society*, **2010**, *132(21)*: 7234-7237.

26. Fu X, Liu J, Yang H, et al. Arrays of Au–TiO2 Janus-like nanoparticles fabricated by block copolymer templates and their photocatalytic activity in the degradation of methylene blue. *Materials Chemistry and Physics*, **2011**, *130(1-2)*: 334-339.

27. Wang T, Chen S R, Jin F, et al. Droplet-assisted fabrication of colloidal crystals from flower-shaped porphyrin Janus particles. *Chemical Communications*, **2015**, *51(7)*: 1367-1370.

28. Berger S, Ionov L, Synytska A. Engineering of Ultra-Hydrophobic Functional Coatings Using Controlled Aggregation of Bicomponent Core/Shell Janus Particles. *Advanced Functional Materials*, **2011**, *21(12)*: 2338-2344.

29. Kirillova A, Ionov L, Roisman I V, et al. Hybrid hairy Janus particles for anti-icing and de-icing surfaces: Synergism of properties and effects. *Chemistry of Materials*, **2016**, *28(19)*: 6995-7005.

30. Kirillova A, Marschelke C, Friedrichs J, et al. Hybrid hairy Janus particles as building blocks for anti-biofouling surfaces. *ACS Applied Materials & Interfaces*, **2016**, *8(47)*: 32591-32603.

31. Van Meer G, Voelker D R, Feigenson G W. Membrane lipids: where they are and how they behave. *Nature reviews Molecular Cell Biology*, **2008**, *9(2)*: 112-124.

32. Wang M, Liu Z, Zhan W. Janus Liposomes: Gel-Assisted Formation and Bioaffinity-Directed Clustering. *Langmuir*, **2018**, *34(25)*: 7509-7518

33. Jesorka, Aldo, and Owe Orwar. "Liposomes: technologies and analytical applications." *Annu. Rev. Anal. Chem.* (**2008**): 801-832

34. Cross R. Without these lipid shells, there would be no mRNA vaccines for COVID-19. *Chem Eng News*, **2021**, *99(8)*: 144.

35. Tenchov R, Bird R, Curtze A E, et al. Lipid Nanoparticles─ From Liposomes to mRNA Vaccine Delivery, a Landscape of Research Diversity and Advancement. *ACS Nano*, **2021**, *15(11)*: 16982-17015.

36. Gross U, Roding J, Stanzl K, et al. Phospholipid-and fluorocarbon-containing cosmetic. *Journal of Fluorine Chemistry*, **1998**, *1(87)*: 125.

37. Genç R, Ortiz M, O'Sullivan C K. Diffusion-controlled synthesis of gold nanoparticles: nano-liposomes as mass transfer barrier. *Journal of Nanoparticle Research*, **2014**, *16(4)*: 1-5.

38. Gudlur S, Sandén C, Matoušková P, et al. Liposomes as nanoreactors for the photochemical synthesis of gold nanoparticles. *Journal of Colloid and Interface Science*, **2015**, *456*: 206-209.

39. Horger K S, Estes D J, Capone R, et al. Films of agarose enable the rapid formation of giant liposomes in solutions of physiologic ionic strength. *Journal of the American Chemical Society*, **2009**, *131(5)*: 1810-1819.

40. Weinberger A, Tsai F C, Koenderink G H, et al. Gel-assisted formation of giant unilamellar vesicles. *Biophysical Journal*, **2013**, *105(1)*: 154-164.

41. D'Onofrio T G, Hatzor A, Counterman A E, et al. Controlling and measuring the interdependence of local properties in biomembranes. *Langmuir*, **2003**, *19(5)*: 1618-1623.

42. Menger F M, Gabrielson K D. Cytomimetic organic chemistry: early developments. *Angewandte Chemie International Edition in English*, **1995**, *34(19)*: 2091-2106.

43. Kuribayashi K, Tresset G, Coquet P, et al. Electroformation of giant liposomes in microfluidic channels. *Measurement Science and Technology*, **2006**, *17(12)*: 3121.

44. Peterlin P, Arrigler V. Electroformation in a flow chamber with solution exchange as a means of preparation of flaccid giant vesicles. *Colloids and Surfaces B: Biointerfaces*, **2008**, *64(1)*: 77-87.

45. Estes D J, Mayer M. Electroformation of giant liposomes from spin-coated films of lipids. *Colloids and Surfaces B: Biointerfaces*, **2005**, *42(2)*: 115-123.

46. Menger F M, Seredyuk V A. Internally catalyzed separation of adhered lipid membranes. *Journal of the American Chemical Society*, **2003**, *125(39)*: 11800-11801.

47. Pautot S, Frisken B J, Weitz D A. Production of unilamellar vesicles using an inverted emulsion. *Langmuir*, **2003**, *19(7)*: 2870-2879.

48. Deshpande S, Caspi Y, Meijering A E C, et al. Octanol-assisted liposome assembly on the chip. *Nature Communications*, **2016**, *7*: 10447.

49. Pattni B S, Chupin V V, Torchilin V P. New developments in liposomal drug delivery. *Chemical Reviews*, **2015**, *115(19)*: 10938-10966.

50. Veatch S L, Keller S L. Separation of liquid phases in giant vesicles of ternary mixtures of phospholipids and cholesterol. *Biophysical Journal*, **2003**, *85(5)*: 3074-3083.

51. Veatch S L, Keller S L. Organization in lipid membranes containing cholesterol. *Physical Review Letters*, **2002**, *89(26)*: 268101.

52. Stottrup B L, Keller S L. Phase behavior of lipid monolayers containing DPPC and cholesterol analogs. *Biophysical Journal*, **2006**, *90(9)*: 3176-3183.

53. Xu X, London E. The effect of sterol structure on membrane lipid domains reveals how cholesterol can induce lipid domain formation. *Biochemistry*, **2000**, *39(5)*: 843-849.

54. Cho E C, Zhang Q, Xia Y. The effect of sedimentation and diffusion on cellular uptake of gold nanoparticles. *Nature Nanotechnology*, **2011**, *6(6)*: 385.

55. Yang Y, Wang J, Shigematsu H, et al. Self-assembly of size-controlled liposomes on DNA nano templates. *Nature Chemistry*, **2016**, *8(5)*: 476.

56. Holzer M, Barnert S, Momm J, et al. Preparative size exclusion chromatography combined with detergent removal as a versatile tool to prepare unilamellar and spherical liposomes of highly uniform size distribution. *Journal of Chromatography A*, **2009**, *1216(31)*: 5838-5848.

57. Mayer L D, Hope M J, Cullis P R. Vesicles of variable sizes produced by a rapid extrusion procedure. *Biochimica et Biophysica Acta (BBA)-Biomembranes*, **1986**, *858(1)*: 161-168.

58. Einstein A. Investigations on the Theory of the Brownian Movement. *Ann. D. Phys.*, **1905**, *17*: 549.

59. Mason T G, Ganesan K, Van Zanten J H, et al. Particle tracking microrheology of complex fluids. *Physical Review Letters*, **1997**, *79(17)*: 3282.

60. Moyses H, Palacci J, Savanna S, et al. Trochoidal trajectories of self-propelled Janus particles in a diverging laser beam. *Soft Matter*, **2016**, *12(30)*: 6357-6364.

61. Zhan W, Jiang K. A modular photocurrent generation system based on phospholipid-assembled fullerenes. *Langmuir*, **2008**, *24(23)*: 13258-13261.

62. Wang M, Chen J, Lian T, et al. Mimicking Photosynthesis with Supercomplexed Lipid Nanoassemblies: Design, Performance, and Enhancement Role of Cholesterol. *Langmuir*, **2016**, *32(29)*: 7326-7338.

63. Asard H, Horemans N, Caubergs R J. Involvement of ascorbic acid and ab-type cytochrome in plant plasma membrane redox reactions. *Protoplasma*, **1995**, *184(1-4)*: 36

64. Deshpande S, Dekker C. On-chip microfluidic production of cell-sized liposomes. *Nature Protocols*, **2018**, *13(5)*: 856-874.

65. Deng N N, Yelleswarapu M, Huck W T S. Monodisperse uni-and multicompartment liposomes. *Journal of the American Chemical Society*, **2016**, *138(24)*: 7584-7591.

66. Zhu C, Li Q, Dong M, et al. Giant Unilamellar vesicle microarrays for cell function study. *Analytical chemistry*, **2018**, *90(24)*: 14363-14367.

67. Liu Z, Cui J, Zhan W. Rapid Access to Giant Unilamellar Liposomes with Upper Size Control: Membrane-Gated, Gel-Assisted Lipid Hydration. *Langmuir*, **2020**, *36(44)*: 13193-13200.

68.Ruysschaert T, Marque A, Duteyrat J L, et al. Liposome retention in size exclusion chromatography. *BMC Biotechnology*, **2005**, *5(1)*: 1-13.

69. Grabielle-Madelmont C, Lesieur S, Ollivon M. Characterization of loaded liposomes by size exclusion chromatography. *Journal of biochemical and biophysical methods*, **2003**, *56(1-3)*: 189-217.

70. Volpe G, Buttinoni I, Vogt D, et al. Microswimmers in patterned environments. *Soft Matter*, **2011**, *7(19)*: 8810-8815.

71. Ismagilov R F, Schwartz A, Bowden N, et al. Autonomous movement and self-assembly. *Angewandte Chemie International Edition*, **2002**, *41(4)*: 652-654.

72. Howse J R, Jones R A L, Ryan A J, et al. Self-motile colloidal particles: from directed propulsion to random walk. *Physical Review Letters*, **2007**, *99(4)*: 048102.

73. Schattling P, Thingholm B, Stadler B. Enhanced diffusion of glucose-fueled Janus particles. *Chemistry of Materials*, **2015**, *27(21)*: 7412-7418.

74. Wang J, Gao W. Nano/microscale motors: biomedical opportunities and challenges. *ACS Nano*, **2012**, *6(7)*: 5745-5751.

75. Gao W, Wang J. Synthetic micro/nanomotors in drug delivery. *Nanoscale*, **2014**, *6(18)*: 10486-10494.

76. Gao W, Uygun A, Wang J. Hydrogen-bubble-propelled zinc-based micro rockets in strongly acidic media. *Journal of the American Chemical Society*, **2012**, *134(2)*: 897-900.

77. Wu Y, Wu Z, Lin X, et al. Autonomous movement of controllable assembled Janus capsule motors. *ACS Nano*, **2012**, *6(12)*: 10910-10916.

78. Wang H, Zhao G, Pumera M. Beyond platinum: Bubble-propelled micromotors based on Ag and MnO2 catalysts. *Journal of the American Chemical Society*, **2014**, *136(7)*: 2719-2722.

79. Wu Y, Dong R, Zhang Q, et al. Dye-enhanced self-electrophoretic propulsion of light-driven TiO 2–Au Janus micromotors. *Nano-Micro Letters*, **2017**, *9(3)*: 30.

80. Ebbens S J, Howse J R. Direct observation of the direction of motion for spherical catalytic swimmers. *Langmuir*, **2011**, *27(20)*: 12293-12296.

81. Volpe G, Buttinoni I, Vogt D, et al. Microswimmers in patterned environments. *Soft Matter*, *2011*, *7(19)*: 8810-8815.

82. Jiang H R, Yoshinaga N, Sano M. Active motion of a Janus particle by self-thermophoresis in a defocused laser beam. *Physical Review Letters*, **2010**, *105(26)*: 268302.

83. Luo M, Li S, Wan J, et al. Enhanced propulsion of urease-powered micromotors by the multilayered assembly of ureases on Janus magnetic microparticles. *Langmuir*, **2020**.

84. Molinero-Fernández Á, Arruza L, López M Á, et al. On-the-fly rapid immunoassay for neonatal sepsis diagnosis: C-reactive protein accurate determination using magnetic graphene-based micromotors. *Biosensors and Bioelectronics*, **2020**, *158*: 112156.

85. Baraban L, Makarov D, Schmidt O G, et al. Control over Janus micromotors by the strength of a magnetic field. *Nanoscale*, **2013**, *5(4)*: 1332-1336.

86. Wu J, Ma S, Li M, et al. Enzymatic/Magnetic Hybrid Micromotors for Synergistic Anticancer Therapy. *ACS Applied Materials & Interfaces*, **2021**, *13(27)*: 31514-31526.

87. Xiao Z, Duan S, Xu P, et al. Synergistic Speed Enhancement of an Electric-Photochemical Hybrid Micromotor by Tilt Rectification. *ACS nano*, **2020**, *14(7)*: 8658-8667.

88. Brown A, Poon W. Ionic effects in self-propelled Pt-coated Janus swimmers. *Soft Matter*, **2014**, *10(22)*: 4016-4027.

89. Xu T, Soto F, Gao W, et al. Ultrasound-modulated bubble propulsion of chemically powered micro engines. *Journal of the American Chemical Society*, **2014**, *136(24)*: 8552-8555.

90. Ebbens S, Gregory D A, Dunderdale G, et al. Electrokinetic effects in catalytic platinum-insulator Janus swimmers. *EPL (Europhysics Letters)*, **2014**, *106(5)*: 58003.

91. Dong R, Zhang Q, Gao W, et al. Highly efficient light-driven TiO2–Au Janus micromotors[J]. *ACS Nano*, **2016**, *10(1)*: 839-844.

92. Zhang Q, Dong R, Wu Y, et al. Light-driven Au-WO3@ C Janus micromotors for rapid photodegradation of dye pollutants. *ACS Applied Materials & Interfaces*, **2017**, *9(5)*: 4674-4683.

93. Dong R, Hu Y, Wu Y, et al. Visible-light-driven BiOI-based Janus micromotor in pure water. *Journal of the American Chemical Society*, **2017**, *139(5)*: 1722-1725.

94. Zhang J, Grzybowski B A, Granick S. Janus particle synthesis, assembly, and application. *Langmuir*, **2017**, *33(28)*: 6964-6977.

95. Wang J. Can man-made nanomachines compete with nature biomotors. *ACS Nano*, **2009**, *3(1)*: 4-9.

96. Sánchez S, Soler L, Katuri J. Chemically powered micro-and nanomotors. *Angewandte Chemie International Edition*, **2015**, *54(5)*: 1414-1444.

97. Wu Y, Wu Z, Lin X, et al. Autonomous movement of controllable assembled Janus capsule motors. *ACS Nano*, **2012**, *6(12)*: 10910-10916.

98. Sengupta S, Dey K K, Muddana H S, et al. Enzyme molecules as nanomotors. *Journal of the American Chemical Society*, **2013**, *135(4)*: 1406-1414.

99. García-Sáez A J, Schwille P. Single molecule techniques for the study of membrane proteins. *Applied Microbiology and Biotechnology*, **2007**, *76(2)*: 257-266

100. Shen H, Tauzin L J, Baiyasi R, et al. Single particle tracking: from theory to biophysical applications. *Chemical Reviews*, **2017**, *117(11)*: 7331-7376.

101. Qian H, Sheetz M P, Elson E L. Single particle tracking. Analysis of diffusion and flow in two-dimensional systems. *Biophys. J.* **1991,** *60(4):* 910-921

102. Jonkman J, Brown C M, Wright G D, et al. Tutorial: guidance for quantitative confocal microscopy. *Nature Protocols*, **2020**, *15(5)*: 1585-1611.

103. Tata B V R, Raj B. Confocal laser scanning microscopy: Applications in material science and technology. *Bulletin of Materials Science*, **1998**, *21(4)*: 263-278.

104. Frallicciardi J, Melcr J, Siginou P, et al. Membrane thickness, lipid phase, and sterol type are determining factors in the permeability of membranes to small solutes. *Nature Communications*, **2022**, *13(1)*: 1-12.

105. Gabba M, Frallicciardi J, van't Klooster J, et al. Weak acid permeation in synthetic lipid vesicles and across the yeast plasma membrane. *Biophysical Journal*, **2020**, *118(2)*: 422-434.

106. Lomize A L, Pogozheva I D. Physics-based method for modeling passive membrane permeability and translocation pathways of bioactive molecules. *Journal of Chemical Information and Modeling*, **2019**, *59(7)*: 3198-3213.

107. Lomize A L, Hage J M, Schnitzer K, et al. PerMM: A web tool and database for analysis of passive membrane permeability and translocation pathways of bioactive molecules. *Journal of Chemical Information and Modeling*, **2019**, *59(7)*: 3094-3099.

108. Mathai J C, Tristram-Nagle S, Nagle J F, et al. Structural determinants of water permeability through the lipid membrane. *The Journal of General Physiology*, **2008**, *131(1)*: 69-76.

109. Walter A, Gutknecht J. Permeability of small nonelectrolytes through lipid bilayer membranes. *The Journal of Membrane Biology*, **1986**, *90(3)*: 207-217.

110. Ghysels A, Krämer A, Venable R M, et al. Permeability of membranes in the liquid-ordered and liquid-disordered phases. *Nature Communications*, **2019**, *10(1)*: 1-12.

111. Mathai J C, Tristram-Nagle S, Nagle J F, et al. Structural determinants of water permeability through the lipid membrane. *The Journal of General Physiology*, **2008**, *131(1)*: 69-76

# CHAPTER 2. Enzymatic Janus Liposome Micromotors

## 2.1 Introduction

Artificial nano-/micromotors have attracted much research interest in recent years owing to their promise for advanced materials with built-in motility. Sophisticated functionality and exotic collective behavior, ranging from on-demand drug delivery, nanorobotics to active matter, have been envisioned.[1-3]As a class of water-dispersed, intrinsically biocompatible colloidal assemblies, liposomes have established diverse and widespread utility in both basic research (e.g., membrane biophysics,[4] protocells [5]and lubrication[6] and commercial (e.g., drug delivery,[7] food,[8] cosmetics[9] and immunoassays[10]) avenues; exploring their physicochemical characteristics and performance as artificial motors, therefore, bears significant fundamental as well as practical implications. Herein, we present a liposome-based micromotor system in which directional particle motion is realized through regionally-executed enzymatic gas production, which, to our knowledge, represents the first example of its kind.

Combining high efficiency/specificity of one with the broken symmetry of the other, enzyme-coated Janus particles provide an attractive approach to artificial motors. Among numerous enzymatic systems [11-15] being investigated, catalase and urease stand out for their effective gas ($O_2$ or $CO_2$) production from naturally-occurring, small-molecule substrates ($H_2O_2$ or urea), conveniently affording design schemes for gas-propelled artificial motors navigating in aqueous media. As for enzyme on-particle placement, conventional bioimmobilization methods (e.g., covalent conjugation and physical adsorption) coupled with various masking schemes have yielded reliable modification of individual inorganic/polymer nanoparticles.[16-18] Performance wise, these enzyme-attached Janus particles typically display enhanced diffusion[14,15] in the presence of

enzymatic substrates – a result from fast rotational diffusion randomizing their directional motion at this length scale.[19-20] Besides size and broken symmetry of Janus particles, other enzyme-associated properties, such as their loading, catalytic efficiency and stability, have also been shown to impact the mobility of these enzyme-powered motors.[11,21] How to maintain enzyme activity during the operation of these artificial motors, in particular, is considered as one of the major issues currently impeding their routine biomedical applications.[1][12][13]

With their minuscule, spherically-sealed lipid bilayer(s) fully immersed in water on both sides, liposomes represent an ideal colloidal platform for anchoring biomolecules while preserving their activity/stability.[22-24] Recognizing these attractive features, Cremer, Velegol, Sen and their coworkers recently investigated microscopic movement of several enzyme-carrying liposome systems.[25-26] Under parallel laminar flow conditions, nanosized liposomes coated with catalase and urease were found to undergo positive and negative chemotaxis, [25] respectively, when subjected to their substrate; in solution, liposomes embedded with ATPase were observed to perform enhanced diffusion in the presence of ATP. [26] Taking further advantage of liposome's encapsulation capability, Patiño, Maspoch, Sánchez and their coworkers developed liposome nanomotors with urease either coated on surface of or encapsulated within liposomes. [27] While the intact urease-encapsulated liposomes display no active motion with urea present outside, disrupting the liposome bilayer, combined with acidic treatments, led to a nearly one-fold mobility increase compared to background diffusion. These results clearly demonstrated the usefulness of liposomes in building enzyme-powered artificial motors.

In this work, we present what we believe the first example of Janus liposome-based, enzyme-powered artificial motor systems. Horseradish peroxidase (HRP), a gas-generating

enzyme, is selectively placed on phase-separated Janus liposomes, using domain-specific sorting of biotinylated lipids followed by enzyme conjugation via avidin/biotin binding. In the presence of HRP's substrate, $H_2O_2$, these HRP-decorated Janus liposomes undergo directional motion, yielding velocities up to three times greater than their thermal diffusion. By contrast, such enhanced mobility is absent from homogenous enzyme-decorated liposomes subjected to similar treatments. The motional characteristics of these enzyme-attached Janus liposome motors are compared with an enzyme-free liposome active motion system [28] we reported recently. Effects of other key experimental factors on liposome motion, including substrate distribution/concentration and liposome Janus ratio, are also examined in detail.

The main goal for this project was to construct enzyme-coated Janus liposome micromotors and place them into the substrate ($H_2O_2$) solution of the enzyme. We hypothesized the active motion of such micromotors could be achieved through regional catalysis reaction and gas generation on the membrane surface of liposomes. Different factors including substrate concentration and Janus ratio that possibly affect such kind of motion behavior of liposome-based micromotor were further investigated.

## 2.2 Experimental Section

### 2.2.1 Reagents and Materials

All lipids employed in this work, including 1,2-dipalmitoyl-sn-glycero-3-phosphocholine (DPPC), 1,2-dioleoyl-sn-glycero-3-phosphocholine (DOPC), 1,2-dioleoyl-sn-glycero-3-phosphoethanolamine-N-(biotinyl) (sodium salt) (biotin-DOPE), 1,2-dioleoyl-sn-glycero-3-phosphoethanolamine-N-(lissamine rhodamine B sulfonyl) (ammonium salt) (rho-DOPE), and 23-(dipyrromethene boron difluoride)-24-norcholesterol (Bodipy-chol), were products of Avanti Polar Lipids (Alabaster, AL). Other chemicals, including chloroform, poly(vinyl alcohol) (PVA, MW:

145 000), cholesterol, NeutrAvidin, and horseradish peroxidase (HRP) conjugated avidin were obtained from Sigma Aldrich. Alexa Fluor 488-conjugated avidin was obtained from Thermo Fisher Scientific. Hydrogen peroxide aqueous solutions (30 wt%) were from Macron Fine Chemicals; thermally curable poly(dimethylsiloxane) (PDMS) kits were from Dow Corning Co. Deionized (DI) water of 18.2 MΩ·cm (Millipore) was used throughout this work.

### 2.2.2 Janus Liposomes preparation procedure

Janus as well as homogeneous liposomes were prepared via gel-assisted hydration as detailed previously.[29] Briefly, dry PVA films were first prepared by spreading drops of a PVA aqueous solution (5 wt%) on precleaned glass slides, followed by drying on a 50 °C hotplate for 0.5 h. On such dry PVA films, lipid stacks were then deposited by spreading small quantities of lipid precursors followed by overnight vacuum drying at room temperature. All lipid precursors used in this work were prepared in chloroform with a total lipid concentration of 5 mM, and for liposome samples intended for enzyme conjugation, in addition contain 1 mol% biotin-DOPE. Unless otherwise specified, the lipid precursor also include 0.2 mol% Bodipy-Chol (for the $l_o$ phase) and rho-DOPE ($l_d$) each as lipid phase indicators. To yield liposomes, finally, such dried lipid films were hydrated in DI water at 45 °C for either 1 h (biotin-free samples) or 2 h (all samples containing biotin-DOPE). Liposomes thus prepared were stored at 4 °C for future use.

### 2.2.3 Protein/Liposome Conjugation

Enzyme surface conjugation on liposomes was accomplished via biotin/avidin binding and depending on the intended downstream usage, two forms of avidin were employed in this work. 1) Alexa Fluor 488-labeled avidin, which was used to fluorescently locate biotin-DOPE in Janus liposomes and determine the optimal avidin/biotin binding ratio in the present system. To facilitate binding, a desired volume of fluorescent-labeled avidin stock solution (0.5 $\mu$M in DI water) was pipetted into a 1-mL liposome solution with its final biotin-DOPE concentration held at ~25 nM. The resulting mixture was briefly vortexed and then incubated for 2 h in the dark at 4 °C. 2) HRP conjugated with avidin which was bound onto fresh and well-prepared Janus liposomes through avidin/biotin conjugation in which the optimized binding ratio was followed by the aforementioned Alexa Fluor 488-labeled avidin experiment condition. To facilitate binding, a desired volume of HRP conjugated avidin stock solution (0.5 $\mu$M in DI water) was pipetted into a 1-mL liposome solution with its final biotin-DOPE concentration held at ~25 nM. The resulting mixture was briefly vortexed and then incubated in the dark in the refrigerator for 1 h.

### 2.2.4 Microporous membrane extrusion of liposomes for size control

The size-controlled liposomes were prepared by extruding above-prepared hydration liposome samples one round through a plunger-based lipid extruder (Mini-Extruder, Avanti Polar Lipids) furnished with polycarbonate filter membranes containing track-etched pores of 5-μm nominal diameter (Whatman Nuclepore™, GE Healthcare). For enzyme-conjugated liposome samples, the extrusion step was performed after the enzyme/liposome conjugation (see next

section). The reported size of these liposomes was determined by the "Analyze Particles" function in ImageJ (version: 2.00-rc-69/1.52n).

### 2.2.5 Liposomes tracking measurement

Fluorescence images of liposomes and video recordings of liposome movement were acquired on a Nikon A1+/MP confocal scanning laser microscope (Nikon Instruments, Melville, NY) using 10x or 20x objectives and excitation laser lines at 488 and 561 nm; the corresponding emission filters are at 525±25 and 595±25 nm, respectively. Using this setup, we monitor liposome movement fluorescently in transparent linear microfluidic channels (dimensions: 200 μm x 200 μm x 18 mm; product model: thinXXS 100182, Cole-Parmer). To avoid channel wall-associated motion complications and ensure run-to-run consistency, only liposomes near the center of microchannels, i.e., ~100 μm away from the channel sides and floor/ceiling, are followed and recorded. Prior to fluorescence recording, each microchannel slide was thoroughly cleaned by sonication for 30 min each in methanol and then DI water; residual solvents were blow dried with nitrogen. Following that, dilute liposome samples suspended in either DI water or aqueous $H_2O_2$ solutions were pipetted into the microchannels and subsequently sealed off from the surrounding at the two inlets with parafilm. Fluorescence videos (in .avi) were typically recorded at 512x512 pixel resolution at 1 frame/s.

Trajectories of liposomes are obtained by analyzing particle movement fluorescence videos using TrackMate, an ImageJ plug-in for single-particle tracking and analysis. The trajectory files (in .xml) thus obtained were then imported into MATLAB to calculate the mean squared displacement (MSD) of particle movement following a published protocol.[43] To ensure data convergence, we typically analyze >500 liposomes for each sample to obtain the ensemble-averaged MSD plot.

### 2.2.6 Fluorescence Microscopy

Fluorescence images and motion videos of giant liposomes were acquired on a Nikon A1+/MP confocal scanning laser microscope (Nikon Instruments, Inc., Melville, NY) using 10× objective and excitation laser lines at 488 and 561 nm. The corresponding green and red emission signals were filtered at 525 ± 25 and 595 ± 25 nm. For each measurement, a 5−8 μL liposome solution was first pipetted into a Poly(dimethylsiloxane) microwell reversibly sealed to a precleaned microscope cover slide (Corning No. 1, 22 × 22 mm, Corning, NY) and then given 1 h to settle under 100% humidity.

## 2.3 Results and Discussion

### 2.3.1 Liposome Motor

A schematic drawing of essential components of our enzymatic liposome motors is shown in Figure 2.1. Composition wise, these liposomes contain mainly three lipids, DOPC/DPPC/cholesterol, in 35/35/30 mole ratio, which together yield a liquid-disordered ($l_d$) lipid domain phase-separated from a liquid-ordered ($l_o$) half within individual liposomes at room temperature, i.e., Janus liposomes.[29] These liposomes are additionally doped with three minor components: fluorescent $l_d$($l_o$) phase indicator, rho-DOPE (Bodipy-Chol), both at 0.2 %, and biotin-DOPE typically held at 1%. The latter is employed to anchor enzymes on the liposome surface through biotin/avidin binding. Importantly, since biotin-DOPE can be prepared to reside in the $l_d$ domain nearly exclusively (see below), the enzyme to be anchored, HRP, will only decorate the outer surface associated with the $l_d$ hemisphere of a liposome upon affinity binding. In the presence of their substrate ($H_2O_2$), accordingly, these regionally-arranged enzymes will generate oxygen primarily near the $l_d$ hemisphere of the host liposome, propelling the latter forward.

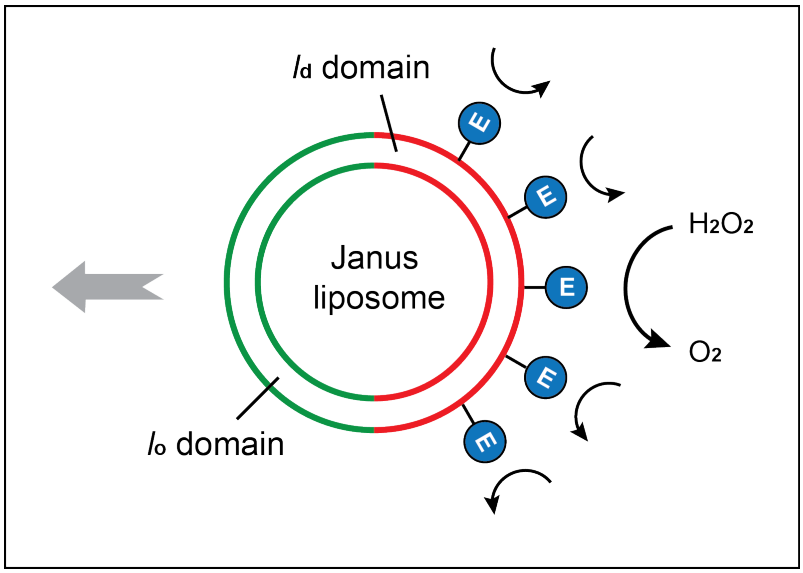


Figure 2.1. Design of enzymatic Janus liposome micromotors. The double circles indicate the lipid bilayer of the liposome, whereas its Janus configuration is denoted by green/red colors. Enzymes (E), such as horseradish hydrogen peroxidase (HRP) investigated here, are conjugated to the outer surface of the $l_d$ domain of Janus liposomes via biotin/avidin binding. The substrate of HRP, hydrogen peroxide ($H_2O_2$), is present both inside and outside Janus liposomes during their movement.

### 2.3.2 Liposome Motor Assembly and Characterization

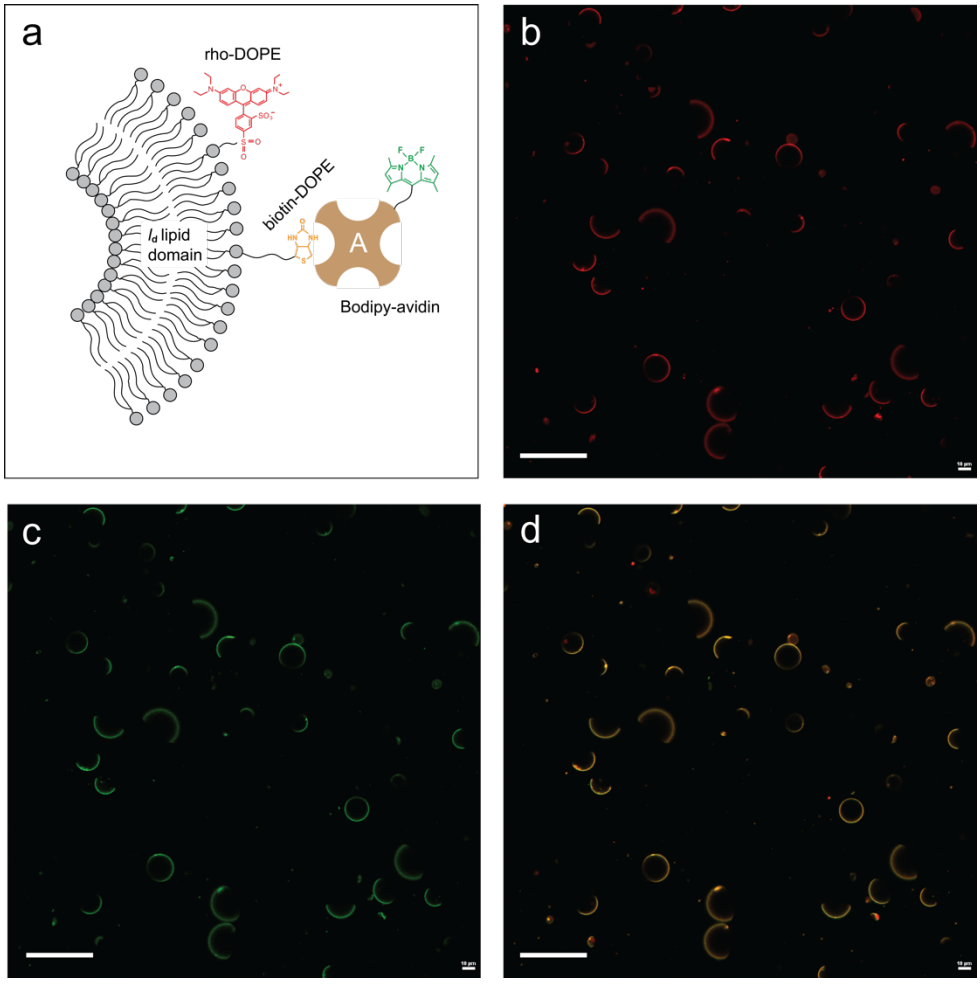


Figure 2.2 Fluorescence microscopic characterization of biotin-DOPE localization in DPPC/DOPC/cholesterol Janus liposomes. a) Cartoon depiction of fluorescently monitoring liposome ld domain (shown in part) with rho-DOPE and biotin-DOPE via Bodipy-labeled avidin. b) Red-channel (rho-DOPE) fluorescence micrograph revealing the $l_d$-domain of Janus liposomes. c) Green fluorescence image showing avidin location of the same liposome sample. The level of avidin is controlled to be roughly 1:5 relative to available biotin-DOPE (see the Experimental Section). d) Merged fluorescence image of b) and c). Scale bar: 50 $\mu$m.

It thus takes two steps to construct such liposome motors: 1) sorting biotin-DOPE into the $l_d$-domain of Janus liposomes, followed by 2) enzyme attachment thereabout via biotin/avidin binding. To maximize gas production, one generally prefers high biotin-DOPE loading in

liposomes (step 1), which, however, could disrupt the lipid organization/phase equilibrium pre-established by DOPC/DPPC/Chol if unchecked. Similarly, the subsequent biotin/avidin-HRP binding (step 2) may introduce additional perturbance to liposomes due to multivalent nature of such binding.

To identify optimal assembling conditions, we examined $l_d$-labeled Janus liposomes subjected to a series of biotin-DOPE doping levels and avidin mixing ratios. As shown in Figure 2.1, biotin-DOPE at 1% doping level remains largely $l_d$-associated in Janus liposomes, consistent with our previous observation. [29] Assuming an even split between $l_d$ and $l_o$ domains, such exclusive association of biotin-DOPE doubles its effective concentration in the $l_d$ domain to 2%. When such biotinylated Janus liposomes were incubated externally with avidin at 5:1 (with biotin in excess to minimize free avidin in solution) mixing ratio, moreover, a fairly even coat of avidin on the $l_d$-hemisphere was obtained (Figure 2c). Higher mixing ratios, for example, 5:1.5 or 5:2, were found to yield denser avidin layers under similar incubation conditions, which, however, were accompanied frequently by liposome morphology changes (e.g., disrupted domains and dotted formations on liposome surfaces) as well as liposome aggregation (as Figure S1). To ensure good enzyme coverage while maintaining integrity/entity of individual Janus liposomes, we thus chose 1% biotin-DOPE 5:1 bound to avidin-HRP to build our liposome motors.

### 2.3.3 Liposome Size Control

In order to be able to quantitatively assess liposome active motion resulted from enzymatic gas production, the passive component of liposome movement, i.e., thermal diffusion, must also be accounted for. According to Stokes-Einstein equation, $D = kT/6\pi\eta r$, where $kT$ is the thermal energy, $\eta$ viscosity of the medium and r radius of the particle, the extent of diffusion of a spherical particle scales inversely proportionally to its size.

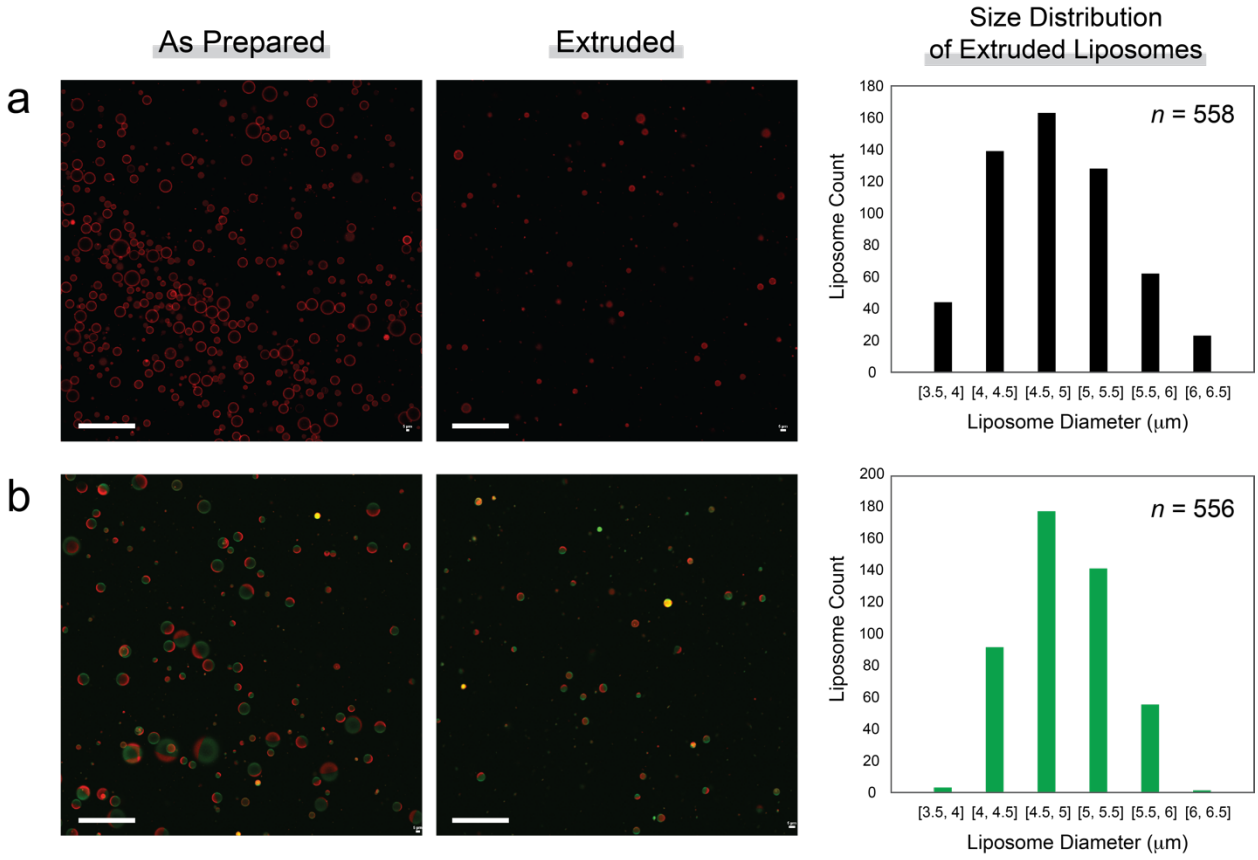


Figure 2.3 Fluorescence images of liposomes before/after size control via extrusion and their size distribution. a) Homogenous DOPC/Chol (70/30, mole ratio) liposomes doped in addition with 0.1% rho-DOPE. b) DPPC/DOPC/Chol (35/35/30) Janus liposomes containing also 0.1% Bodipy-Chol and rho-DOPE each. Liposome counts are reported in 0.5-μm size groups. Scale bar: 50 μm.

To keep liposome diffusion at a relatively constant level, we thus sought to control their size using membrane extrusion (Experimental Section). As shown in Figure 3, liposome samples as prepared display a wide range of sizes, which, upon extrusion through 5-$\mu$m-diameter porous membranes, can be effectively narrowed down to be around 5 $\mu$m. For Janus liposomes, importantly, the Janus configuration in the end product appears to be relatively unaffected after such hydraulic treatment. It is possible to prepare smaller liposomes by extrusion employing membranes with finer pores, which, however, makes it challenging to reliably discern the two domains in Janus liposomes. What need to be mentioned here, the size histogram distribution data present here is different from the measurement data in some degree because the software Image J excluded the smaller liposomes (less then 3.5 $\mu$m )out automatically in the analysis process.

### 2.3.4 Substrate ($H_2O_2$) Distribution in the System

With all lipid constituents dynamically assembled into a bilayer-enclosed architecture, liposomes differ fundamentally from their inorganic/polymer counterparts for building motors. Their structural thinness and softness, first and foremost, directly impact their mechanical stability and hence the integrity of resultant motors. This is especially the case for microsized liposomes studied here, in which microscopic membrane undulations are largely decoupled with nanoscopic bending from individual lipids and thus respond freely to surface tension and other environmental agitations.[30-32] If, for example, a species with limited permeability to the liposome bilayer is only present on one side of the liposome, a concentration gradient would result across the bilayer. This, in turn, will produce an osmotic pressure that can be too great for the liposome to withstand – a detrimental outcome for its intended application.

To determine whether $H_2O_2$ poses any osmotic shock to liposomes investigated here, we next monitored liposome samples subjected to a sudden $H_2O_2$ concentration jump in the surroundings. As shown in Figure 4, Janus liposomes upon exposure to ~80 mM $H_2O_2$ were able to maintain not only their phase-separated morphology, but, to a great extent, also their size.

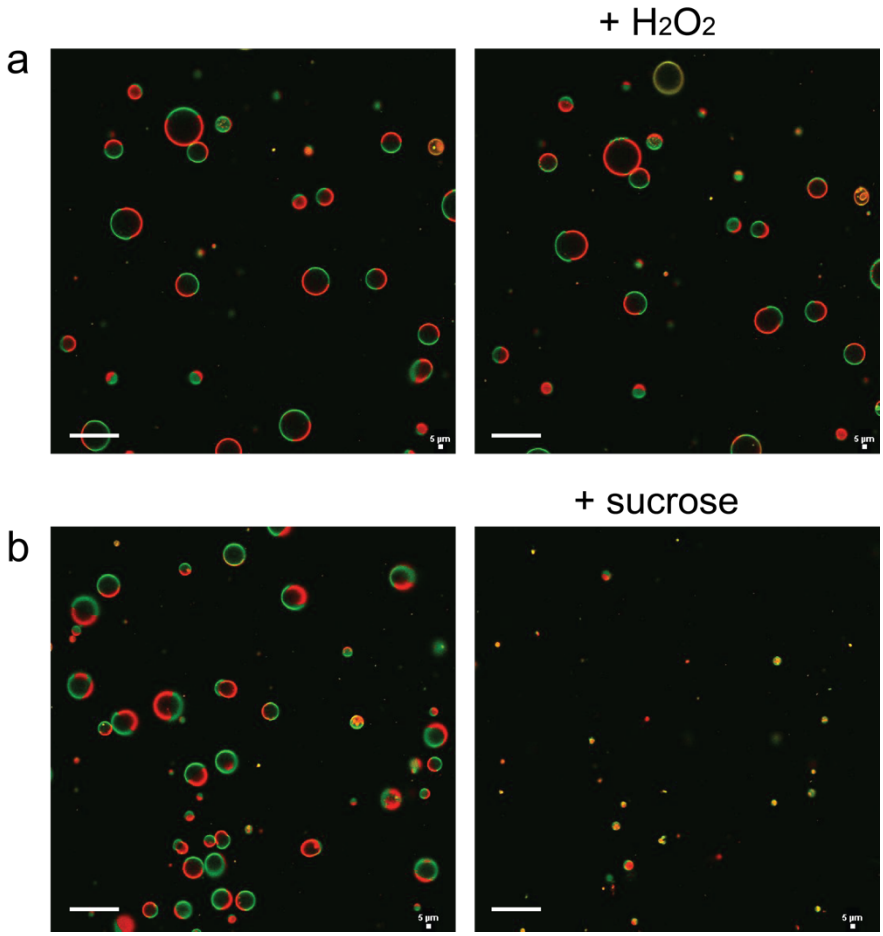


Figure 2.4 fast permeation/equilibration of H2O2 across the lipid bilayer of Janus liposomes. a) Fluorescence snapshots of Janus liposomes before/after being treated with H2O2. The effective H2O2 concentration upon homogenization is ~80 mM. b) Fluorescence snapshot of Janus liposomes samples before/after being similarly treated with ~24 mM sucrose. Same liposome sample (DPPC/DOPC/Chol, 35/35/30, with 0.1% Bodipy-Chol and rho-DOPE) was employed; in both cases, the two frames are taken a few seconds apart. Scale bar: 50 $\mu$m.

Similar observations were also obtained from homogeneous DOPC liposomes (data not shown). These results thus suggest that $H_2O_2$ readily permeates and equilibrates across DOPC/DPPC/Chol bilayers, at least on the second (s) timescale if not much faster.[33] Permeability coefficients of $H_2O_2$ across $l_d$ and $l_o$ lipid bilayers became available just recently, with the former measured to be at 1 x $10^{-3}$ cm/s level for DOPC/POPG/Chol liposomes. [34] For reference, this value is roughly an order of magnitude greater than water permeation across Chol-mixed lipid membranes, [35] whereas oxygen, the product of $H_2O_2$ enzymatic breakdown, permeates much more facilely (on the order of 1 x $10^2$ cm/s).[3 Also included in Figure 2.4 are control measurements of Janus liposomes similarly treated with sucrose instead. Owing to its high water-solubility and low lipid permeability, sucrose is frequently employed as an osmolyte to enforce osmotic imbalance across lipid membranes.[37] Its hydrogen-bonding capability and high density (relative to water alone), in addition, are quite useful in liposome preparation and sedimentation.[22][38] According to van 't Hoff equation, $\Delta\Pi = \Delta ckT$, where $\Delta c$ is the concentration gradient and $\Delta\Pi$ the resultant osmotic pressure, 24 mM sucrose introduced externally would exert an osmotic pressure of nearly 60 kPa across the liposome bilayers. The resulting force, in turn, squeezes and crushes the liposome all around, quickly shrinking the latter into a much smaller particle with crumpled and intermixed lipid domains (Figure 4b).

### 2.3.5 Enzymatic Gas-Driven Motion of Janus Liposomes

With background diffusion properly controlled and substrate distribution in the system known, we next investigated liposome movement trajectories and speed under various conditions. In each case, we perform mean square displacement (MSD) analysis on >500 liposome trajectories to obtain a robust, ensemble-averaged displacement plot (Experimental Section). As shown in

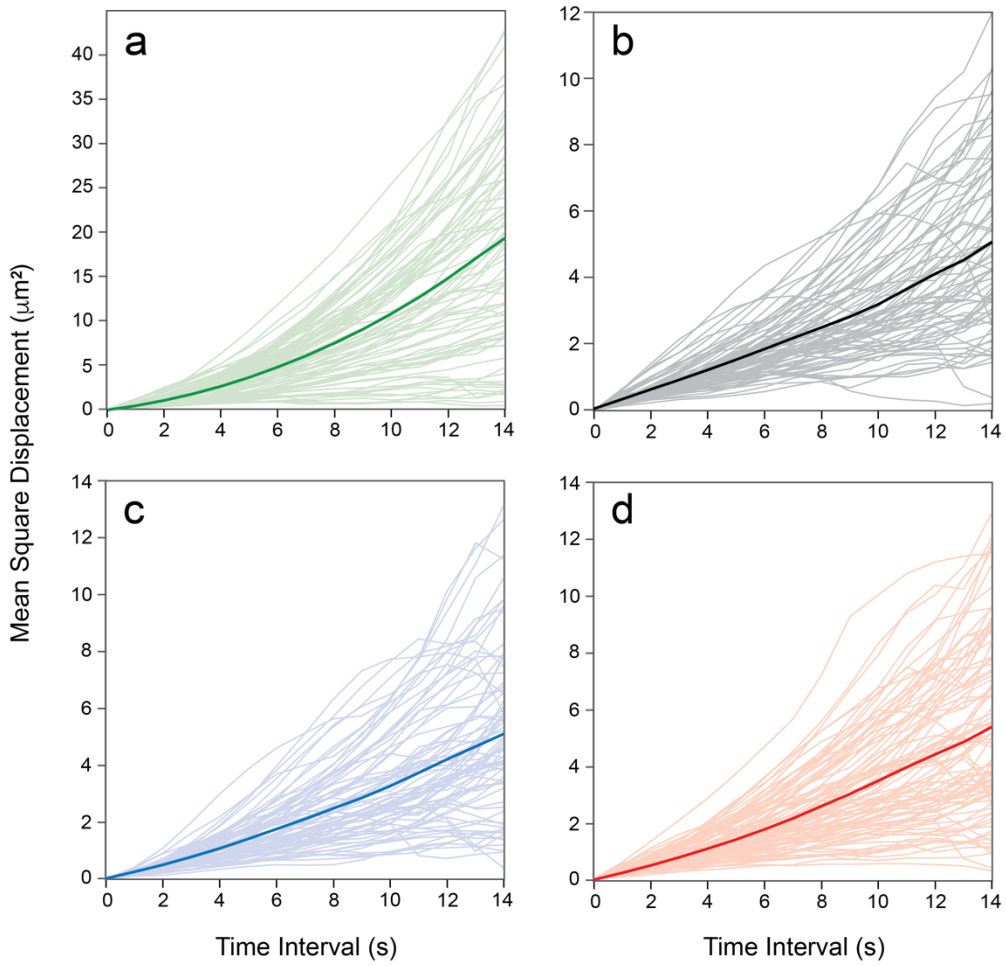


Figure 2.5. Mean square displacement (MSD) plots of Janus liposome movement under either enzymatic conversion or control conditions. In each case, the light-color traces in the background represent MSD plots averaged from all particles sampled in individual fluorescence videos, whereas the thick colored line is the ensemble-averaged MSD plot of all particles. a) MSD plots of HRP-$l_d$-attached Janus liposomes in the presence of 1 wt% $H_2O_2$. Liposome composition: 35/35/30 DOPC/DPPC/Chol with additional 1% biotin-DOPE; average liposome size: ~4.5 $\mu$m, n = 638. b) MSD plots of HRP-$l_d$-attached Janus liposomes in water alone. n = 559. c) MSD plots of HRP-free Janus liposomes in the presence of 1 wt% $H_2O_2$. . n = 494. d) MSD plots of HRP-coated homogeneous liposomes in the presence of 1 wt% $H_2O_2$. Liposome composition: 70/30 DOPC/Chol with additional 1% biotin-DOPE; n = 585.

Figure 2.5a, HRP-$l_d$-attached Janus liposomes in the presence of $H_2O_2$ collectively yield an upward-bending MSD plot, indicative of presence of active motion component in the system that is superimposed with background diffusion. When either the enzyme or its substrate is taken out

of the system, in contrast, only sublinear MSD plots characteristic of diffusion-dominant motion[19,20] were obtained (Figure 5b,c). These negative controls thus point to enzymatic gas production as the driving force of liposome active motion. Furthermore, when homogeneous DOPC liposomes were used as motor construct in place of Janus liposomes (while keeping both HRP and $H_2O_2$ in the system), only background-level displacements were observed (Figure 5d). This result stresses once again the importance of particle asymmetry in achieving liposome active motion: [28] interfacial reactivity (i.e., gas generation), a necessary condition for particle propulsion, can fall insufficient if it gets canceled out around the particle due to latter's spherical symmetry.

Fitting the ensemble-averaged MSD plot in Figure 5a into to the diffusion-with-flow model,[19][39] $MSD(t) = v_0^2t^2 + 4Dt$, we then obtained the active motion velocity ($v_0$) and translational diffusivity (D), 2.7 x $10^{-1}$ $\mu$m $s^{-1}$ and 8.6 x $10^{-2}$ $\mu m^2$ $s^{-1}$, of the system being tested. Treating the three negative controls as diffusion-only cases, we in turn estimated their diffusivity: 8.7 x $10^{-2}$ $\mu m^2$ $s^{-1}$ (substrate-free), 9.4 x $10^{-2}$ $\mu m^2$ $s^{-1}$ (enzyme-free), 9.7 x $10^{-2}$ $\mu m^2$ $s^{-1}$ (homogeneous liposomes), respectively, following MSD(t) = 4Dt. These MSD-derived diffusivity values are in general agreement with that predicted (1.0 x $10^{-1}$ $\mu m^2$ $s^{-1}$) by the Stokes-Einstein equation for spherical particles of 4.5-$\mu$m diameter. Using the same liposome size, we further obtained Péclet number (Pe) [19] of 14.1 associated with the active case, from $Pe = 2rv_0/D$, which denotes the magnitude of active motion component relative to diffusion.

Different levels of liposome movement among these samples are also evident from examining representative trajectories of individual liposomes (Figure 6). While particles in control groups typically display clustered trajectories featuring short stepwise displacements over the 15-s monitoring window, liposomes undergoing active motion tend to produce more extended traces. Closer examination further reveals that the majority of these active liposomes (45%) move in a

directional fashion, in that the particle tends to move along the direction defined by the initial orientation of its $l_d$(rear) and $l_o$(front) domains (Figure 6d). Due to thermal randomization and liposome rotational motion, trajectories that display overall sideway as well as backward movement were also found, which occur at lower frequencies.

### 2.3.6 Effect of $H_2O_2$ Concentration on Liposome Active Motion

Since liposome active motion is propelled by enzymatic gas generation, the extent of which is directly proportional to the substrate concentration, we next examined movement of HRP-coated Janus liposomes under different $H_2O_2$ concentrations. As shown in Figure 7, a small enhancement in liposome motion became appreciable in the presence of 0.01% $H_2O_2$ (~1 mM). As the concentration increases, the resultant MSD plots tick upward accordingly. The extent of increase, however, appears to level out toward higher concentrations, which may be due to substrate saturation.

In terms of enzymatic action, HRP first binds $H_2O_2$ with 1:1 stoichiometry to produce a highly oxidizing precursor, which, upon encountering and oxidizing two equivalents of a reductant ($AH_2$), regenerates the enzyme together with water as a coproduct as follows.[40]

$$HRP + H_2O_2 \longrightarrow HRP{\bullet}H_2O_2 \qquad 1)$$

$$HRP{\bullet}H_2O_2 + 2AH_2 \longrightarrow HRP + 2AH^{\bullet} + H_2O \qquad 2a)$$

In this sequence, therefore, $H_2O_2$ acts as an oxidant. When no reductant substrates are present in the system, alternatively, $H_2O_2$ will fill in as the reductant in the second step: [41,42]

$$HRP{\bullet}H_2O_2 + 2H_2O_2 \longrightarrow HRP + O_2 + 2H_2O \qquad 2b)$$

In this case, therefore, HRP behaves analogously to catalase, converting $H_2O_2$ to release oxygen and water. It is thus this alternative pathway by which our liposome motor operates. Kinetically,

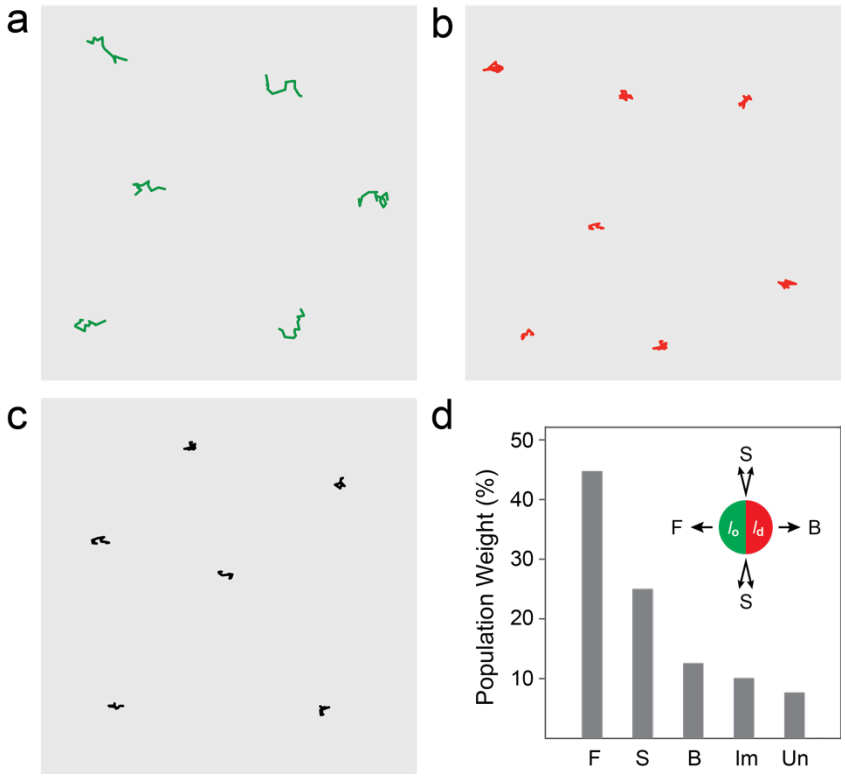


Figure 2.6. Trajectories of liposome movement under enzymatic conversion conditions and their direction relative to the initial orientation of Janus liposomes. a) Representative trajectories of HRP-$l_d$-attached Janus liposomes in the presence of 1 wt% $H_2O_2$. Liposome composition: 35/35/30 DOPC/DPPC/Chol with additional 1% biotin-DOPE; average liposome size: ~4.5 $\mu$m. b) Representative trajectories of HRP-free Janus liposomes in the presence of 1 wt% $H_2O_2$. c) Representative trajectories of HRP-attached homogenous DOPC/Chol liposomes in 1 wt% $H_2O_2$. In each case, a gray box of 200x200 $\mu$m is given as size reference. d) Trajectory development vs. Janus liposome initial orientation of sample in a): forward (F, with liposome's $l_o$ domain as the front), backward (B), sideway (S), immobile (I) and undetermined (Un) particles; n = 555.

the initial HRP/$H_2O_2$ binding proceeds quite facilely ($k = 2 \times 10^7$ $M^{-1}$ $s^{-1}$), whereas an apparent rate constant of ~1.8 $s^{-1}$ was determined directly from oxygen production for the catalase-like pathway.[41] In these steady-state, solution-based measurements, the speed of oxygen production was found to increase with higher $H_2O_2$ concentrations, reaching saturation at about 40 mM. [42] Physiologically, this pathway has been proposed as a defense mechanism for plants in response to $H_2O_2$ burst during pathogenic attack.

### 2.3.7 Effect of Janus Ratio on Activity of Janus Liposome Micromotors

A unique feature associated with phase-separated Janus liposomes is their tunable $l_d$-to-$l_o$ area ratio, i.e., Janus ratio, which is accessible through control of lipid composition as long as it operates within the liquid-liquid coexistence region defined by the lipid phase diagram.[29] Previously, we have shown that Janus ratio of DOPC/DPPC/Chol Janus liposomes can be tuned by nearly an order of magnitude through adjusting the mixing ratio of the three components.[29] Since the relative size of $l_d$ domain directly defines the active, enzyme-coated portion of Janus liposomes, we next examined whether different Janus ratios directly impact mobility of resultant motors.

As shown in Figure S2, MSD plots obtained from $l_d$-major (DOPC/DPPC/Chol: 50/30/20; Janus ratio: ~3:1) and $l_d$-minor (20/50/30; ~1:3) Janus liposomes appear closely comparable, both slightly less active than domain-even-split samples (35/35/30). Such closeness in particle displacement may result from the same doping level (1%) of biotin-DOPE in all three samples, which would accommodate same load of enzymes with different surface densities. Assuming comparable gas production per particle among the three samples, furthermore, geometry considerations favor liposome motors with 1:1 Janus ratio: While propulsion only exerts on a small portion of the particle in $l_d$-minor liposomes, gas production past the liposome equator, as the case for $l_d$-major samples, can lead to partial cancelation of propulsion. In line with the observed results, this interpretation should be taken with caution, however. Several other complicating factors, such as variations in liposome size, Janus ratio (within the same population) as well as secondary modifications caused by extrusion, may as well even out their differences in motion that would otherwise be present.Comparison of Different Types of Janus Liposome Micromotors. Recently, we reported another liposome motor system based on asymmetrical lipid efflux.[28] As Janus

liposomes of similar lipid composition and size were employed in both studies, we now move on to a direct comparison of the two in this last section.

Due to fundamentally different mechanisms involved, several distinctive characteristics can be identified between the two systems. 1) Driving force. The present enzymatic system is based on gas generation/propulsion, whereas the other employs lipid extraction/efflux. In both cases, liposome asymmetry is found to be essential to achieve particle directional motion; 2) Fuel location/availability. The present system uses $H_2O_2$ as fuel, which is homogeneously present in the system. By contrast, the other system uses cholesterol, which is present only the liposome bilayer; 3) Active motion direction. In our enzyme-based system, liposomes move predominantly in the $l_d$-to-$l_o$ direction; whereas the opposite is true for the other system; 4) Identity/impact of effectuator(s). In both cases, the level of fuel present in the system is found to impact liposome active motion directly and significantly. Of the reaction partner to the fuel, the effect of enzyme loading remains to be explored; whereas the level (but not type) of extracting agents was found to be insignificant in the concentration range tested for the other system; 5) Effect of Janus ratio. While Janus ratio is found to be largely unimpactful here, nearly one-fold difference in liposome mobility was observed in the other study.

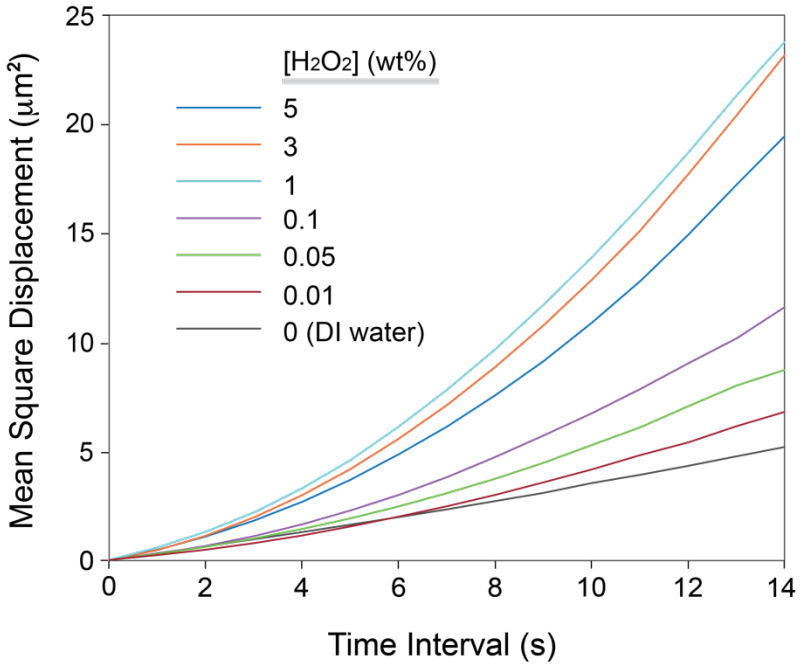


Figure 2.7. Effect of H2O2 concentration on Janus liposome movement under enzymatic conversion conditions. In each case, HRP-$l_d$-attached Janus liposomes consisting 35/35/30 DOPC/DPPC/Chol and 1% biotin-DOPE were used; average liposome size: ~4.5 $\mu$m. The $H_2O_2$ concentration was varied from 0 to 5 wt%.

### 2.3.8 Motion behavior test for catalase-bound Janus liposomes in the hydrogen peroxide solution

In order to further confirm and improve the motion speed of our size controlled enzyme based Janus liposomes, we tested a high efficient and high turned over number to hydrogen peroxide enzyme, catalase, bound onto the hemisphere membrane of Janus liposomes. In this process, it takes two steps reaction for catalase (obtained from NANOCS) binding onto the Janus liposomes because the catalase enzyme is biotin conjugated commercial available. The bound procedure is described in the aforementioned experimental section in detail. Once acquired the well-prepared catalase bound Janus liposomes solution with size controlled, we just repeat the previous classic single particle tracking (SPT) method which can provide dynamic information for different kind

of micro/nano-particles motion behavior in bulk solution. To facilitate the data more representative, we explored the motion behavior of catalase bound Janus liposomes in 1% $H_2O_2$ solution in a linear microfluidic channel. The total mean square displacement (MSD) data for these catalase bound Janus liposomes (~500) in 1% $H_2O_2$ and control groups were displayed in figure 2.8 below. From the MSD data comparison, we could clearly find that the motion speed of biotin bound Janus liposomes was obvious improved about three folds compared with the three control groups. In this process, the propulsion force for the active motion behavior of these biotin bound Janus liposomes was from the hydrogen catalysis reaction and oxygen bubble production on one hemisphere of the membrane. The combine mean MSD plots for motion behavior test of catalase bound Janus liposomes in 1% $H_2O_2$ with three control groups was displayed in figure 2.9. Considering the high

catalysis efficiency of catalase enzyme to $H_2O_2$ compared with horseradish peroxidase (HRP), we

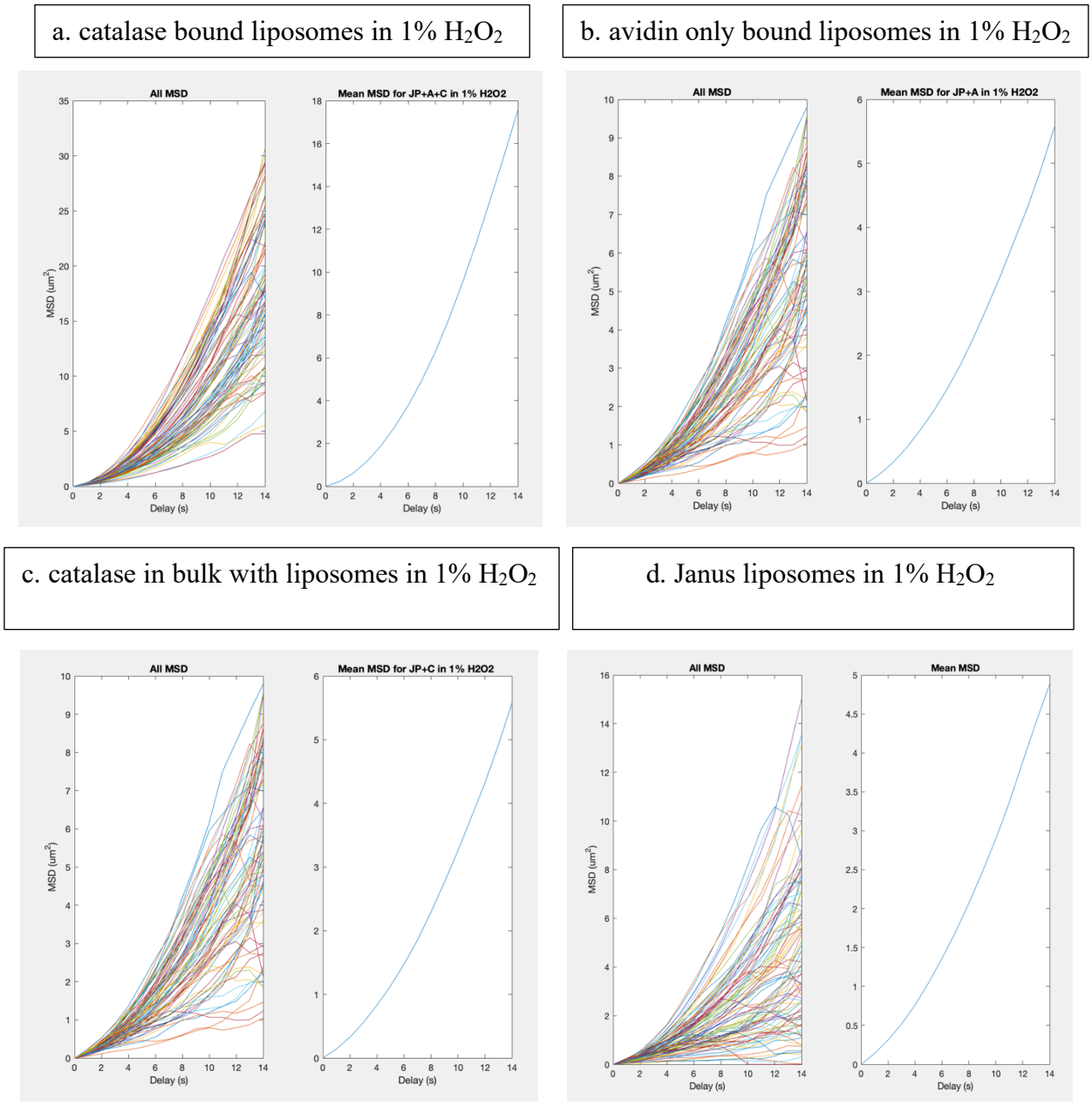


Figure 2.8. Total mean square displacement (MSD) analysis catalase bound Janus liposomes (~500) in 1% H2O2 and three control groups. a. total MSD for catalase bound liposomes in 1% $H_2O_2$; b. total MSD for avidin bound only on Janus liposomes in 1% $H_2O_2$; c. total MSD for catalase in bulk with liposomes in 1% $H_2O_2$; d. total MSD for Janus liposomes in 1% $H_2O_2$

expected the much faster motion behavior of catalase bound Janus liposomes then HRP bound Janus liposomes in 1% $H_2O_2$. While the mean MSD results of catalase bound Janus liposomes displayed a lower motion speed compared with the HRP bound one in figure 2.15. This unexpected result was possibly due to large size of catalase enzyme which could hinder the oxygen bubble leaving from the nearby surface or the longer space arms of biotin-to-avidin-to-biotin conjugation on the membrane surface of Janus liposomes. With the detail systematically study for the active motion behavior of these two enzyme (HRP and Catalase ) bound Janus liposomes in 1% $H_2O_2$ ,

| a. combined MSD for catalase bound liposomes in 1% $H_2O_2$ with controls | b. Mean MSD for catalase bound liposomes vs HRP bound liposomes |
|---|---|

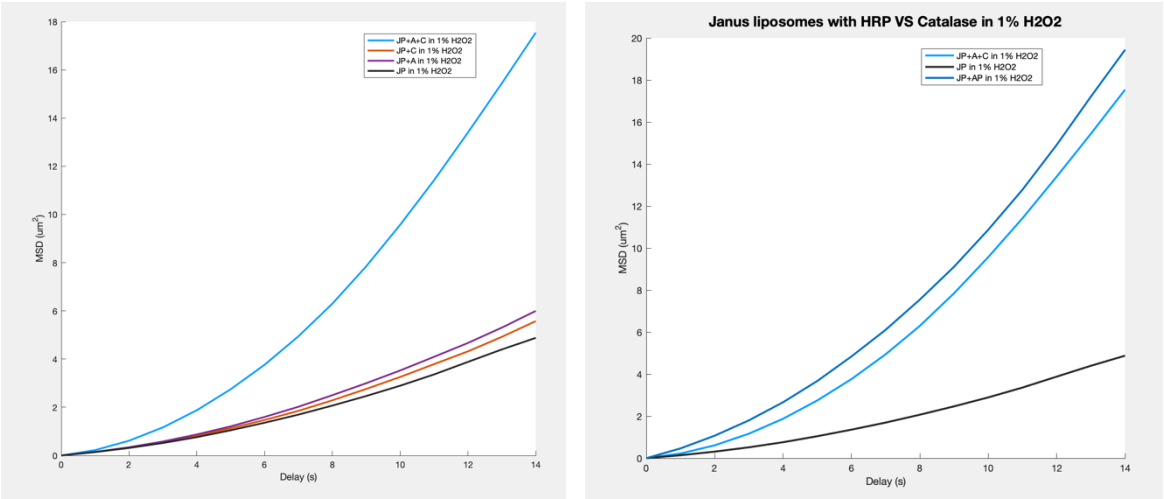


Figure 2.9. Mean MSD data for catalase bound Janus liposomes in 1% H2O2. a. combined MSD for catalase bound liposomes in 1% H2O2 with control groups: Janus liposomes with catalase in bulk in 1% $H_2O_2$, Janus liposomes with avidin only in 1% $H_2O_2$, Janus liposomes in 1% $H_2O_2$ respectively. b. Mean MSD for catalase bound liposomes vs HRP bound liposomes;

we first explored the propulsion of the enzyme based soft Janus liposomes which makes the directional motion of these Janus liposomes being possible. These results could offer valuable guidance for researchers interested in the liposomes based drug delivery test.

### 2.3.9 Conclusions

We present in this work the first Janus liposome-based micromotor system propelled by regional enzymatic conversion and gas generation. A general strategy for local placement of enzymes is laid out, utilizing domain-specific lipid sorting together with biotin/avidin affinity binding, which can be readily extended to many other water-soluble enzymes to build new liposome micromotors and study other types of asymmetrical lipid-assembled, enzyme-attached colloids. In relation to our recent work [28] on liposome active motion using lipid efflux, this study stresses once gain the importance of particle asymmetry in achieving directional motion and in addition, displays several distinctive features. Sorting out how these features can be controlled and their effects maximized, through fine chemical/structural control of Janus liposomes, is one area on which our ongoing investigation is focused.

## 2.4 Reference


1. Sánchez, S.; Soler, L.; Katuri, J. Chemically Powered Micro- and Nanomotors. *Angew. Chem. Int. Ed.* **2015**, *54*, 1414-1444.

2. Zhang, J.; Luijten, E.; Grzybowski, B. A.; Granick, S. Active Colloids with Collective Mobility Status and Research Opportunities. *Chem. Soc. Rev.* **2017**, *46*, 5551-5569.

3. Wang, L.; Song, S.; van Hest, J.; Abdelsohsen, L. K. E. A.; Huang, X.; Sánchez, S. Biomimicry of Cellular Motility and Communication Based on Synthetic Soft-Architectures. *Small* **2020**, *16*, 1907680.

4. Menger, F. M.; Keiper, J. S. Chemistry and Physics of Giant Vesicle as Biomembrane Models. *Curr. Opin. Chem. Biol.* **1998**, *2*, 726-732.

5. Trantidou, T.; Friddin, M.; Elani, Y.; Brooks, N. J.; Law, R. V.; Seddon, J. M.; Ces, O. Engineering Compartmentalized Biomimetic Micro- and Nanocontainers. *ACS Nano* **2017**, *11*, 6549-6565.

6. Goldberg, R.; Klein, J. Liposomes as Lubricants: Beyond Drug Delivery. *Chem. Phys. Lipids* **2012**, *165*, 374-381.

7. Chang, H.-I.; Yeh, M.-K. Clinical Development of Liposome-Based Drugs: Formulation, Characterization, and Therapeutic Efficacy. Int. J. *Nanomedicine* **2012**, *7*, 49-60.

8. Shahidi, F.; Han, X.-Q. Encapsulation of Food Ingredients. *Crit. Rev. Food Sci. Nutr.* **1993**, *33*, 501-547.

9. Betz, G.; Aeppli, A.; Menshutina, N.; Leunenberger, H. In Vivo Comparison of Various Liposome Formulations for Cosmetic Application. *Int. J. Pharm.* **2005**, *296*, 44-54.

10. Rongen, H. A. H.; Bult, A.; van Bennekom, W. P. Liposomes and Immunoassays. J. *Immunol. Methods* **1997**, *204*, 105-133.

11. Patiño, T.; Arqué, X.; Mestre, R.; Palacios, L.; Sánchez, S. Fundamental Aspects of Enzyme-Powered Micro- and Nanoswimmers. *Acc. Chem. Res.* **2018**, *51*, 2662-2671.

12. Mathesh, M.; Sun, J.; Wilson, D. A. Enzyme Catalysis Powered Micro/Nanomotors for Biomedical Applications. J. *Mater. Chem. B* **2020**, *8*, 7319-7334.

13. Safdar, M.; Khan, S. U.; Jänis, J. Progress toward Catalytic Micro- and Nanomotors for Biomedical and Environmental Applications. *Adv. Mater.* **2018**, *30*, 1703660.

14. Ma, X.; Jannasch, A.; Albrecht, U.-R.; Hahn, K.; Miguel-López, A.; Schäffer, E.; Sánchez, S. Enzyme-Powered Hollow Mesoporous Janus Nanomotors. *Nano Lett.* **2015**, *15*, 7043-7050.

15. Dey, K. K.; Zhao, X.; Tansi, B. M. Méndez-Ortiz, W. J.; Córdova-Figueroa, U. M.; Golestanian, R.; Sen, A. Micromotors Powered by Enzyme Catalysis. *Nano Lett.* **2015**, *15*, 8311-8315.

16. Jiang, S.; Chen, Q.; Tripathy, M.; Luijten, E.; Schweizer, K. S.; Granick, S. Janus Particle Synthesis and Assembly. *Adv. Mater.* **2010**, *22*, 1060-1071.

17. Loget, G.; Kuhn, A. Bulk Synthesis of Janus Objects and Asymmetric Patchy Particles. J. *Mater. Chem.* **2012**, *22*, 15457-15474.

18. Walther, A.; Muller, A. H. E. Janus Particles: Synthesis, Self-Assembly, Physical Properties, and Applications. *Chem. Rev.* **2013**, *113*, 5194-5261.

19. Zöttl, A.; Stark, H. Emergent Behavior in Active Colloids. *J. Phys.: Condense. Matter* **2016**, *28*, 253001.

20. Moran, J. L.; Posner, J. D. Phoretic Self-Propulsion. *Annu. Rev. Fluid Mech.* **2017**, *49*, 511-540.

21. Patiño, T.; Feiner-Gracia, N.; Arqué, X.; Miguel-López, A.; Jannasch, A.; Stumpp, T.; Schäffer, E.; Albertazzi, L.; Sánchez, S. Influence of Enzyme Quantity and Distribution on the Self-Propulsion of Non-Janus Urease-Powered Micromotors. *J. Am. Chem. Soc.* **2018**, *140*, 7896-7903.

22. Szoka, Jr. F.; Papahadjopoulos, D. Comparative Properties and Methods of Preparation of Lipid Vesicles (Liposomes). *Ann. Rev. Biophys. Bioeng.* **1980**, *9*, 467-508.

23. New, R. R. C. Liposome: A Practical Approach. Oxford University Press: Oxford, UK, 1990.

24. Fouladi, F.; Steffen, K. J.; Mallik, S. Enzyme-Responsive Liposomes for the Delivery of Anticancer Drugs. *Bioconjugate Chem.* **2017**, *28*, 857-868.

25. Somasundar, A.; Ghosh, S.; Mohajerani, F.; Massenburg, L. N.; Yang, T.; Cremer, P. S.; Velegol, D.; Sen, A. Positive and Negative Chemotaxis of Enzyme-Coated Liposome Motors. *Nat. Nanotech.* **2019**, *14*, 1129-1134.

26. Ghosh, S.; Mohajerani, F.; Son, S.; Velegol, D.; Butler, P. J.; Sen, A. Motility of Enzyme-Powered Vesicles. *Nano Lett.* **2019**, *19*, 6019-6026.

27. Hortelão, A. C.; García-Jimeno, S.; Cano-Sarabia, M.; Patiño, T.; Maspoch, D.; Sánchez, S. LipoBots: Using Liposomal Vesicles as Protective Shell of Urease-Based Nanomotors. *Adv. Funct. Mater.* **2020**, *30*, 2002767.

28. Cui, J.; Jin, H.; Zhan, W. Enzyme-Free Active Liposome Motion via Asymmetrical Lipid Efflux. *Langmuir* **2022**, *38*, 11468-11477.

29. Wang, M.; Liu, Z.; Zhan, W. Janus Liposomes: Gel-Assisted Formation and Bioaffinity-Directed Clustering. *Langmuir* **2018**, *34*, 7509-7518.

30. Seifert, U. Configurations of Fluid Membranes and Vesicles. *Adv. Phys.* **1997**, *46*,13-137.

31. Israelachvili, J. N. Intermolecular and Surface Forces, 3rd Ed. Elsevier Inc. The Netherlands, **2011**.

32. Deserno, M. Fluid Lipid Membranes: From Differential Geometry to Curvature Stresses. *Chem. Phys. Lipids* **2015**, *185*, 11-45.

33. The time resolution of our measurements here is limited both instrumentally (1 frame/s recording speed) and by $H_2O_2$ diffusion. Also see the Experimental Section.

34. Orrico, F.; Lopez, A. C.; Saliwonczyk, D.; Acosta, C.; Rodriguez-Grecco, I.; Mouro-Chanteloup, I.; Ostuni, M. A.; Denicola, A.; Thomson, L.; Möller, M. N. The Permeability of Human Red Blood Cell Membranes to Hydrogen Peroxide Is Independent of Aquaporins. *J. Biol. Chem.* **2022**, *298*, 101503.

35. Ghysels, A.; Krämer, A.; Venable, R. M.; Teague, W. E. Jr; Lyman, E.; Gawrisch, K.; Pastor, R. W. Permeability of Membranes in the Liquid Ordered and Liquid Disordered Phases. *Nat. Commun.* **2019**, *10*, 5616.

36. Subczynski, W. K.; Hyde, J. S.; Kusumi, A. Oxygen Permeability of Phosphatidylcholine-Cholesterol Membranes. *Proc. Natl. Acad. Sci. USA* **1989**, *86*, 4474-4478.

37. White, G. F.; Racher, K. I.; Lipski, A.; Hallett, F. R.; Wood, J. M. Physical Properties of Liposomes and Proteoliposomes Prepared from Escherichia coli Polar Lipids. *Biochim. Biophys. Acta* **2000**, *1468*, 175-186.

38. Motta, I.; Gohlke, A.; Adrien, V.; Li, F.; Gardavot, H.; Rothman, J. E.; Pincet, F. Formation of Giant Unilamellar Proteo-Liposomes by Osmotic Shock. *Langmuir* **2015**, *31*, 7091-7099.

39. Qian, H.; Sheetz, M. P.; Elson, E. L. Single Particle Tracking. Analysis of Diffusion and Flow in Two-Dimensional Systems. *Biophys. J.* **1991**, *60*, 910-921.

40. Dunford, H. B.; Stillman, J. S. On the Function and Mechanism of Action of Peroxidases. Coord. *Chem. Rev.* **1976**, *19*, 187-251.

41. Hernández-Ruiz, J.; Arnao, M. B.; Hiner, A. N. P.; García-Cánovas, F.; Acosta, M. Catalase-like Activity of Horseradish Peroxidase: Relationship to Enzyme Inactivation by $H_2O_2$. *Biochem. J.* **2001**, *354*, 107-114.

42. Arnao, M. B.; Acosta, M.; del Río, J. A.; Varón, R.; García-Cánovas, F.; A Kinetic Study on the Suicide Inactivation of Peroxidase by Hydrogen Peroxide. *Biochim. Biophys. Acta* **1990**, *1041*, 43-47.

43. Tinevez, J.-T.; Perry, N.; Schindelin, J.; Hoopes, G. M.; Reynolds, G. D.; Laplantine, E.; Bednarek, S. Y.; Shorte, S. L.; Eliceiri, K. W. TrackMate: *An Open and Extensible Platform for Single-Particle Tracking*. *Methods* **2017**, *115*, 80-90.

# CHAPTER 3. Enzyme-Free Liposome Active Motion Driven by Asymmetrical Lipid Efflux

## 3.1 Introduction

Inspired by the elegance of natural microswimmers and enabled by recent advancement in material synthesis and microfabrication, research in microscopic artificial motors has blossomed into a field of extensive activity in recent years [1-3]. Such pursuit has been truly multidisciplinary, with chemists, engineers and physicists often working side-by-side on the preparation, characterization and theoretical formulation of these motors. Among the vast material and design choices being explored, spherical micromotors stand out for their simple geometry (with it, well-understood hydrodynamics) and ease of fabrication, and thus have been essential to what the field has become today. With Janus particles prepared from oxide/polymer microbeads with partial metal coatings alone, for example, researchers have discovered several suitable mechanisms for building such motors, exploiting chemical catalytic [4-6], photothermal [7-9] and photocatalytic processes [10-11] of various metals. In the majority of these cases, a local gradient across the particle/fluid interface drives the motion, whereas the broken symmetry of the particle imparts direction [12-14]. With motion as a built-in feature along with their small size, these artificial motors promise exciting new application possibilities, including targeted drug delivery and microrobotics. To this end, however, the potential biotoxicity of these materials and their clearance from biological hosts often stand as significant issues to be contemplated with [1, 3, 15].

As a closed spherical lipid assembly rich in surface/interfacial characteristics, liposomes represent an important class of water-dispersed colloids. Compared to their inorganic/polymer counterparts, from which the vast majority of existing nano- and micromotors are made, liposomes

are ultimately economical in formation (i.e., all constituents surface bound and no hard/solid core) and biocompatible (i.e., few toxic effects or clearance issues). These attractive features account for much of the industrial and medical use of liposomes [16], e.g., in food [17], drug delivery [18]and cosmetics[19]. With added motility, particularly when furnished in a controlled and environmentally responsive manner, these liposome carriers will have much to gain in functionality and effectiveness.

Only a handful of studies have been reported using liposomes to achieve directional/active motion, however. Taking a biohybrid approach, Kurakazu and coworkers attached flagella of Chlamydomonas, a biflagellate unicellular alga, to microsized liposomes, which display enhanced diffusion in the presence of ATP [20]. Similarly, Vanderlick et al. used E. coli to drive liposomes of different sizes [21]. Interestingly, while the bacterial transporter succeeded in propelling liposomes of 0.2- to 2-μm diameter (with velocities in tens μm/s), only Brownian motion observed with larger liposomes (10 to 20-μm). Working with enzyme-coated liposomes with diameter on the order of 100 nm, researchers at Penn State have recently demonstrated enhanced (up to 25%) diffusion [22] as well as positive/negative chemotaxis [23] of liposomes in the presence of enzyme substrates. As functional auxiliaries, liposomes have also been incorporated into artificial micromotor systems recently. For example, Städler et al. showed that the disintegration of liposomes coated on 0.8-μm silica beads could propel the latter along a gradient of lipid-dissolving agents [24]. All these studies, noticeably, are based on symmetrical liposomes with homogeneous surface makeup. On the use of Janus liposomes to achieve active/directional motion, only a couple of reports have appeared so far. In the first, Inaba and coworkers demonstrated light-induced liposome propulsion using photocleavable peptides [25]. In our own work, we showed recently that dipolar (+/–) Janus liposomes undergo directional, domain orientation-specific motion driven

either by an external electric field or interparticle electrostatic interactions [26]. These results point directly to the broken symmetry in Janus liposomes as an additional degree of freedom in manipulating liposome motion.

In this work, we investigate how interfacial lipid release from liposomes impacts their hydrodynamic behavior and demonstrate liposome active motion under asymmetrical efflux conditions. Structurally, such asymmetry is realized via cholesterol-modulated liquid/liquid lipid phase separation within individual liposomes, yielding Janus colloidal particles with two distinctive domains. Adding β-cyclodextrin (β-CD), a cholesterol-extracting agent [27, 28], at low-mM levels to the aqueous bulk then triggers cholesterol release from these Janus liposomes, which occurs at one domain an order of magnitude faster than the other. This asymmetrical material outflow, in turn, drives directional liposome movement against their Brownian diffusion. We further show how the active motion is correlated with liposome asymmetry and cholesterol extraction, the latter a surface-limited process sustained by continuous inter-domain cholesterol transfer. We explore various experimental parameters as well as mechanical details responsible for such motion. This work thus reveals a uniquely distinctive design principle based entirely on the intrinsic physicochemical properties of lipid assemblies to achieve active motion.

The main goal for this project was trying to build up an enzyme-free system of liposome micromotors. We hypothesized that the active motion of such enzyme-free based liposomes was achieved through cholesterol extraction from the membrane bilayer with the extracting agent, β-cyclodextrin. In this process, we expected that both the Janus configuration of liposomes and the concentration of extracting reagent would affect the motion behavior most. What's more, we also hypothesize that the motion was directional in some extent.

## 3.2 Materials and Methods

### 3.2.1 Liposomes Preparation

Janus as well as homogeneous liposomes were prepared by following the gel-assisted hydration method by Marques et al. [80] with minor modifications [33]. Briefly, dry poly(vinyl alcohol) (PVA, MW: 145,000, Sigma-Aldrich) films were first prepared by spreading drops of a PVA aqueous solution (5 wt%) on precleaned glass slides, followed by drying at 50°C for 0.5 h. On such dry PVA films, lipid stacks were then deposited by spreading small quantities of lipid precursors (e.g., 5 μL at 1 mM total lipids dissolved in chloroform) followed by further drying under vacuum for overnight at room temperature. In the final step, such dried lipid films were hydrated in DI water at 45°C to yield liposomes. Depending on lipid composition, the hydration time varies: 1h for homogeneous DPPC/Chol and DOPC/Chol liposomes; 2h for DPPC/DOPC/Chol and DPPC/DPhPC/Chol Janus liposomes. The exact lipid compositions are specified in the main text. For the purpose of fluorescence microscopy, lipid-conjugated indicator dyes, 23-(dipyrromethene boron difluoride)-24-norcholesterol (Bodipy-Chol, Avanti Polar Lipids) and/or 1,2-dioleoyl-sn-glycero-3-phosphoethanolamine-N-(lissamine rhodamine B sulfonyl) (ammonium salt) (Rho-DOPE, Avanti Polar Lipids), were also included in the liposome formation at 0.2 mol%. Thus prepared liposomes were stored at 4 °C for future use.

The size-controlled liposomes were prepared by extruding above-prepared hydration liposome samples through a plunger-based lipid extruder (Mini-Extruder, Avanti Polar Lipids) furnished by polycarbonate filter membranes with 5-μm diameter pores (Whatman Nuclepore™, GE Healthcare). The reported size of these liposomes was determined by the "Analyze Particles" function in ImageJ (version: 2.00-rc-69/1.52n).

### 3.2.2 Liposome Movement Tracking

Fluorescence images and videos of liposomes were acquired on a Nikon A1+/MP confocal scanning laser microscope (Nikon Instruments, Melville, NY) using 10x or 20x objectives and excitation laser lines at 488 and 561 nm. The corresponding green and red emission signals were filtered at 525±25 and 595±25 nm, respectively. For fluorescence recording, microscope-compatible, linear microfluidic channel slides (thinXXS 100182; dimensions: 200 μm x 200 μm x 18 mm; Cole-Parmer) were used as reservoirs to hold liposome samples. To avoid channel wall-associated motion complications and ensure run-to-run consistency, only particles near the center of microchannels, i.e., ~100 μm away from the sides and above from the channel floor/ceiling, are monitored and recorded. Before each measurement, these microchannel slides were thoroughly cleaned by sonication for 30 min each in methanol and then DI water; residual solvents were blow dried with a nitrogen stream. For PS bead and liposome diffusion measurements, dilute liposome samples in DI water were first pipetted into the microchannels. To achieve fluid quiescence, the liposome solution in the microchannel was sealed off from the surrounding at the two inlets with parafilm. For liposome active motion measurement, dilute liposome samples in DI water were first mixed with cyclodextrin aqueous solutions of desired concentration, which were immediately injected into the microchannel, sealed and secured on the stage of the fluorescence microscope. The whole procedure from sample mixing to the start of video recording is typically controlled under 2 min. Fluorescence videos were then recorded at 512x512 pixel resolution at 1 frame/s.

### 3.2.3. Particle Trajectory Analysis

Monodisperse green fluorescent PS microbeads (diameters: 0.5±0.03, 1.0±0.05 and 2.0±0.2 $\mu$m, Bangs Laboratories) were used to verify tracking accuracy of this procedure. Trajectories of

polystyrene (PS) beads and liposomes are obtained by analyzing particle movement videos recorded with the fluorescence microscope using TrackMate, a single-particle tracking tool embedded in ImageJ. The trajectory files thus obtained were then imported into MATLAB to calculate the mean squared displacement of particle movement following a published protocol (37).

## 3.3 Results and Discussion

### 3.3.1 Liposome Motor Design and Tracking

The Janus configuration in individual liposomes is achieved through lipid phase separation in ternary lipid systems [29-31] consisted of a high-melting component (e.g., DPPC, melting temperature, $T_m$: 41 °C), a low-melting one (e.g., DOPC, $T_m$: −17 °C) and cholesterol (Chol), which yields a liquid-ordered ($l_o$) hemispherical bilayer domain and a liquid-disordered ($l_d$) half sharing a circular, quasi-1D phase boundary at room temperature. Compositionally, the $l_o$ domain is enriched with DPPC/Chol and the $l_d$ domain with DOPC [32]. By varying their mixing ratio at the stage of liposome formation, in addition, we can modify the relative size of the two domains in the end products [33]. To make these liposomes fluorescently accessible, we add low levels of rhodamine-labeled DOPE (rho-DOPE) and(/or) Bodipy-labeled cholesterol (Bodipy-chol) in the lipid precursors. Of the two, rho-DOPE resides almost exclusively in the $l_d$ domain [34], whereas Bodipy-chol is distributed in both domains with $l_o$-phase enrichment proportional to Chol [35, 36]. Dilute suspensions (i.e., with volumetric fractions <0.01%) of thus-labelled liposomes are loaded in transparent microchannel reservoirs, and their movement is then followed and recorded by a confocal fluorescence microscope (Fig. 1A).

Upon addition of β-CD into the system, selective inclusion binding of Chol inside the former's cavity triggers a global Chol extraction from Janus liposomes. As detailed below, this

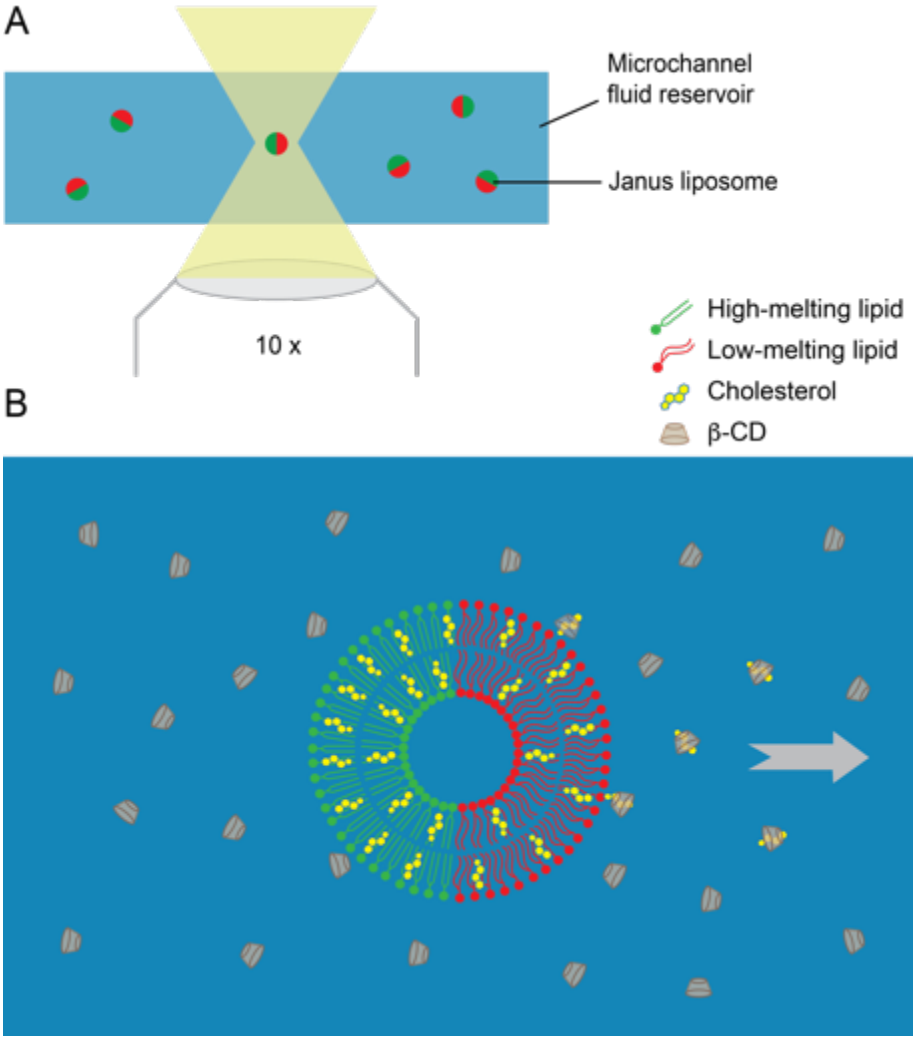


Figure.3 1 (A) Experimental setup for detection of liposome movement. (B) Schematic illustration of liposome micromotor design, which features Janus liposomes comprised of a high-melting lipid, a low-melting lipid and cholesterol (Chol), together with β-CD, a Chol-extracting agent. Arrow indicates the predominant liposome movement direction.

interfacial material release takes place predominantly via the $l_d$ domain, and, the resultant anisotropic traffic about the liposome causes the latter to move toward the extraction front against

their Brownian diffusion (Fig. 1B). When either liposome asymmetry or Chol extraction is absent from the system, such directional motion ceases to occur. In the following sections, we present experimental evidence to confirm this new mode of active motion, and analytically establish correlations between the extraction kinetics and active motion speed and finally, discuss the processes/factors responsible to such motion.

### 3.3.2. Particle Trajectory Analysis Procedure and Benchmarking

To assess liposome movement quantitatively, we perform mean-square-displacement (MSD) analysis on individual liposomes using TrackMate, an open-source single-particle tracking program[37]. In 2D, this time-dependent quantity is expressed as: $MSD(t) = \langle (x_{i+n} - x_i)^2 + (y_{i+n} - y_i)^2 \rangle$, where $x_{i+n}$ and $y_{i+n}$ denote coordinates of the particle's new location after time interval, n, whereas $x_i$ and $y_i$ represent its initial position. For spherical particles performing random walk only [38, 39], i.e., 2D diffusion, the ensemble-averaged MSD is related to their translational diffusion coefficient, D, by the linear relationship: $MSD(t) = 4Dt$. In case that there exist additional motional components in the system besides diffusion, the MSD plots obtained tend to deviate from linearity [39, 40]. Due to the stochastic nature of thermal agitation, time-to-time and run-to-run fluctuations in MSD naturally occur even for the same-sized particles being tracked. To uncover particle motion characteristics against such thermal randomness sufficiently accurately, it is thus necessary to sample sizeable populations of liposomes so robust statistical analysis may be ensured. In our hands, we find that such data convergence in standard microbeads when more than 200 particles are sampled (SI Appendix, Fig. S1). A similar trend has been observed by others [41]. For our liposome samples that are more polydisperse than the particle standards, we typically track and analyze 450-500 particles throughout this investigation.

To test the effectiveness of our tracking procedure, we first studied the movement of fluorescent polystyrene (PS) microbeads (diameters: 0.5±0.03, 1.0±0.05 and 2.0±0.2 μm) suspended in water. In each case, we obtained a linear ensemble-averaged MSD plot (SI Appendix, Fig. S2), indicative of pure Brownian diffusion. From the slope of these MSD plots, we then derived their diffusion coefficients (Fig. 2A-C), which are in good agreement with values predicted independently by Stokes-Einstein equation, $D = kT/6\eta r$, where kT is the thermal energy term (4.07 x $10^{-14}$ $cm^2$ g $s^{-2}$ at 22 °C), η viscosity of the medium (9.54 x $10^{-3}$ g $cm^{-1}$ $s^{-1}$ for water at 22 °C) and r radius of the particle: 2.26 x $10^{-9}$ $cm^2$ $s^{-1}$ (2.0 μm), 4.53 x $10^{-9}$ $cm^2$ $s^{-1}$ (1.0 μm), and 9.06 x $10^{-9}$ $cm^2$ $s^{-1}$ (0.5 μm). These are uniformly greater than the MSD-derived values by 5-7%, which may be attributable to tracking inaccuracy, bead size distribution as well as slight fluctuations in temperature and viscosity.

### 3.3.3. Janus Liposomes Execute Active Motion Under Cholesterol Extraction Conditions

To test the feasibility of exploiting lipid efflux for active liposome motion, we next examined liposome movement in the presence of β-CD. Owing to their high extraction efficiency and two-way binding dynamics, β-CD and its derivatives are widely employed in manipulating and controlling Chol level both in artificial and cellular lipid membranes [42-44]. Administered at relatively low (mM) levels, moreover, such extraction is Chol specific, with other coexisting lipid components such as phospholipids remain largely intact during the process [45-47].

As shown in Fig. 3A (traces in green and red), the MSD plots obtained from homogenous DPPC/Chol and DOPC/Chol liposomes remain largely linear in the presence of 2.0 mM β-CD. Their MSD-derived diffusion coefficients, 9.2 x $10^{-2}$ $\mu m^2$ $s^{-1}$ (DPPC/Chol) and 9.3 x $10^{-2}$ $\mu m^2$ $s^{-1}$ (DOPC/Chol), compare closely to those obtained in pure water. Strikingly, for Janus liposomes

subjected to similar treatment, the resultant MSD plot displays greater stepwise displacements that yield an overall upward-bending profile (Fig. 3a, blue trace), indicating the presence of active motion in the system aside from diffusion [39, 40]. A very similar trend is also observed when we extend the test to another Janus liposome system based on diphytanoylphosphatidylcholine (DPhPC) together with DPPC and Chol (Fig. 3a, black trace). The motional difference between homogenous and Janus liposomes is also evident from individual particle trajectories recorded (Fig. 3A, inset). Since Chol extraction is expected to proceed similarly on homogeneous liposomes vs. their corresponding domains on Janus liposomes (more below), the active motion observed most likely originates from the broken symmetry, i.e., the opposing $l_d/l_o$ domains, associated with the latter.

Fitting these plots according to the two-component model [12, 39], $MSD(t) = v_0^2t^2 + 4Dt$, we further obtained the active motion velocity ($v_0$) and diffusivity (D) of the two Janus systems: 1.9 x $10^{-1}$ μm $s^{-1}$ and 1.5 x $10^{-1}$ $\mu m^2$ $s^{-1}$ (DPPC/DOPC/Chol); 2.0 x $10^{-1}$ μm $s^{-1}$ and 1.6 x $10^{-1}$ $\mu m^2$ $s^{-1}$ (DPPC/DPhPC/Chol), respectively. Of the former, the calculated diffusivity is ~50% greater than that obtained in pure water, suggesting that diffusion is coupled with and enhanced by the active motion[12, 13] in the present case. From these values, we also calculated Péclet number (Pe) associated with the active motion by $Pe = 2rv_0/D$: 6.2 (DPPC/DOPC/Chol) and 6.5 (DPPC/DPhPC/Chol). A dimensionless quantity, Pe characterizes the relative contribution of active vs. diffusive components to overall particle movement, with $Pe \gg 1$ if active motion dominates in the system and $Pe \ll 1$ when it is negligible. Thus, our Janus liposome system, as the way it is being measured, yields an intermediate case in which the active component is greater than but not dominant over diffusion. Notice that, due to time needed for solution mixing and injection (Experimental Section), we have to miss the initial stage of the extraction for particle tracking

when the Chol efflux is the highest. Otherwise, we expect to see more prominent liposome active motion.

A close examination of individual trajectories obtained from DPPC/DOPC/Chol Janus liposomes in addition reveals a direct correlation between the liposome trajectory placement and their initial domain orientation. Here, three out of four liposomes have their trajectories developed in front of their $l_d$ domain (Fig. 3B). Expanding this analysis to the entire population, we find similar correlation in >50% of the particles, more than twice the liposomes displaying trajectories toward the opposite direction, 24%; in addition to these two groups, 22% liposomes being monitored move sideways (Fig. 3C).

A related factor to consider here is liposome's rotational motion, which as thermal noise randomizes liposome orientation. For 5-μm-diameter liposomes, we estimate their rotational diffusion coefficient ($D_r$) to be $1.03 \times 10^{-2}$ $s^{-1}$, by $D_r = kT/(8\eta r^3)$. From this value, we then obtain the persistence time associated with liposome motion ($\tau_r$) at 48.5 s, following $\tau_r = [(d - 1)D_r]^{-1}$, where d (=3) is the spatial dimension of rotation. Within the 15-s time window of liposome tracking, therefore, liposome active motion is expected to remain correlated with their initial orientation (12, 13), consistent with our experimental observation.

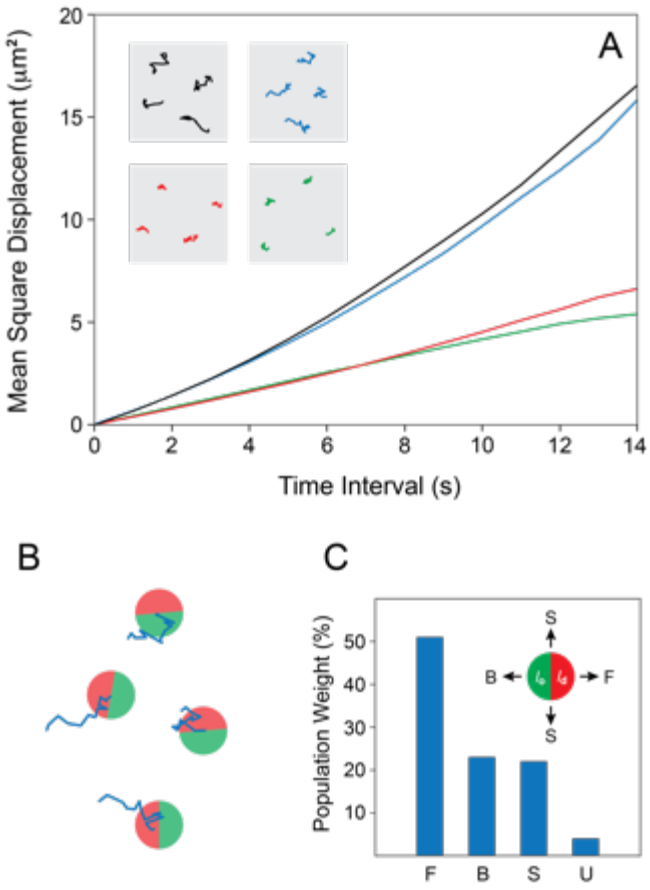


Figure. 3.2 (A) MSD plots of homogeneous and Janus liposomes in the presence of 2 mM β-CD. Colors used for different samples: homogeneous DOPC/Chol (red), DPPC/Chol (green), DPPC/DOPC/Chol Janus (blue) and DPPC/DPhPC/Chol Janus (black). Insets: representative liposome movement trajectories; same color code applies. In each case, four liposome trajectories obtained from the same recording are placed in a 25x25 μm box (in gray). The distance between liposomes in the actual is much greater (no interparticle interactions). (B) Trajectory development vs. Janus liposome initial orientation of the DPPC/DOPC/Chol sample. (C) Population-wise analysis of liposome trajectory placement vs. initial liposome orientation. A total of 458 liposomes were assigned into four categories of movement: forward (F, with liposome's $l_d$ domain as the front), backward (B), sideway (S) and undetermined (U).

### 3.3.4 Cholesterol Extraction from Liposomes by β-CD is Lipid Dependent and Domain Specific

To quantitatively assess Chol efflux in different lipid systems and thus identify its correlation with liposome motion, we next investigated Chol extraction kinetics by fluorescently following its analog, Bodipy-Chol. Combining Bodipy's compact size and charge neutrality with Chol's main structural features in a small package, this probe has been found to closely track the distribution/transport of Chol in both model [35, 36] and cellular lipid environments [37, 38]. Moreover, Bodipy-Chol maintains similar emission characteristics in both $l_d$ and $l_o$ lipid domains [48, 49], enabling its use in following Chol partitioning among complex membrane phases. By combining fluorescence detection of Bodipy-Chol with external standard calibration (Experimental Section), we can thus quantify Chol levels in different liposomes and lipid domains.

As a preliminary test, our single-point fluorescence imaging reveals appreciably faster extraction on DOPC/Chol vs. homogenous liposomes. Upon 16-min continuous extraction, for example, Bodipy-Chol fluorescence is mostly retained in DPPC/Chol liposomes, but largely lost from DOPC/Chol liposomes (Fig. 4A). This trend is further confirmed by detailed time-dependent measurements, which identify first-order Chol extraction kinetics for both cases (Fig. 4B). Specifically, it proceeds an order of magnitude faster in DOPC ($k = 0.056\ s^{-1}$, $t_{1/2} = 9.5$ min) compared to DPPC ($k = 0.005\ s^{-1}$, $t_{1/2} = 143$ min). This result is in accord with previous findings that Chol displays a higher tendency (activity) to escape from disordered lipid domains, a result due to complex interplay between Chol/lipid binding, lipid matrix order (with it, Chol's accessibility), and entropy [50-52]. Fast Chol extraction also appears evident at the $l_d$ domain in Janus liposomes (Fig. 4A).

Detailed kinetic analysis reveals several additional features unique to Janus liposomes (Fig. 4B). To start, a rate constant of $0.031\ s^{-1}$ ($t_{1/2} = 20$ min) is found for Chol extraction at the $l_o$ domain, which is 6 times higher than that from homogenous DPPC liposomes. At the DOPC-enriched $l_d$

domain, interestingly, the level of extraction appears to first rise at the beginning of the process before setting into a continuous decay (open circles in red, Fig. 4B). The first-order fitting of the latter returns $k = 0.061\ s^{-1}$ ($t_{1/2} = 5.3$ min), which is quite comparable to that from homogenous DOPC liposomes. Of the initial rise, it corresponds to a level of Chol traffic at the $l_d$ domain that temporarily surpasses the local Chol availability. Since there exists no external Chol supply in the system, this greater Chol traffic can only be sustained by an internal Chol transfer, i.e., from the $l_o$ to $l_d$ domain of the same Janus liposome. The existence of this internal route is also consistent with the observation of fast Chol depletion observed from the $l_o$ domain, serving as the internal Chol reserve in the process. As suggested previously by Sanchez and coworkers [53,54], Chol distribution between $l_o/l_d$ domains maintains a dynamic equilibrium dictated by the amount/type of lipids present in the liposome. When a preexisting equilibrium is tipped off by fast extraction taking place at one domain of the liposome, such internal Chol transfer acts to reestablish the global equilibrium.

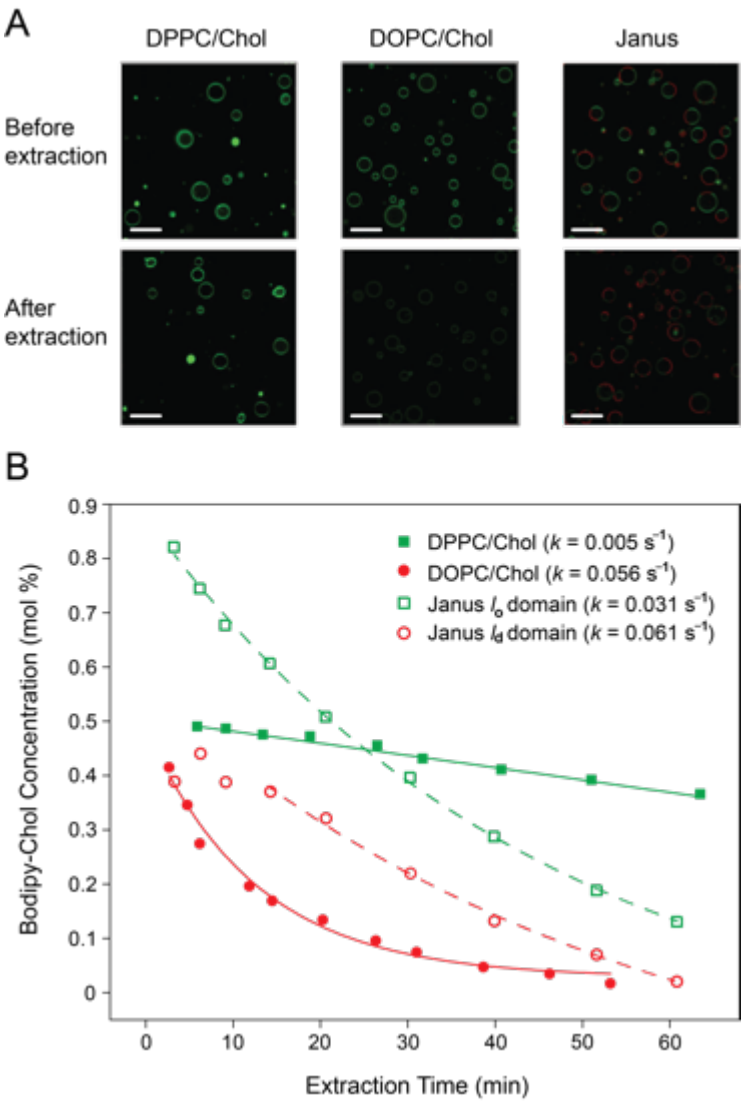


Figure.3.3 β-CD extraction of Chol from homogeneous and Janus liposomes. (A) Fluorescence micrographs of liposome samples before/after 16-min extraction with 2 mM β-CD. All samples contain 1% Bodipy-Chol as the fluorescence label for Chol. Scale bar: 50 μm. (B) Bodipy-Chol concentration decrease in homogeneous (solid squares and circles) and Janus liposomes (open squares and circles) over time as a result of β-CD extraction. Solid and dashed lines are fitting curves obtained from first-order kinetics. In the case of Janus $l_d$ domain, only the last six data points were used to produce the fit (more in main text).

### 3.3.5 Contributing Factors to Liposome Active Motion

Keeping the nominal liposome size constant at 5 μm, we next examined the impact of various extraction-related experimental variables on liposome motion. As for the concentration of the extracting agent, we find the MSD plot obtained with 0.5 mM β-CD to be closely comparable to the case of 2 mM β-CD (Fig. 5A). When [β-CD] is raised to 4 mM, only a small (~10%) increase in liposome displacement is obtained (trace in purple, Fig. 5A). Such insensitivity of active motion to CD concentration could be due partially to β-CD accumulation at the liposome surface as a result of H-bonding, which provides a constant pool of β-CD during extraction. A more likely cause, however, lies in the fast depletion of Chol from liposomes under high β-CD concentrations. For example, we found early on that, with 4 mM β-CD, the Chol extraction can progress to ~90% completion in less than 2 min (data not shown). At still higher concentrations, e.g., 5 mM, substantial liposome morphological changes and rupturing prevent us from accurately identifying $l_d/l_o$ domains. Interestingly, when we replace β-CD out from the system with methyl-β-CD (at 1 mM), a more efficient Chol-extracting agent than the former [55, 56], we observe a 35% enhancement in the resulting MSD (trace in orange, Fig. 5A). Higher methyl-β-CD concentrations are not tested due to extensive lipid domain fusion and liposome rupturing. Another factor investigated is the relative size of $l_d$ vs. $l_o$ domains, i.e., the Janus ratio, in Janus liposomes, which can be controlled by adjusting the mixing ratio of the three main lipids [33]. Here, we identify a clear correlation, in that liposomes generally move more actively as their $l_d$ domain becomes larger (Fig. 5B). Of the three samples tested, the one prepared from DPPC/DOPC/Chol mixed at 50/20/30 (Janus ratio: ~1:3) produces the least active MSD plot, which is still significantly more active (by 90%) than

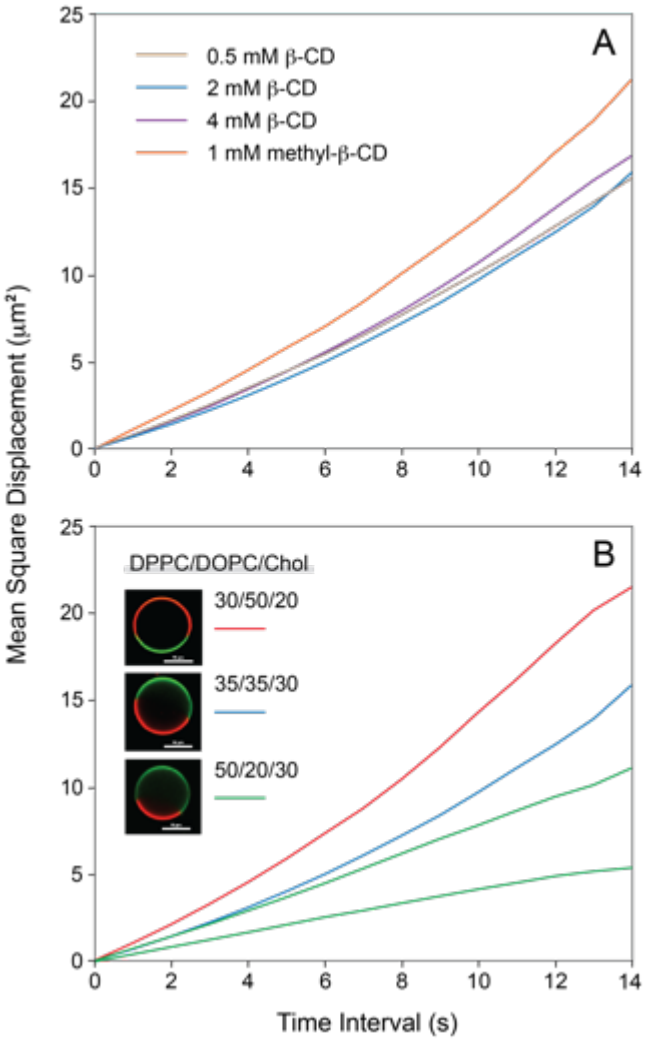


Figure.3.4. (A) MSD plots of Janus liposome movement were obtained from different CD concentrations and types. (B) MSD plots of Janus liposome movement were obtained from samples with different Janus ratios. Inlet: fluorescence micrographs of representative liposomes with different relative Ld/Lo domain sizes and their lipid mixing ratios. To clarify, these are taken from liposome samples without size control (extrusion).

that obtained from homogeneous liposomes under similar conditions. In comparison, the 35/35/30 sample (Janus ratio: ~1:1) is 20% more active, which, in turn, is 47% slower than that from 30/50/20 mixed sample (Janus ratio: ~3:1). Of the latter, it is important to note that its highest mobility is achieved despite its lowest Chol level expected in the $l_d$ domain among the three [32]. While these results point directly to the deciding role of liposome surface area on the liposome active motion, other factors, such as Chol anchoring strength and its heterogeneous liposome exit [57], cannot be ruled out fully without further examination.

### 3.3.6. Molecular Interactions, Driving Forces and Hydrodynamics Involved

We now move on to a mechanistic discussion of the liposome active motion observed, focusing on the molecular interactions, interfacial forces, and hydrodynamics involved.

Starting from the extractant, β-CD, its α-1,4-linked, 7-member glucose ring system possesses a truncated-cone shaped structure when dispersed in water, featuring a shallow hydrophobic cavity furnished distally by two (6-positioned) hydroxyl groups at the narrow end and four (2,3-positioned) hydroxyl groups at the other [27]. These peripherical hydroxyls render hydrogen bonding prominent in much of β-CD interaction with other species, be it a solvent (water primarily) or a binding partner. As to the cavity, it is important to recognize that it is "preloaded" with several water molecules inside, e.g., ~6 from neutron diffraction evidence [58]. Due to structural confinement presented by the cavity, moreover, these trapped water molecules can only attain partial H-bonding, as opposed to the ideal four-fold arrangement, with their neighbors. As such, they are highly disordered and mobile. When a binding partner enters β-CD's cavity to form an inclusion complex, out go these frustrated water molecules (Fig. 6A). Energetically, it is the

release of these high-energy waters to the bulk, thus restoring their H-bonding order, that primarily drives such formations [59-61].

Once being added into a liposome solution, β-CD starts to accumulate around liposomes driven by H-bonding with the lipid headgroups [62]. From there, it would either thermally relax back to the bulk or more eventfully, encounter a cholesterol nearby, whose hydroxyl group is positioned at the lipid/water interface but less accessible to β-CD compared to co-assembled phospholipids. Such encounters then trigger highly efficient Chol extraction from the liposome host, with $\Delta G$ estimated to be –40 kJ $mol^{-1}$ for $l_d$-like lipid systems [63]. To pull the relatively long Chol fully out, the addition of second β-CD is favored so as to shield Chol's entire hydrophobic body from direct water exposure. This 2:1 CD⊃Chol complex stoichiometry is generally supported by experimental [64, 65] and simulation [63, 66] results. Once the extraction is complete, the resultant CD⊃Chol complex tends to diffuse away from the liposome surface – as a new entity, its concentration is the highest there. Such departure is also facilitated by the unbound β-CDs, which continuously diffuse in to replace those Chol-loaded ones from liposome surface and thus sustain the extraction. A two-way traffic of extractants, therefore, arises at the liposome/water interface (Fig. 6B).

Mechanically, the extraction process can be viewed as an intermolecular tug-of-war between Chol's complexation with β-CD on one hand and Chol's anchoring in lipid matrices on the other. From recent single-molecule force studies, the former interaction registers a force of >30 pN [61], exceeding the latter measured for both $l_o$ (22 pN) and $l_d$ (12 pN) bilayers [67] under comparable conditions. These results not only underscore β-CD's high extraction efficiency toward Chol; but, more importantly, they also hint at the pulling force that the liposome must experience as Chol exits its host. As 2D liquids, $l_o/l_d$ lipid bilayers are viscous matrices that exhibit

internal friction. As the force imbalance causes Chol to accelerate from a relatively stationary starting position inside these matrices, part of momentum carried by Chol will be transferred to the liposome via such internal friction, resulting in a pull along the same direction, i.e., roughly perpendicular to the local bilayer plane.[66] Of the two CDs tested, methyl β-CD bears a deeper hydrophobic pocket that affords more favorable inclusion of Chol compared to β-CD [68], thus registering a stronger pull. Its two H-bonds vs. β-CD's six also translates to a smaller desorption energy barrier [66]. This pulling force, moreover, multiplies as the Chol efflux increases. Take, homogenous DOPC/Chol liposomes, for example. From the cross-section area each lipid occupies in a mixed lipid bilayer, 0.6 (DOPC) and 0.2 $nm^2$ [69], we can estimate their average number in a 5-μm-diameter unilamellar liposome: 2.2 x $10^8$ and 1.0 x $10^8$, respectively. Relating the latter with the extraction half time obtained earlier ($t_{1/2}$ = 9.5 min), we can then obtain a rough estimate of average Chol efflux: 1.1 x $10^3$ $\mu m^{-2}$ $s^{-1}$, which, notably, compares closely to the rate of β-CD-facilitated Chol desorption from monolayers [42].

Such Chol extraction-induced pulling does not produce directional liposome motion outright, however. Another key factor is the geometric asymmetry of Janus liposomes, which enables anisotropic chol efflux over the liposome surface and hence, external force development about the structure. By contrast, the spherical symmetry of homogeneous liposomes leads to net cancelation of interfacial forces around the particles. As a result, their motion remains largely diffusive despite their ongoing Chol extraction (Fig. 2).

As the most abundant species present, water, particularly its hydration effect and associated hydrodynamics, need specific consideration. To start, there exists a layer of water bound to the liposome surface, i.e., the hydration shell [70, 71], which structurally makes up the outermost layer of liposomes interacting with water and extractant molecules in the bulk. Mechanistically, the

former interaction (between bound and free waters) manifests itself through liposome Brownian diffusion, whereas the latter presents a physical barrier for the extractant to overcome before Chol extraction could take place. Closely related to its existence, there is also hydration's dependence on lipid type. It has been generally established that, for example, more waters are bound with DOPC than DPPC bilayers on a per lipid basis [70, 72, 73], which accentuates different water binding strength and penetration depth between these two lipid systems. If water/lipid interactions are lipid specific, then, can they "propagate" through the system and manifest themselves on the level of liposome movement?

Our liposome tracking results clearly point to the negative. For both homogeneous and Janus liposomes (Fig. 2), we observe ideal Brownian motion fully described by diffusion of a rigid sphere at low Reynolds numbers [38, 74]. Such absence of lipid specificity in liposome motion can be understood on several levels. Microscopically, liposome diffusion results from uncompensated random thermal collisions by water molecules in the bulk. The bound waters, on the other hand, display much slower translational dynamics [75-77] and to a good approximation, may be considered frozen during the collision process. In this sense, the bound water layer is as much on the receiving end of the collision as the liposome itself. Another important factor to consider here is Chol's well-known condensing/ordering effects [78,79]. By replacing bulk waters from forming H-bonding network with the lipid headgroups at the lipid/water interface, it decreases the level of water penetration into the lipid bilayer; by softening DPPC matrix on one hand and ordering DOPC on the other, moreover, it effectively levels the mechanical distinction between the two lipid domains. Note also that, rotational diffusion is not fast enough to average out such a difference for the size of liposomes studied here, as discussed earlier.

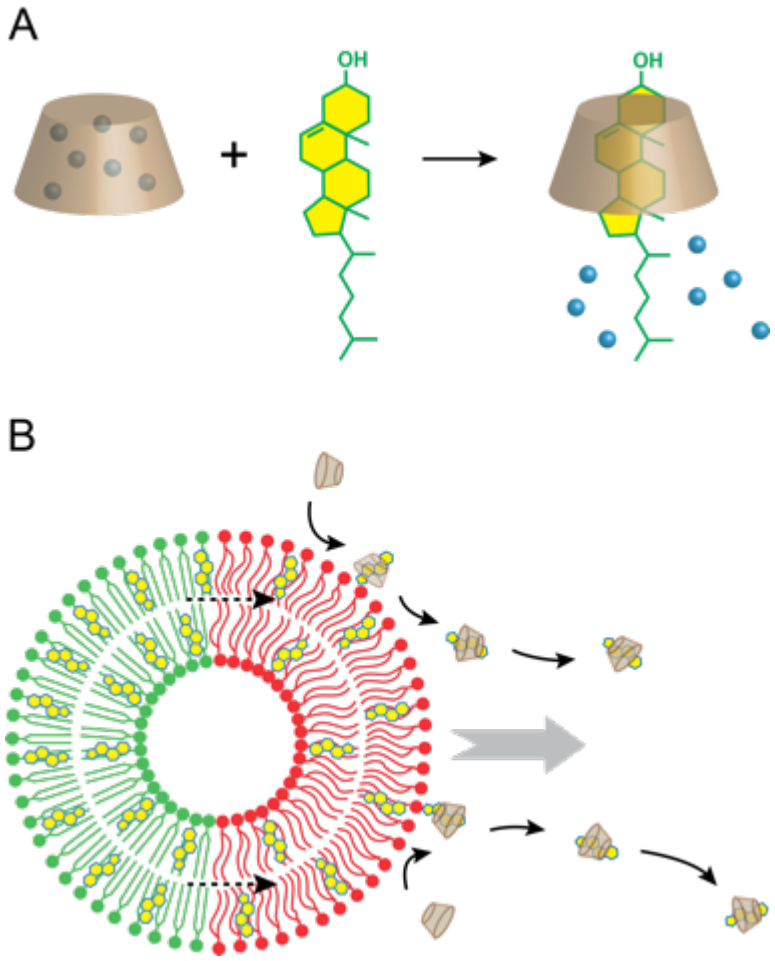


Figure. 3.5 (A) Schematic of CD/Chol inclusion complex formation and associated water release from CD's cavity. (B) Cartoon depiction of the driving force, lipid transfer (indicated by dashed arrows) and efflux (solid arrows) involved in the directional motion (gray arrow) of Janus liposomes.

### 3.3.7. Conclusions

This work demonstrates liposome active motion through asymmetrical lipid efflux from Janus liposomes. Sustained by continuous Chol release from liposomes and inter-domain Chol transfer, the observed active motion exceeds the background diffusion by nearly two-fold. By exploiting intrinsic material properties of lipid assemblies, such as lipid phase separation and extraction, this work represents a significant departure from existing liposome-based motor design strategies. Applied orthogonally together with the latter, it should enable further development of multi-responsive, function-programmable liposome motors. Largely a proof of concept in itself, this work outlines a hierarchical design principle that should be applicable to other lipid systems operating on alternative intermolecular interactions and interfacial properties. One of such exploration possibilities is lipid-active enzymes. Ongoing work in this laboratory is geared toward this area as well as improving the speed and robustness (e.g., under osmotic pressure or in crowded environments) of these liposome motors.

### 3.4 Reference

1. S. Sánchez, L. Soler, J. Katuri, Chemically powered micro- and nanomotors. Angew. Chem. Int. Ed. 54, 1414-1444 (2015).

2. F. Wong, K. K. Dey, A. Sen, Synthetic micro/nanomotors and pumps: fabrication and applications. Annu. Rev. Mater. Res. 46, 407-432 (2016).

3. M. Safdar, S. U. Khan, J. Jänis, Progress toward catalytic micro- and nanomotors for biomedical and environmental applications. Adv. Mater. 30, 1703660 (2018).

4. J. G. Gibbs, N. A. Fragnito, Y. Zhao, Asymmetric Pt/Au coated catalytic micromotors fabricated by dynamic shadowing growth. Appl. Phys. Lett. 97, 253107(2010).

5. W. Gao, A. Pei, R. Dong, J. Wang, Catalytic iridium-based Janus micromotors powered by ultralow levels of chemical fuels. J. Am. Chem. Soc. 136, 2276-2279 (2014).

6. X. Ma, S. Jang, M. N. Popescu, W. E. Uspal, A. Miguel-Lopez, K. Hahn, D.-P. Kim, S. Sánchez, Reversed Janus micro/nanomotors with internal chemical engine. ACS Nano. 10, 8751-8759 (2016).

7. Y. Wu, T. Si, X. Lin, Q. He, Near infrared-modulated propulsion of catalytic Janus polymer multilayer capsule motors. Chem. Commun. 51, 511-514 (2015).

8. B. Jang, A. Hong, H. E. Kang, C. Alcantara, S. Charreyron, F. Mushtaq, E. Pellicer, R. Büchel, J. Sort, S. S. Lee, B. J. Nelson, S. Pane, Multiwavelength light-responsive Au/B-$TiO_2$ Janus micromotors. ACS Nano. 11, 6146-6154 (2017).

9. W. Liu, W. Wang, X. Dong, Y. Sun, Near-Infrared light-powered Janus nanomotor significantly facilitates inhibition of amyloid-β fibrillogenesis. ACS Appl. Mater. Interfaces 12, 12618-12628 (2020).

10. L. Xu, F. Mou, H. Gong, M. Luo, J. Guan, Light-driven micro/nanomotors: from fundamentals to applications. Chem. Soc. Rev. 46, 6905-6926 (2017).

11. R. Dong, Y. Cai, Y. Yang, W. Gao, B. Ren, Photocatalytic micro/nanomotors: from construction to applications. Acc. Chem. Res. 51, 1940-1947 (2018).

12. A. Zöttl, H. Stark, Emergent behavior in active colloids. J. Phys.: Condense. Matter 28, 253001 (2016).

13. C. Bechinger, R. D. Leonardo, H. Löwen, C. Reichhardt, G. Volpe, G. Volpe, Active Particles in Complex and Crowded Environments. Rev. Mod. Phys. 88, 045006 (2016).

14. J. L. Moran, J. D. Posner, Phoretic self-propulsion. Annu. Rev. Fluid Mech. 49, 511-540 (2017).

15. T. Xu, W. Gao, L.-P. Xu, X. Zhang, S. Wang, Fuel-free synthetic micro-/nanomachines. Adv. Mater. 29, 1603250 (2017).

16. D. D. Lasic, Novel applications of liposomes. Trends Biotech. 16, 307-321 (1998).

17. B. F. Gibbs, S. Kermasha, I. Alli, C. N. Mulligan, Encapsulation in the food industry: a review. Int J. Food Sci. Nutr. 50, 213-224 (1999).

18. H.-I. Chang, M.-K. Yeh, Clinical development of liposome-based drugs: formulation, characterization, and therapeutic efficacy. Int J. Nanomedicine 7, 49-60 (2012).

19. G. J. Nohynek, J. Lademann, C. Ribaud, M. S. Roberts, Grey goo on the skin? Nanotechnology, cosmetic and sunscreen safety. Crit. Rev. Toxicol. 37, 251-277 (2008).

20. T. Kurakazu, M. Takinoue, K. Kuribayashi-Shigetomi, S. Takeuchi, Flagella-driven liposomes: liposomes actuated by attached flagella. 14th International Conference on Miniaturized Systems for Chemistry and Life Sciences, 3-7 October 2010, Groningen, The Netherlands.

21. N. Dogra, H. Izadi, T. K. Vanderlick, Micro-motors: a motile bacteria based system for liposome cargo transport. Sci. Rep. 6, 29369 (2016).

22. S. Ghosh, F. Mohajerani, S. Son, D. Velegol, P. J. Butler, A. Sen, Motility of enzyme-powered vesicles. Nano Lett. 19, 6019-6026 (2019).

23. A. Somasundar, S. Ghosh, F. Mohajerani, L. N. Massenburg, T. Yang, P. S. Cremer, D. Velegol, A. Sen, Positive and negative chemotaxis of enzyme-coated liposome motors. Nat. Nanotech. 14, 1129-1134 (2019).

24. F. Mazur, M. Fernández-Medina, N. Gal, O. Hovorka, R. Chandrawati, B. A. Städler, Locomotion of micromotors due to liposome disintegration. Langmuir 36, 7056-7065 (2020).

25. H. Inaba, A. Uemura, K. Morishita, T. Kohiki, A. Shigenaga, A. Otaka, K. Matsuura, Light-induced propulsion of a giant liposome driven by peptide nanofibre growth. Sci. Rep. 8, 6243 (2018).

26. Z. Liu, J. Cui, W. Zhan, Dipolar Janus liposomes: formation, electrokinetic motion and self-assembly. Soft Matter 16, 2177-2184 (2020).

27. J. Szejtli, Introduction and General Overview of Cyclodextrin. Chem. Rev. 98, 1743-1753 (1998).

28. K. Uekama, F. Hirayama, T. Irie, Cyclodextrin drug carrier systems. Chem. Rev. 98, 2045-2076 (1998).

29. S. L. Veatch, S. L. Keller, Separation of liquid phases in giant vesicles of ternary mixtures of phospholipids and cholesterol. Biophys. J. 85, 3074-3083 (2003).

30. S. L. Veatch, I. V. Polozov, K. Gawrisch, S. L. Keller, Liquid domains in vesicles investigated by NMR and fluorescence microscopy. Biophys. J. 86, 2910-2922 (2004).

31. J. H. Davis, J. J. Clair, J. Juhasz, Phase equilibria in DOPC/DPPC-$d_{62}$/cholesterol mixtures. Biophys. J. 96, 521-539 (2009).

32. S. L. Veatch, O. Soubias, S. L. Keller, K. Gawrisch, critical fluctuations in domain-forming lipid mixtures. Proc. Natl. Acad. Sci. USA 104, 17650-17655 (2007).

33. M. Wang, Z. Liu, W. Zhan, Janus liposomes: gel-assisted formation and bioaffinity-directed clustering. Langmuir 34, 7509-7518 (2018).

34. M. V. Gudheti, M. Mlodzianoski, S. T. Hess, Imaging and shape analysis of GUVs as model plasma membranes: effect of trans DOPC on membrane properties. Biophys. J. 93, 2011-2023 (2007).

35. F. S. Ariola, Z. Li, C. Cornejo, R. Bittman, A. A. Heikal, Membrane fluidity and lipid order in ternary giant unilamellar vesicles using a new Bodipy-cholesterol derivative. Biophys. J. 96, 2696-2708 (2009).

36. D. Wüstner, L. Solanko, E. Sokol, O. Garvik, Z. Li, R. Bittman, T. Korte, A. Herrmann, Quantitative assessment of sterol traffic in living cells by dual labeling with dehydroergosterol and BODIPY-cholesterol. Chem. Phys. Lipids 164, 221-235 (2011).

37. J.-T. Tinevez, N. Perry, J. Scindelin, G. M. Hoopes, G. D. Deynolds, E. Laplantine, S. Y. Bednarek, S. Shorte, K. W. Eliceiri, Trackmate: An open and extensible platform for single-particle tracking. Methods 2017, 115, 80-90.

38. H. C. Berg, Random Walks in Biology (Princeton University Press, Princeton, NJ, 1983).

39. H. Qian, M. P. Sheetz, E. L. Elson, Single particle tracking. Analysis of diffusion and flow in two-dimensional systems. Biophys. J. 60, 910-921 (1991).

40. M. J. Saxton, K. Jacobson, Single particle tracking: Applications to membrane dynamics. Annu. Rev. Biophys. Biomol. Struct. 26, 373-399 (1997).

41. Y. Zhang, H. Hess, Chemically-powered swimming and diffusion in the microscopic world. Nat. Chem. 5, 500-510 (2021).

42. H. Ohvo, J. P. Slotte, Cyclodextrin-mediated removal of sterols from monolayers: Effects of sterol structure and phospholipids on desorption rate. Biochemistry 35, 8018-8024 (1996).

43. R. Leventis, J. R. Silvius, Use of cyclodextrins to monitor transbilayer movement and differential lipid affinities of cholesterol. Biophys. J. 81, 2257-2267 (2001).

44. R. Zidovetzki, I. Levitan, Use of cyclodextrins to manipulate plasma membrane cholesterol content: evidence, misconceptions and control strategies. Biochim. Biophys. Acta 1768, 1311-1324 (2007).

45. E. P. C. Kilsdonk, P. G. Yancey, G. W. Stoudt, F. W. Bangerter, W. J. Johnson, M. C. Phillips, G. H. Rothblat, Cellular cholesterol efflux mediated by cyclodextrins. J. Biol. Chem. 270, 17250-17256 (1995).

46. S.-L. Niu, B. J. Litman, Determination of membrane cholesterol partition coefficient using a lipid vesicle–cyclodextrin binary system: effect of phospholipid acyl chain unsaturation and headgroup composition. Biophys. J. 83, 3408-3415 (2002).

47. L. Szente, É. Fenyvesi, Cyclodextrin-lipid complexes: cavity size matters. Struc. Chem. 28, 479-492 (2017).

48. S. Sankaranarayanan, G. Kellner-Weibel, M. de la Llera-Moya, M. C. Phillips, B. F. Asztalos, R. Bittman, and G. H. Rothblat, A sensitive assay for ABCA1-mediated cholesterol efflux using BODIPY-cholesterol. J. Lipid Res. 52, 2332-2340 (2011).

49. E. Sezgin, F. B. Can, F. Schneider, M. P. Clausen, S. Galiani, T. A. Stanly,* D. Waithe, A. Colaco, A. Honigmann, D. Wüstner, F. Platt, C. Eggeling, A comparative study on fluorescent cholesterol analogs as versatile cellular reporters. Chem. Phys. Lipids 57, 299-309 (2016).

50. H. M. McConnell, M. Vrljic, Liquid-liquid immiscibility in membranes. Annu. Rev. Biophys. Biomol. Struct. 32, 469-492 (2003).

51. H. Ohvo-Rekilä, B. Ramstedt, P. Leppimäki, J. P. Slotte, Cholesterol interactions with phospholipids in membranes. Prog. Lipid Res. 41, 66-97 (2002).

52. Y. Lange, T. L. Steck, Cholesterol homeostasis and the escape tendency (activity) of plasma membrane cholesterol. Prog. Lipid Res. 47, 319-332 (2008).

53. S. A. Sanchez, M. A. Tricerri, E. Gratton, Interaction of high density lipoprotein particles with membranes containing cholesterol. J. Lipid Res. 48, 1689-1700 (2007).

54. S. A. Sanchez, G. Gunther, M. A. Tricerri, E. Gratton, Methyl-□-cyclodextrins preferentially remove cholesterol from the liquid disordered phase in giant unilamellar vesicles. J. Membrane Biol. 241, 1-10 (2011).

55. R. Zidovetzki, I. Levitan, Use of cyclodextrins to manipulate plasma membrane cholesterol content: evidence, misconceptions and control strategies. Biochim. Biophys. Acta 1768, 1311-1324 (2007).

56. E. P. C. Kilsdonk, P. G. Yancey, G. W. Stoudt, F. W. Bangerter, W. J. Johnson, M. C. Phillips, G. H. Rothblat, Cellular cholesterol efflux mediated by cyclodextrins. J. Biol. Chem. 270, 17250-17256 (1995).

57. K. Bacia, D. Scherfeld, N. Kahya, P. Schwille, fluorescence correlation spectroscopy relates rafts in model and native membranes. Biophys. J. 87, 1034-1043 (2004).

58. C. Betzel, W. Saenger, B. E. Hingerty, G. M. Brown, Circular and flip-flop hydrogen bonding in □-cyclodextrin undecahydrate: a neutron diffraction study. J. Am. Chem. Soc. 106, 7545-7557 (1984).

59. H.-J. Schneider, Binding mechanisms in supramolecular complexes. Angew. Chem. Int. Ed. 48, 3924-3977 (2009).

60. F. Biedermann, W. M. Nau, H.-J. Schneider, The hydrophobic effect revisited – Studies with supramolecular complexes imply high-energy water as a noncovalent driving force. Angew. Chem. Int. Ed. 53, 11158-11171 (2014).

61. S. Pandey, Y. Xiang, D. V. D. W. Kankanamalage, J. Jayawickramarajah, Y. Leng, H. Mao, Measurement of single-molecule forces in cholesterol and cyclodextrin host-guest complexes. J. Phys. Chem. B 125, 11112-11121 (2021).

62. W. Khuntawee, P. Wolschann, T. Rungrotmongkol, J. Wong-ekkabut, S. Hannongbua, Molecular dynamics simulations of the interaction of beta cyclodextrin with a lipid bilayer. J. Chem. Inf. Model. 55, 1894-1902 (2015).

63. C. A. López, A. H. de Vries, S. J. Marrink, Computational microscopy of cyclodextrin mediated cholesterol extraction from lipid model membranes. Sci. Rep. 3, 2071 (2013).

64. A. Tsamaloukas, H. Szadkowska, P. J. Slotte and H. Heerklotz, Interactions of cholesterol with lipid membranes and cyclodextrin characterized by calorimetry. Biophys. J. 89, 1109-1119 (2005).

65. E. Christoforides, A. Papaioannou, K. Bethanis, Crystal structure of the inclusion complex of cholesterol in β-cyclodextrin and molecular dynamics studies. Beilstein J. Org. Chem. 14, 838-848 (2018).

66. C. A. López, A. H. de Vries, S. J. Marrink, Molecular mechanism of cyclodextrin mediated cholesterol extraction. PLoS Comput. Biol. 7, e1002020 (2011).

67. F. W. S. Stetter, L. Cwiklik, P. Jungwirth, T. Hugel, Single lipid extraction: The anchoring strength of cholesterol in liquid- ordered and liquid-disordered phases. Biophys. J. 107, 1167-1175 (2014).

68. Y. Yu, C. Chipot, W. Cai, X. Shao, Molecular dynamics study of the inclusion of cholesterol into cyclodextrins. J. Phys. Chem. B 110, 6372-6378 (2006).

69. S. A. Pandit, S.-W. Chiu, E. Jakobsson, A. Grama, H. L. Scott, Cholesterol packing around lipids with saturated and unsaturated chains: a simulation study. Langmuir 24, 6858-6865 (2008).

70. C. Ho, S. J. Slater, and C. D. Stubbs, Hydration and order in lipid bilayers. Biochemistry 34, 6188-6195 (1995).

71. E. A. Disalvo, F. Lairion, F. Martini, E. Tymczyszyn, M. Frías, H. Almaleck, G. J. Gordillo, Structural and functional properties of hydration and confined water in membrane interfaces. Biochim. Biophys. Acta 1778, 2655-2670 (2008).

72. A. S. Ulrich, A. Watts, molecular response of the lipid headgroup to bilayer hydration monitored by $^{2}$H-NMR. Biophys. J. 66, 1441-1449 (1994).

73. W. Pohle, C. Selle, H. Fritzsche, H. Binder, Fourier transform infrared spectroscopy as a Probe for the study of the hydration of lipid self-assemblies. I. Methodology and general phenomena. Biospectroscopy 4, 267-280 (1998).

74. G. K. Batchelor, An Introduction to Fluid Dynamics (Cambridge University Press, New York, NY, 1967).

75. S. König, E. Sackmann, D. Richter, R. Zorn, C. Carlile, T. M. Bayerl, Molecular dynamics of water in oriented DPPC multilayers studied by quasielastic neutron scattering and deuterium-nuclear magnetic resonance relaxation. J. Chem. Phys. 100, 3307-3316 (1994).

76. J. Fitter, R. E. Lechner, N. A. Dencher, Interactions of hydration water and biological membranes studied by neutron scattering. J. Phys. Chem. B 103, 8036-8050 (1999).

77. J. Yang, C. Calero, J. Martí, Diffusion and spectroscopy of water and lipids in fully hydrated dimyristoylphosphatidylcholine bilayer membranes. J. Chem. Phys. 140, 104901 (2014).

78. K. Simon, W. L. C. Vaz, Model Systems, lipid rafts, and cell membranes. Annu. Rev. Biophys. Biomol. Struct. 33, 269-295 (2004).

79. T. Róg, M. Pasenkiewicz-Gierula, I. Vattulainen, M. Karttunen, Ordering effects of cholesterol and its analogues. Biochim. Biophys. Acta 1788, 97-121 (2009).

80. A. Weinberger, F.-C. Tsai, G. Koenderink, T. F. Schmidt, R. Itri, W. Meier, T. Schmatko, A. Schoder, C. Marques, Gel-assisted formation of giant unilamellar vesicles. Biophys. J. 105, 154-164 (2013).

# CHAPTER 4. Photoelectrochemically-Driven Active Motion of $Ru(bpy)_3^{2+}$-Labeled Liposomes

## 4.1 Introduction

The advancement of synthesis and fabricating technologies for Janus particles have brought about various designing of micro/nanomotors and devices, which mainly take advantage of converting other forms of energy into mechanical energy to propel motion for the particles.[1] These brilliant designs greatly stimulated the imagination of researchers who developed micromotors or nanomotors propelled by chemical reactions [2-5] as well as external fields including magnetic field,[6-7] electric field,[8] acoustic field, [9-10]temperature gradients [11-12]and light-driven. [13-16] Chemically powered motors based on forming the chemical gradients or bubbles on the asymmetrical structure of Janus particles to trigger the particle's motion were the most widely investigated case in the past decades. [5,17] The most classic nanomotors focusing on chemically powered mechanism was Pt-Au bimetallic featured Janus rods (1um length ) in aqueous hydrogen peroxide solution fabricated by Vincent H. Crespi and his group in 2004.[18] In their specific auto-motors, the Janus rod moved autonomously along their axis in the direction of the Pt end with speeds up to 10 body lengths per second in 2-3% $H_2O_2$ solution. Since then, there was an increasing number of demonstrations related to Pt-based catalytic Janus motors in hydrogen peroxide as well as some enzyme-based biocompatible motors reported by researchers. [4,5,17] Even though this chemically powered kind of motor holds a lot of advantages such as convenient fabrication, high diversity of design, and wide applications, the “fuel molecules” are indispensable for these motors. Besides, it retained large challenges to control the happening and end of the

chemical reaction until the “fuel molecules” were exhausted in most reports. Such catalytically driven artificial motors displayed inherent biocompatible and controllable limitations including when considering employing them in the biological system. Therefore fuel-free autonomous micro/nanomotors systems have attracted intense attention from researchers. Among all the fuel-free Janus motors, light-driven micro/nanomotors which are converting light energy into mechanical energy exhibited extraordinary advantages compared with other types of active motion devices. Light has been regarded as one the of most efficient and versatile physical stimuli to facilitate and regulate the propulsion of micro-/nanomotors.[13] While utilizing harmless and renewable visible light to provide energy to power micro-/nanomotors in a fluid environment encounters a great challenge. To achieve such locomotion through a light-driven based mechanism, the particles have to be made of or coated with photoactive materials including photocatalytic materials, photothermal materials, and photochromic materials.[1] These applied photoactive materials are capable of performing a photochemical reaction, photothermal conversion, and photoisomerization respectively via absorbing light energy and generating the asymmetric field of energy across the surface of the particle to power the motion. According to the previous reports of light-driven motors, the common constructing strategy of preparing such light-based micro/nanomotors can be classified into two main groups: one is designing asymmetric structure (Janus particles) with photoactive materials and the other is to create nonuniform photo-exposure upon a photoactive material. In the past few years, different metal-based micro-/nanomotors propelled by photocatalytic activities were reported due to transition metals widely employed in sensitizers such as TiO2-based tubular micro engine[19-20] by light-induced bubble formation; BiOI-based micromotors powered by visible-light-driven in pure water[13].

Combined the great advantages of liposomes as environmentally friendly drug delivery candidates and biocompatible to the human system with light-driven based motors, we herein fabricated $Ru(bpy)_3^{2+}$-labeled Janus liposomes which were further utilized into soft photoelectrically-driven micromotors. As a versatile and stable ruthenium-coordinated compound with excellent photoactivity, tris(2,2'-bipyridine)ruthenium(II) ($Ru(bpy)_3^{2+}$) has been broadly employed as a photosensitizer in many applications ever since its first synthesis in the 1960s.[21-22] Photoexcitation of $Ru(bpy)_3^{2+}$ ($\lambda_{max}$: ~450 nm), for example, readily populates its metal-to-ligand charge-transfer excited state, $Ru(bpy)_3^{2+*}$, which is characterized by a long lifetime, i.e., typically in hundreds of nanoseconds.[23-24] To begin with our liposomes-based micromotors investigation, the membrane phase of liposomes labeling photosensitizer $Ru(bpy)_3^{2+}$-DOPE was synthesized according to the protocol in our previous reports.[25] The synthesized $Ru(bpy)_3^{2+}$-DOPE was utilized to label the $L_d$ phase membrane of Janus liposomes which replaced the original rhodamine-DOPE labeling followed by $Ru(bpy)_3^{2+}$-labeled Janus liposomes were generated successfully. To achieve active motion of $Ru(bpy)_3^{2+}$ labeled Janus liposomes, selecting effective chemical fuels in the solution become crucial. Based on the electron transfer and mass transfer property of $Ru(bpy)_3^{2+}$, different fuel system candidates including ascorbate/ $Ru(bpy)_3^{2+}$; oxalate/ $Ru(bpy)_3^{2+}$; persulfate/ $Ru(bpy)_3^{2+}$; bromate/ $Ru(bpy)_3^{2+}$ and methyl viologen/EDTA/$Ru(bpy)_3^{2+}$ were tested under confocal microscope upon 405nm laser exposure. In terms of reactivity under the laser light, the methyl viologen/EDTA/$Ru(bpy)_3^{2+}$ system was found to be the most promising one. Moreover, the active motion behaviors of these size-controlled Janus liposomes which were extruded by micropores attached membrane were investigated when exposed to blue laser light stimuli in the present report. To evaluate the active motion velocity of $Ru(bpy)_3^{2+}$ labeled Janus liposomes by photoelectrochemically driven, we analyzed the mean square displacement (MSD)

of the motion trajectory. After comparing the MSD of these Janus liposomes' trajectory with and without fuel molecules present, we found the motion of these special light-driven liposomes were indeed enhanced compared with under control condition. However, the motion efficiency wasn't reached our expectations and more details will be explained in the results part of this chapter.

The main goal of this project was to construct the $Ru(bpy)_3^{2+}$ labeled Janus liposome micromotors through light-driven active motion. We hypothesized these Janus liposomes could be propelled with the mass transfer and electron transfer process happened on the surface with liposomes membrane when placed them into the reactive fuel reagents solution. In addition, we expected the light-driven active motion could be adjusted by the exposure light intensity and reagent molecule solution.

## 4.2 Experimental Section

### 4.2.1 Reagents and Materials

All lipids used including 1,2-dipalmitoyl-sn-glycero-3-phosphocholine (DPPC, 13.623mM ), 1,2-dioleoyl-sn-glycero-3-phosphocholine (DOPC, 12.720mM), 1,2-dioleoyl-sn-glycero-3-phosphoethanolamine (DOPE, 13.44mM) and 23-(dipyrrometheneboron difluoride)-24-norcholesterol (Bodipy-chol, 0.867mM) were products of Avanti Polar Lipids (Alabaster, AL). Other chemicals including poly(vinyl alcohol) (PVA, MW: 145 000), Cholesterol, bis(2,20 -bipyridine)-40-methyl-4-carboxybipyridine-rutheniumN-succinimidyl-ester(hexafluorophosphate) ($Ru(bpy)_3^{2+}$-NHS), N,N-dimethylformamide(DMF), triethylamine, 4-(2-hydroxyethyl)piperazine-1-ethanesulfonic acid (HEPES), methyl viologen dichloride hydrate (MV2þ), L-ascorbic acid sodium salt (sodium ascorbate), potassium persulfate, bromate acid, Chloroform (>=99.5%) were

obtained from Sigma Aldrich; hydrogen peroxide solution (30%) from Maron Fine Chemicals; Poly(dimethylsiloxane) (PDMS) from DOW Corning CO. Deionized (DI) water of 18.2 MΩ·cm (Millipore) was used throughout this work. Polycarbonate (PC) filter membranes employed in this work were either Whatman Nuclepore (GE Healthcare; thickness: 7−22 μm) or isospory (Millipore Sigma, thickness: 21−27 μm) membranes with pore sizes of 5 μm and nominal thickness of 0.25 mm; Plunger-based lipid extruder (Mini-Extruder, Avanti Polar Lipids). Linear microfluidic channels employed in motion recording test from Cole-Parmer Company.

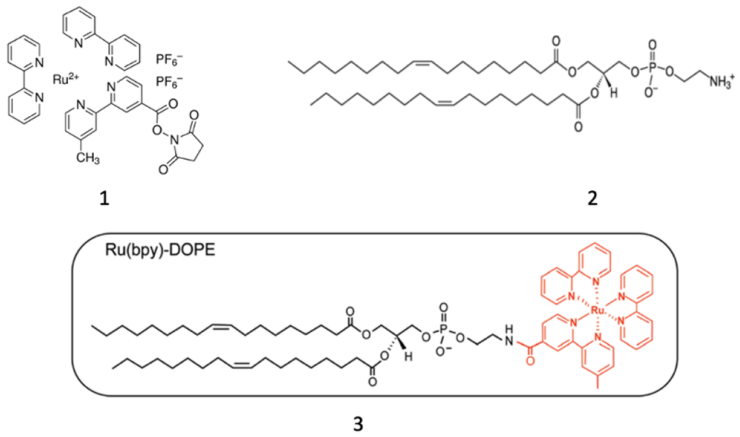


Figure 4.1 Three components for the synthesized experiment products. 1. Ru(bpy)32+-NHS; 2. DOPE; 3. Ru(bpy)32+-DOPE.

### 4.2.2 Synthesis of $Ru(bpy)_3^{2+}$- DOPE

$Ru(bpy)_3^{2+}$- DOPE is synthesized by ourselves in the lab on account that it was not commercially available. The synthesis protocol was mainly followed by the previous report in our lab with a few modifications.[25] To begin with the one-step reaction of $Ru(bpy)_3^{2+}$-NHS and DOPE, 2.5 μmol of DOPE (186μL, 13.44mM) in chloroform was added to a cleaned round flask and dried with a nitrogen blowing stream, to which 0.8mL of high purity DMF and 25 μmol of triethylamine (3.5 μL )were added to the flask and kept stirring under nitrogen gas environment

for 30mins. Then 5 μmol of $Ru(bpy)_3^{2+}$-NHS (about 5mg total) dissolved completely in DMF and injected into the aforementioned flask and mixed thoroughly with a stir bar on the stirring plate overnight at room temperature in the dark. All the reaction process was implemented in the pure nitrogen gas environment and the final reaction volume was close to 1 mL. Later the resulting products were dried by nitrogen blowing stream and purified on a silica gel column (15cm length, 200-400 mesh) using chloroform and chloroform/methanol/water (90:10:0.5) and then 65:25:4 v/v/v) as mobile phase. In the purification process, the production of $Ru(bpy)_3^{2+}$- DOPE was confirmed by TLC spots comparison and $^1H$ NMR in $CDCl_3$ and finally, the purification was examined by EIS-MS. The collected $Ru(bpy)_3^{2+}$- DOPE was concentrated and dissolved in chloroform with 5mM concentration which would be applied to further label the Janus liposomes in the following part. Figure 4.1 displayed the structures of two reaction reagents $Ru(bpy)_3^{2+}$-NHS and DOPE as well as the synthesized product $Ru(bpy)_3^{2+}$- DOPE. Figures 4.2 and 4.3 demonstrated the $^1H$ NMR in the $CDCl_3$ spectrum and EIS Mass spectrum (calculated at 1353.7 )respectively of our final synthesized product $Ru(bpy)_3^{2+}$- DOPE.

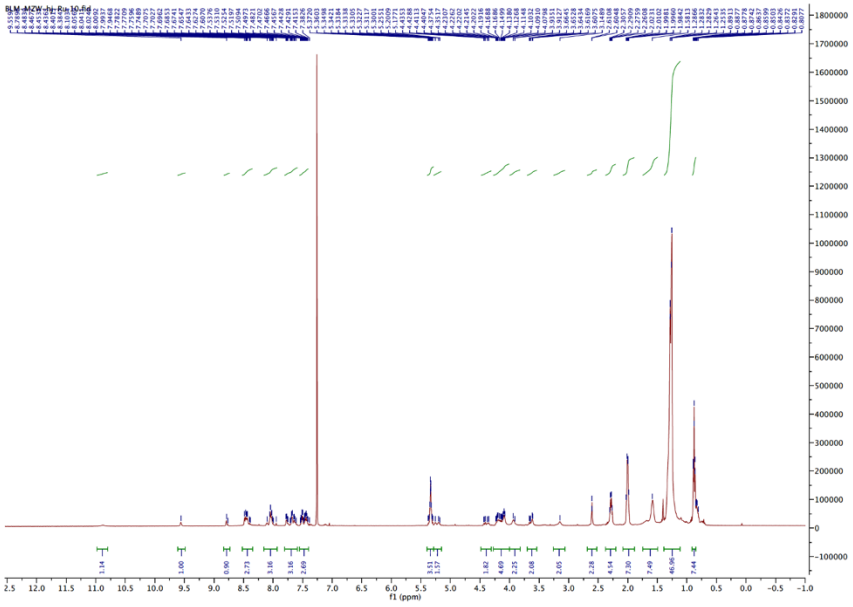

Figure 4.2 1H NMR in CDCl3 spectrum for the fresh synthesized Ru(bpy)32+- DOPE product. The main peak between 1.5 and 1 represents the structure of our product.

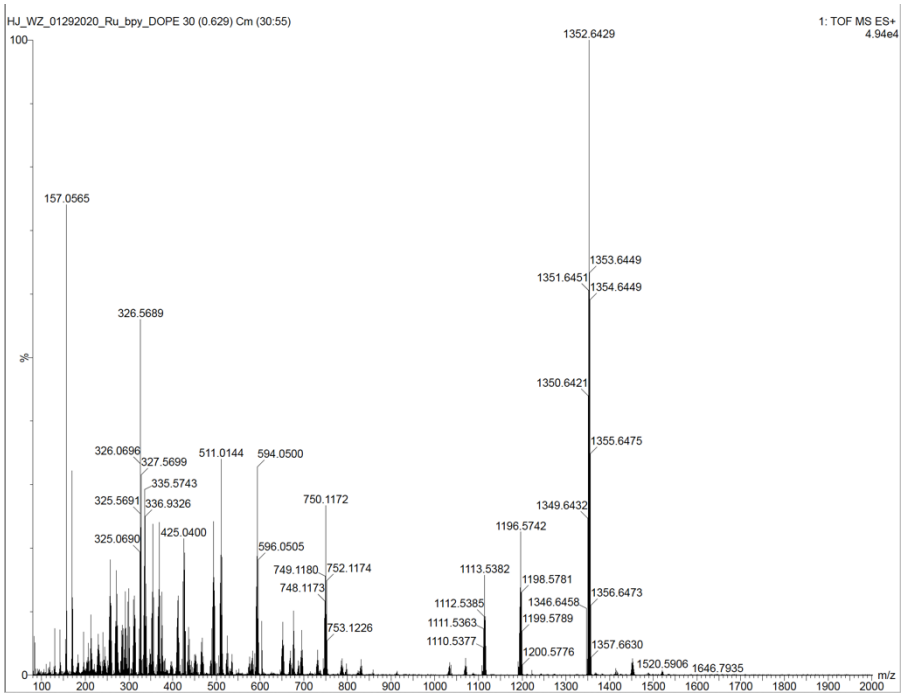


Figure 4.3 ESI-Mass spectrum for fresh synthesized Ru(bpy)32+- DOPE in methanol. The main peak displayed at around 1352.6 was close to the calculated value of 1353 which further confirmed our target product.

### 4.2.3 $Ru(bpy)_3^{2+}$-labeled Janus liposomes preparation

In terms of preparing $Ru(bpy)_3^{2+}$ labeled Janus liposomes, we mainly followed the procedure in our previous report [26] in which the rhodamine-DOPE was replaced by $Ru(bpy)_3^{2+}$-DOPE to label $L_o$ phase. In the detailed process, there were several successive operations and steps including (1) Material/substrate preparation, which includes poly(vinyl alcohol) (PVA) solution, glass

substrates, and lipids precursor solutions. The PVA aqueous solution used in this procedure contains 5 wt % polymer, which is dissolved by continuously stirring the polymer in DI water maintained at 80 °C, whereas the glass slides (VWR, 1 × 1 in, 1 mm thickness) are cleaned by sonication in acetone, DI water, dilute detergent aqueous solutions, and DI water again and then blow-dried by a nitrogen stream. All lipid precursors used in this work are prepared in chloroform with a total lipid concentration of 5mM, and their compositions are including DPPC/DOPC/cholesterol/ $Ru(bpy)_3^{2+}$-DOPE/Chol-bodipy. (2) PVA gel preparation, which is done by first evenly spreading 100 μL of the PVA solution on a precleaned glass slide at room temperature and then drying it on a hot plate at 50 °C for 30mins. (3) Lipid deposition on PVA gel. To achieve this, a 5 μL lipid precursor is first cast on the PVA gel film prepared above using a micro-syringe. This quickly produces a lipid thin film upon solvent evaporation, which is further dried under a vacuum overnight in the dark at room temperature. (4) Liposome production, which is carried out by hydrating the lipid films deposited on PVA gel with 1 mL of DI water at 45 °C for 2hours. After a brief shake of the hydration homemade cap housing the lipid deposits/gel/glass substrate, thus-produced liposomes are harvested with a pipette and stored at room temperature. An extended hydration period is found to be beneficial to the coalescence process of biotinylated Janus liposomes.

### 4.2.4 Characterization of Janus liposomes by fluorescence microscopy

The fluorescence images and motion videos of $Ru(bpy)_3^{2+}$ labeled Janus liposomes were acquired on a Nikon A1+/MP confocal scanning laser microscope (CSLM, Nikon Instruments, Inc., Melville, NY) using 20× objective and excitation laser lines at 405 and 488 nm. As a special sensitizer of metal-ligand complex phosphor, $Ru(bpy)_3^{2+}$ owns maximum excitation at around

450nm (close to the blue light wavelength) and emission peak at 625nm. The corresponding green and red emission signals were filtered at 525 ± 25 and 595 ± 25 nm. For each measurement, a 10−15 μL liposome solution was first pipetted into a Poly(dimethylsiloxane) microwell reversibly sealed to a precleaned microscope cover slide (Corning No. 1, 22 × 22 mm, Corning, NY) and then given 30mins to settle under 100% humidity.

### 4.2.5 Characterization of motion behaviors for Janus liposomes by photoelectrochemically-driven

Generally, there exist several different diffusion coefficient measurements for micro- or nanomotors so far including particle tracking by mean square displacement (MSD) analysis, fluorescence correlation spectroscopy (FCS), dynamic light scattering (DLS), and diffusion nuclear magnetic resonance (NMR).[29] Among all these methods, MSD analysis has been widely used as a standard measurement to determine diffusion coefficients of microswimmers due to reliability for a large number of particle tracks and reproducibility. Here the diffusion behavior of the as-obtained membrane extruded $Ru(bpy)_3^{2+}$ labeled Janus was characterized CCD camera coupled to the laser scanning microscope and then processed through the MSD analysis method. The detailed procedure for this MSD analysis could be summarized into the following steps: (1) the good quality Janus liposomes were extruded by micropores contained membrane to get size controlled (5um) liposomes; (2) the extruded $Ru(bpy)_3^{2+}$ labeled Janus liposomes solution was mixed with an equivalent volume of different concentration persulfate solutions (5mM,10mM) in the dark environment to prevent photo quenching; (3) the solution mixtures were loaded into a precleaned linear microfluidic channel quickly and set onto the confocal stage plate; (4) Once turned on the blue laser (405nm filtered), the motion behavior was recorded by CCD camera (at

a frame rate of about 25 fps) equipped with Nikon inverted microscope in which the 20x objective was attached. Based on the single particle tracking method, the recording images and videos of liposomes motion were processed and analyzed by the well-known software Image J to acquire motion trajectories files; (5) These trajectory files were further analyzed through MATLAB software with home-written codes to calculate the mean square displacement (MSD) curves which could properly describe and classify the motion behaviors of micro/nano-particles. According to the previous particles motion study, the corresponding MSD fitting equation in a short time interval can be expressed as follows:

$$MSD(\Delta t) = 4D\Delta t + v^2\Delta t^2 \text{ [27]}$$

where D is the diffusion coefficient, $\Delta t$ is the interval time, and v is the movement speed of the particle.

### 4.3 Results and Discussion

#### 4.3.1 Experiment design

As introduced earlier, the experiment design for the photoelectrochemically driven-based active motion of liposomes was demonstrated in Figure 4.1 in which once the $Ru(bpy)_3^{2+}$-labeled Janus liposomes mixed with electron donor or acceptor fuel molecules and exposed under blue laser light (450nm wavelength), the active motion of liposomes were induced by chemo-phoretic propulsion energy formation due to the electron transfer reaction only happened on one hemisphere of liposome membrane surface ($L_d$). Owned various special photochemistry properties, $Ru(bpy)_3^{2+}$ could achieve electron transferring with a bunch of different electron donors or acceptors fuels including ascorbate, oxalate, persulfate, bromate, methyl viologen/EDTA. The motion direction

of these liposomes here was from $L_d$ domain side to the $L_o$ domain side as a consequence of new chemical species chemical gradient formation on the two-hemisphere membrane.

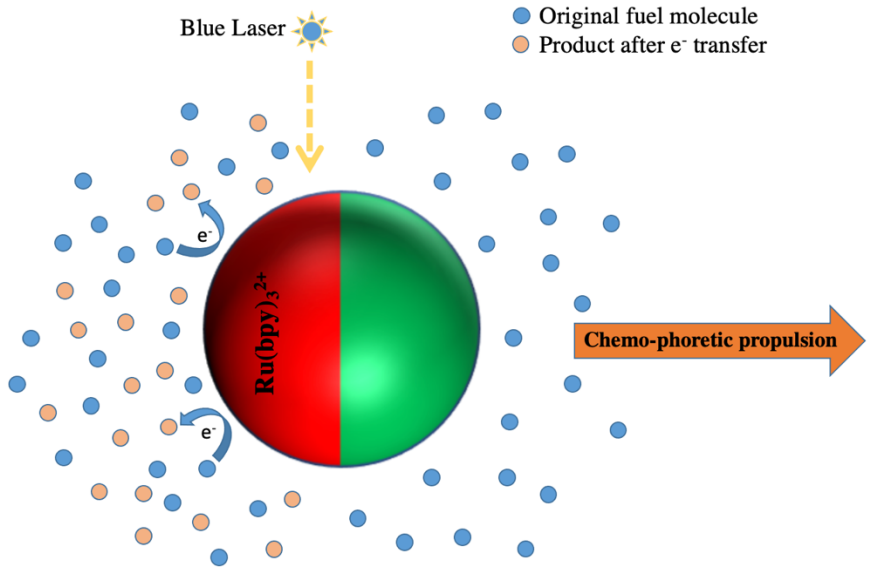


Figure 4.4 Schematic of photoelectrochemically-driven active motion process for Ru(bpy)32+-labeled Janus liposome in fuel chemicals environment exposed under blue laser light in which the red hemisphere represents Ru(bpy)32+-labeled Ld phase and the green one represents bodipy labeled Lo phase. The arrow indicates the motion direction.

### 4. 3. 2 Fluorescence configuration of $Ru(bpy)_3^{2+}$-labeled Janus liposomes

The aforementioned well-prepared Janus liposomes by gel-assisting swelling hydration method were characterized by confocal laser scanning microscope to examine the liposomes quality. The phase separation of Ld and Lo domain on the membrane was clearly distinguished as figure 4.5 (a) showed means that $Ru(bpy)_3^{2+}$-DOPE mainly partitioned preferentially into one domain (Ld) to form Janus liposomes. Based on these Janus liposomes images, we demonstrated that the fluorescence dye rhodamine conventionally applied in labeling Ld of the liposomes could be replaced by $Ru(bpy)_3^{2+}$ molecules. Besides, the production yield of Janus liposomes was still as

high as the rhodamine-labeled case. Considering the low quantum yield (0.042±0.002) of $Ru(bpy)_3^{2+}$ in solutions, in order to acquire clear and bright images, especially for the red domain of the liposomes membrane, the Janus liposomes sample needs to be exposed to higher laser

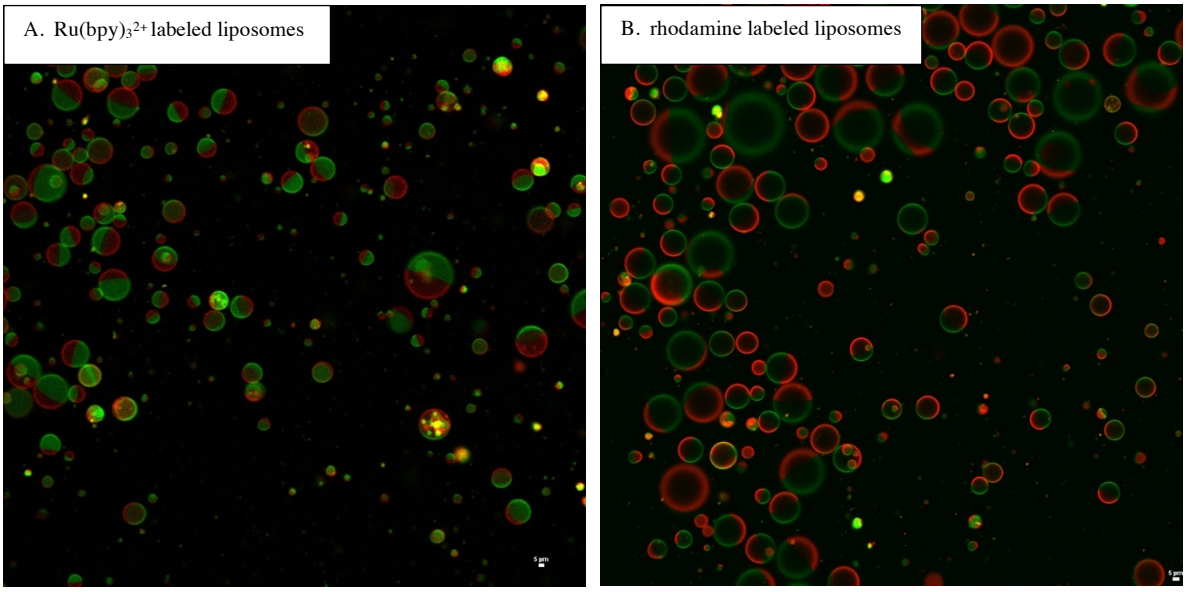


Figure 4.5. Confocal fluorescence microscopy images for Ru(bpy)32+ labeled Janus liposomes (A) and rhodamine-labeled liposomes (B). Here both of the two green domains were labeled by the same kind of green dye Bodipy.

intensity. Due to the special ligand-metal center structure, $Ru(bpy)_3^{2+}$ owned two separated adsorption peaks respectively at 290nm and 450nm especially the latter one (450nm) displays a great promising configuration in the labeling. The large gap between the adsorption peak and emission peak (630nm) which avoids fluorescence self-adsorption makes it become an extraordinary fluorescence candidate.[23] In our experiment, the $Ru(bpy)_3^{2+}$ was excited at 405nm laser and the emission light was filtered at 595nm ± 20nm making the great loss of photons on the camera which indeed resulted in decreasing brightness of the Janus liposomes $L_d$ membrane. When comparing the $Ru(bpy)_3^{2+}$ labeled Janus liposomes images with the aforementioned rhodamine-

labeled liposomes earlier under confocal microscopy as figure 4.3, the Ld domain of the rhodamine-labeled liposomes were much brighter than $Ru(bpy)_3^{2+}$ labeled ones.

$$2Ru(bpy)_3^{2+} + S_2O_8^{2-} \xrightarrow{h\nu} 2Ru(bpy)_3^{3+} + 2SO_4^{2-} \quad (1)$$

$$Ru(bpy)_3^{2+} \xrightarrow{h\nu} Ru(bpy)_3^{2+*} \quad (2)$$

$$Ru(bpy)_3^{2+*} + S_2O_8^{2-} \xrightarrow{k_q} Ru(bpy)_3^{3+} + SO_4^{-}\cdot + SO_4^{2-} \quad (3)$$

$$Ru(bpy)_3^{2+} + SO_4^{-}\cdot \xrightarrow{\text{fast}} Ru(bpy)_3^{3+} + SO_4^{2-} \quad (4)$$

Figure 4.6 Mechanism of the photochemistry of $Ru(bpy)_3^{2+}$ -$S_2O_8^{2-}$ system (Copyright by *The Journal of Physical Chemistry*)[28]

### 4. 3. 3 Electron transfer test between $K_2S_2O_8$ and $Ru(bpy)_3^{2+}$ molecules

As a special sensitizer and metal-ligand fluorophore, the triplet excited state of $Ru(bpy)_3^{2+}$ has both stronger oxidizing and reducing properties than its ground state. This unique physical character makes it widely used as both an electron donor and acceptor when reacting with some other oxidizing or reducing chemical species such as ascorbate, oxalate, persulfate, bromate, and methyl viologen. In order to investigate the electron transfer efficiency between $Ru(bpy)_3^{2+}$ and these mentioned electron acceptors or donors, we chose the persulfate ions as the representative example for our further experiment research. Based on the previous findings about electron transfer between $Ru(bpy)_3^{2+}$ and $S_2O_8^{2-}$, the main mechanism could be summarized into four chemical reactions as Figure 4.5 presented. In this specific process, both the generated excited $Ru(bpy)_3^{2+*}$ by exposure under the blue laser and $Ru(bpy)_3^{2+}$ could directly react with persulfate ions in which the electron transfer between them happened. In other words, the excited $Ru(bpy)_3^{2+}$

molecules could be quenched effectively by the persulfate ions when exposed to light. To further prove this quenching efficiency, the UV-vis spectroscopy absorbance measurement for $Ru(bpy)_3^{2+}$ and $S_2O_8^{2-}$ ions mixture was implemented. From the absorbance reading (Figure 4.6) for different concentrations of $Ru(bpy)_3^{2+}$ mixed with a fixed concentration of $S_2O_8^{2-}$, we found that both under

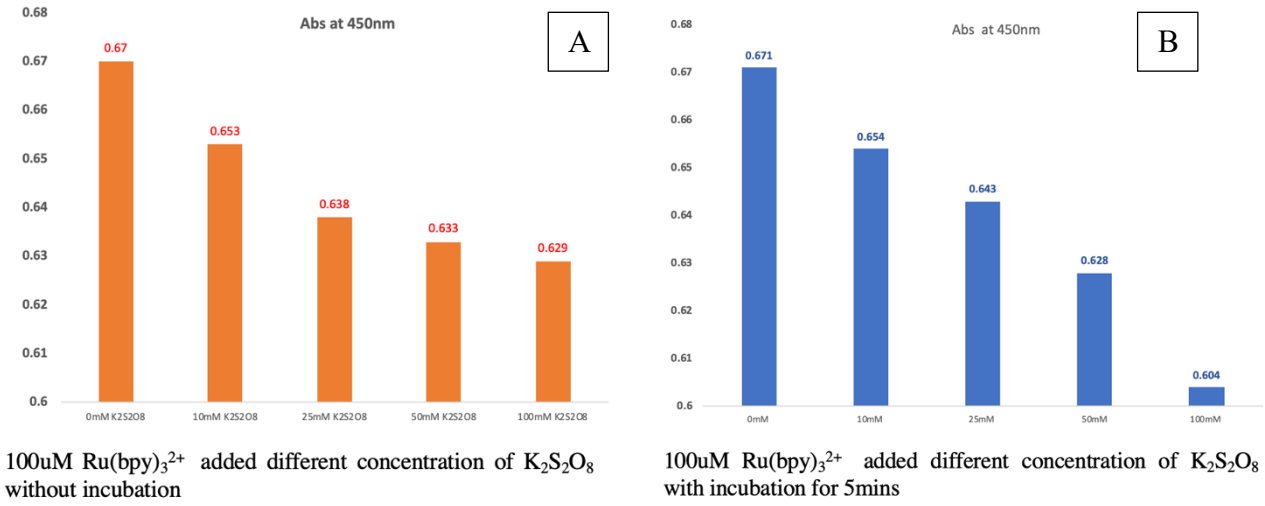


100uM $Ru(bpy)_3^{2+}$ added different concentration of $K_2S_2O_8$ without incubation

100uM $Ru(bpy)_3^{2+}$ added different concentration of $K_2S_2O_8$ with incubation for 5mins

Figure 4.7 UV-vis spectroscopy absorbance measurements at 450nm for $S_2O_8^{2-}$ quenching $Ru(bpy)_3^{2+}$. A is for mixture absorbance without incubation; B is for mixture incubation for 5mins.

incubation condition for 5mins and without incubation condition, the absorbance of the $Ru(bpy)_3^{2+}$ and $K_2S_2O_8$ mixture continued decreasing with the increased concentration of $K_2S_2O_8$ solution. However, not all the $Ru(bpy)_3^{2+}$ were fully quenched even though the mixing ratio of $K_2S_2O_8$ to $Ru(bpy)_3^{2+}$ improved to 1000 folds in this process. These spectroscopy absorbance results demonstrated that the quenching efficiency through electron transferring was not as high as we expected. In accordance with the above experimental procedure, the quenching efficiency was further tested on the membrane surface of $Ru(bpy)_3^{2+}$ labeled Janus liposomes in which the well-prepared Janus liposomes solution was mixed with different concentrations of $K_2S_2O_8$ solution

(5mM, 10mM 25mM) followed by characterizing these quenched Janus liposomes through a confocal microscope. From the confocal images as Figure 3.6 displayed, the red fluorescence from $Ru(bpy)_3^{2+}$ labeled $L_d$ domain gradually disappeared with the concentration of $K_2S_2O_8$ quenchers increasing which indicated that the quenching reaction for $Ru(bpy)_3^{2+}$ by $K_2S_2O_8$ on the bilayer membrane was also achieved. In the presence of 10mM $K_2S_2O_8$, almost all of the $Ru(bpy)_3^{2+}$ molecules have been quenched under the laser light without affecting the shape of liposomes while once the concentration of quencher solution improved to 25mM, some of the liposomes shapes were changed due to the osmatic pressure enlarged between the inner and outer side of the bilayer membrane.

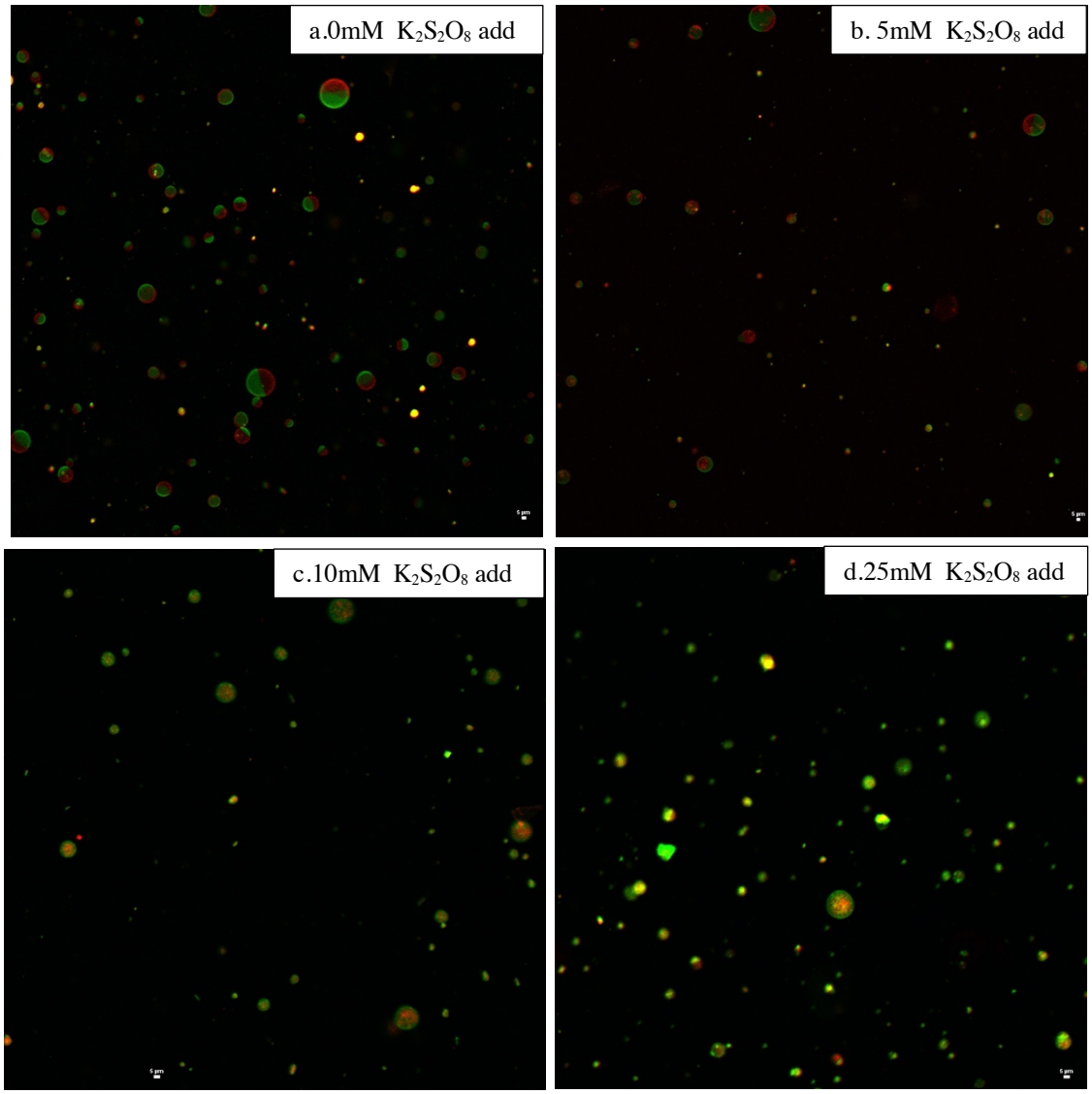


Figure 4.8 Quenching test of $Ru(bpy)_3^{2+}$ labeled Janus liposomes membrane. equivalent volume from the same batch of $Ru(bpy)_3^{2+}$ labeled Janus liposomes sample mixed with different concentrations of K2S2O8 solution respectively (a.0mM, b.5mM, c.10mM d. 25mM) and exposed under 405nm laser to acquire the confocal images.

These findings proved that the electron transfer, as well as mass transfer, happened on the membrane of the liposomes which is the effective support of later active motion experiments. In order to determine if the potassium ions would affect the quenching behavior, $K_2S_2O_8$ was replaced

by $(NH_4)_2S_2O_8$ (ASP) to repeat the whole aforementioned quenching process. The final confocal images data (shown here) demonstrated a similar quenching trend which proved that it was $S_2O_8^{2-}$ ions quenched the $Ru(bpy)_3^{2+}$ fluorescence.

### 4.3.4 Photoelectrochemically driven active motion test for $Ru(bpy)_3^{2+}$ labeled Janus liposomes in $K_2S_2O_8$

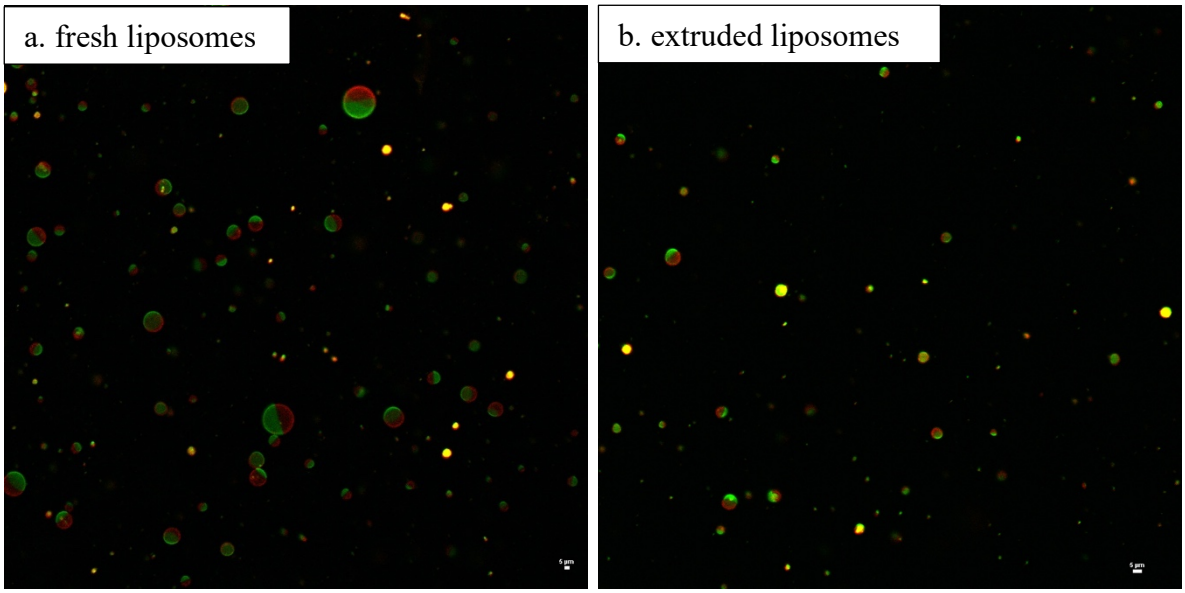


Figure 4.9 (a) Confocal images for fresh $Ru(bpy)_3^{2+}$ labeled liposomes via gel-assisted swelling hydration method; (b) size-controlled liposomes by membrane extrusion.

In terms of the good quality of Janus liposomes, the present Janus phase morphology of liposomes was estimated over 90% among the total particles. As **Figure 3.7** (a) displayed, the good quality of $Ru(bpy)_3^{2+}$ attached Janus liposomes were well prepared and extruded through 5um membrane extrusion **Figure 3.7 (b)**. The size uniform liposomes were loaded into the linear microfluidic channel to measure and further study the motion behaviors in the fueling environment

($K_2S_2O_8$). In accordance with the prementioned motion behavior and trajectory analysis procedure of these specific size-controlled liposomes, the mean square displacement (MSD) as a function of

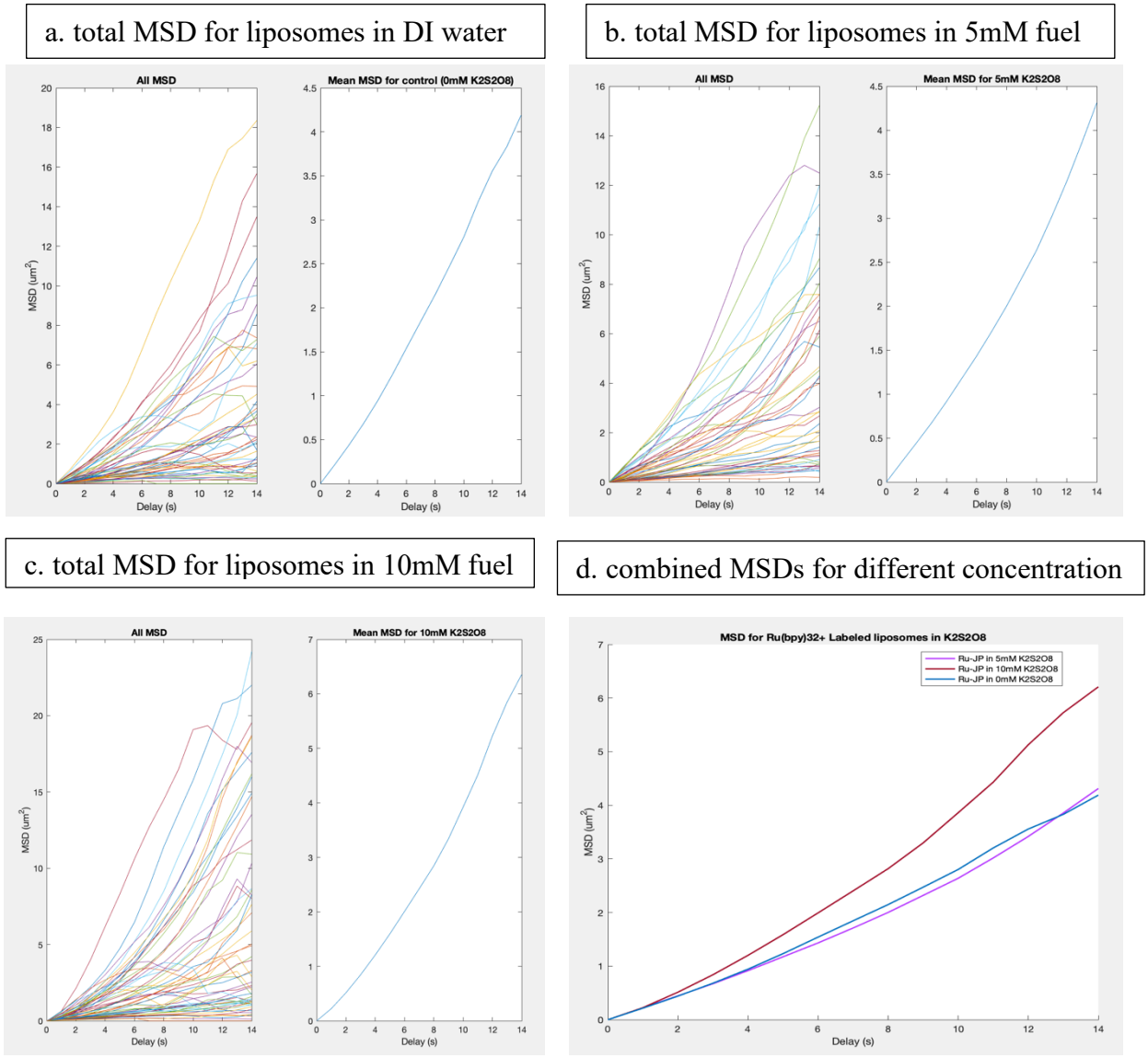


Figure 4.10 MSD characterization of motion behaviors of photoelectrochemically driven Ru(bpy)32+ labeled Janus liposomes in persulfate environment condition. a. Janus liposomes in DI water (total 283 tracks);b. Janus liposomes in 5mM $K_2S_2O_8$(total 364 tracks); c. Janus liposomes in 10mM K2S2O8(total 277 tracks);d. combined MSD for different concentrations.

the time interval was approximated by extracting the x-y coordinates from tracking trajectories. In our motion experiment, we only recorded liposomes movement in the channel for a time scale of 15 seconds length. Due to the $Ru(bpy)_3^{2+}$ molecules only asymmetrically labeled on one hemisphere side of the liposomes membrane, the active motion behavior of these particles should be different compared with the control group. Whereas, after calculating the MSD of these Janus liposomes' trajectories in the different $K_2S_2O_8$ concentration environments (5mM and 10mM), the active movement hasn't increased as fast as our expectation. After calculating about 300 tracks of liposome movement, we observed that the mean MSD after 15 seconds period delay in the presence of 5mM $K_2S_2O_8$ displayed a similar value as the control group in the absence of $K_2S_2O_8$. Even though in the presence of 10mM $K_2S_2O_8$, the mean MSD value (close to 6) only improved by about 40% compared with the control group. Since a much higher concentration of $K_2S_2O_8$ (for example 25mM) would affect the spherical shape of liposomes in bulk solution, we haven't further explored the motion behavior of liposomes in such a $K_2S_2O_8$ environment. These results demonstrated that the migration speed of most $Ru(bpy)_3^{2+}$ liposomes were rather slow or kept stationary in these fuel environment. There were several possible reasons that contributed to this phenomenon. Firstly, we assumed that the quenching reaction that happened on the surface of the membrane is not efficient enough to form the chemical gradient potential to propel the motion. Then it could be the extra fuel molecules surrounding the surface membrane of liposomes affected the redistribution of the Lo and Ld phase during the reaction process and it would lead to the disappearance of liposomes' Janus boundary. Furthermore, the osmotic pressure between the outside and inside of the liposome lost balance by these added fuel molecules which affect the phase redistribution of the membrane as well. In the meanwhile, the low quantum yield of $Ru(bpy)_3^{2+}$ molecule under the shift of

maximum absorbance peak of blue laser light reduced the electron transfer and mass transfer which also affected the liposomes movement. Besides, the strong oxidizing property of $K_2S_2O_8$ to $Ru(bpy)_3^{2+}$ which make an immediate reaction of them during the liposomes loading process results in the motion behavior ending too early to be observed. In summary, the motion behavior of $Ru(bpy)_3^{2+}$ labeled Janus liposomes self-propelled under the $K_2S_2O_8$ environment was rather slower compared with other previously reported light-driven micromotors[30-33] which offered another possibility of some new mild fuel candidates to $Ru(bpy)_3^{2+}$.

### 4.3.5 Photoelectrochemically driven active motion test for $Ru(bpy)_3^{2+}$ labeled Janus liposomes in Sodium Oxalate ($Na_2C_2O_4$)

$$Ru(bpy)_3^{2+} - e \rightarrow Ru(bpy)_3^{3+}$$

$$Ru(bpy)_3^{3+} + C_2O_4^{2-} \rightarrow Ru(bpy)_3^{2+} + C_2O_4^{\bullet-}$$

$$C_2O_4^{\bullet-} \rightarrow CO_2^{\bullet-} + CO_2$$

$$Ru(bpy)_3^{3+} + CO_2^{\bullet-} \rightarrow Ru(bpy)_3^{2+*} + CO_2$$

$$Ru(bpy)_3^{2+} + CO_2^{\bullet-} \rightarrow Ru(bpy)_3^{+} + CO_2$$

$$Ru(bpy)_3^{3+} + Ru(bpy)_3^{+} \rightarrow Ru(bpy)_3^{2+*} + Ru(bpy)_3^{2+}$$

$$Ru(bpy)_3^{2+*} \rightarrow Ru(bpy)_3^{2+} + h\nu$$

Figure 4.11 Proposed electron transfer process between Ru(bpy)32+ and Oxalate ions (C2O42-) on the electrode surface. (Copyright by *Chemical Reviews* 2008)

Since the light-driven active motion of $Ru(bpy)_3^{2+}$ labeled liposomes in the persulfate solution ($K_2S_2O_8$) has not reached our expectation, we tried to further explore new fuel candidates that could initiate a reaction with $Ru(bpy)_3^{2+}$ on the surface of the membrane. Considering the special

chemical property of $Ru(bpy)_3^{2+}$, a lot of mild oxidizing or reducing reagents could be applied as fuel molecules to activate the motion of $Ru(bpy)_3^{2+}$ labeled liposomes. Based on the previously reported photoinduced electrochemical reaction about $Ru(bpy)_3^{2+}$, sodium oxalate was a classic alternative candidate in the electron transfer process [34]. As Figure 3.9 displayed, both $Ru(bpy)_3^{2+}$ and $Ru(bpy)_3^{3+}$ could react with oxalate ions and especially the latter one can generate excited $Ru(bpy)_3^{2+*}$ species which produce fluorescence light. As the assumed reversible reaction, once we mixed sodium oxalate and $Ru(bpy)_3^{2+}$ and then exposed the mixture under blue light, the fluorescence light generated via excited $Ru(bpy)_3^{2+*}$ would be quenched by oxalate ions due to electron transfer. In order to confirm this assumption, we examined the quenching efficiency of oxalate to $Ru(bpy)_3^{2+}$ on the membrane by mixing the sodium oxalate with $Ru(bpy)_3^{2+}$ labeled liposomes. From the quenching result displayed in figure 3.10, we observed the red domain on the

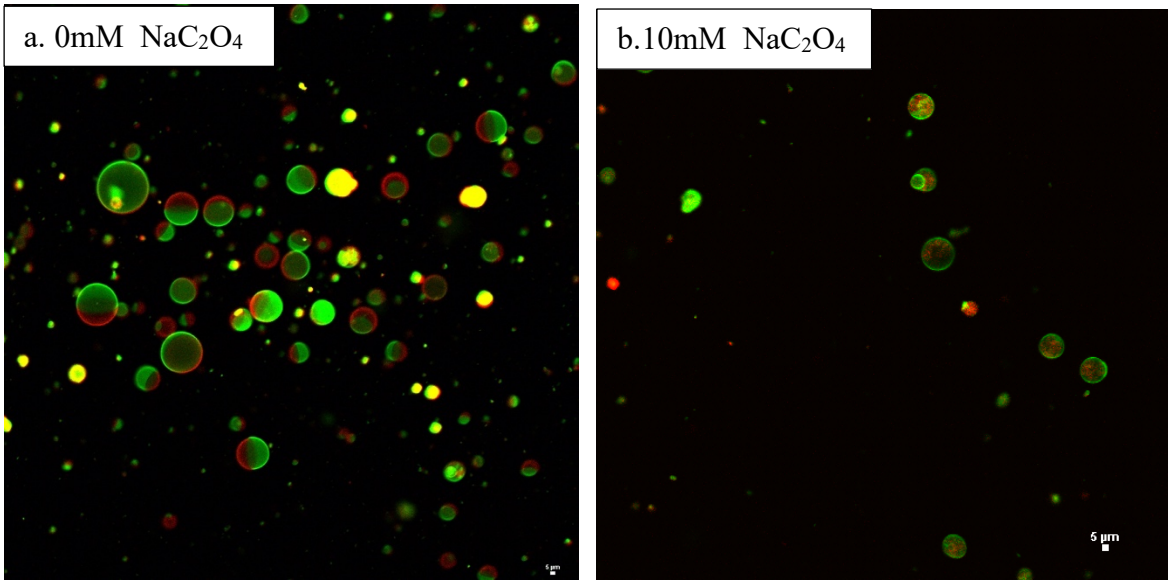


Figure 4.12 Quenching test of $Ru(bpy)_3^{2+}$ labeled Janus liposomes membrane by $Na_2C_2O_4$ .(a). fresh prepared $Ru(bpy)_3^{2+}$ labeled Janus liposomes without adding $Na_2C_2O_4$; (b).fresh $Ru(bpy)_3^{2+}$ labeled Janus liposomes with 10mM $Na_2C_2O_4$.

the membrane was gradually disappeared after 10mM $Na_2C_2O_4$ added into the $Ru(bpy)_3^{2+}$ labeled Janus liposomes which means $Ru(bpy)_3^{2+}$ molecules on the membrane were quenched by $C_2O_4^{2-}$ ions through electron transfer. In this process, the $Ru(bpy)_3^{2+}$ molecule distribution on the $L_d$ domain was greatly affected and some of the liposomes' shapes were also influenced due to the osmatic pressure change between the outside and inside of the bilayer membrane. In the meanwhile, a higher concentration of $Na_2C_2O_4$ (25mM, 50mM ) solution was also mixed with the same batch of fresh prepared $Ru(bpy)_3^{2+}$ labeled Janus liposomes to check the quenching performance of $Ru(bpy)_3^{2+}$. However, most of the liposomes were broken (data not showing here) under this situation (25mM and 50mM) because of the osmatic pressure change. This quenching reaction between $Ru(bpy)_3^{2+}$ and Oxalate ions makes the electron transfer or mass transfer on the membrane achieved.

To further explore the photoelectrochemically driven effect of $Ru(bpy)_3^{2+}$ labeled Janus liposomes under the $Na_2C_2O_4$ environment, we examined the real-time motion of these Janus liposomes through the aforementioned process in which the mixture solution including liposomes and $Na_2C_2O_4$ was introduced into a linear microfluidic chamber and subsequently the chamber device was placed onto the confocal stage. Then the sample was probed in the fluorescence field imaging mode to observe the motion of these vesicles. What needed to be mentioned here is the dimension of the linear microfluidic chamber was (L * W * H) 1.8mm x 400um x 200um, and it was carefully sealed the two channel ends to prevent evaporation. The liposome's motion video scans were recorded by a high-sensitivity charged-coupled device camera at an optical magnification of 20x and maintaining the scan rate at 25 fps for 15 seconds total video time under blue laser (405nm). After recording the videos, they were analyzed through the well-known software Image J to extract the trajectory of these active liposomes and quantify their motion

behavior at different $Na_2C_2O_4$ concentrations. Once extracted the trajectory data from the optical tracking of at least 6 to 8 vesicles, the mean square displacements (MSD) of these vesicles ensemble at different time intervals were calculated using MATLAB software and plotted in Figure 3.11. As can be seen from the mean MSD curves of membrane extruded $Ru(bpy)_3^{2+}$ labeled Janus liposomes in the presence of 5mM $Na_2C_2O_4$ and 10mM $Na_2C_2O_4$ compared with the control group, the curves of them displayed was almost linear and the final value remained similar as

a. mean MSD for liposomes in DI water

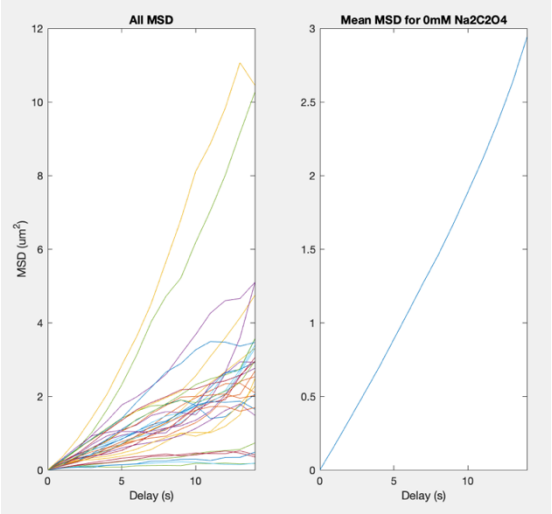


b. mean MSD for liposomes in 5mM $Na_2C_2O_4$

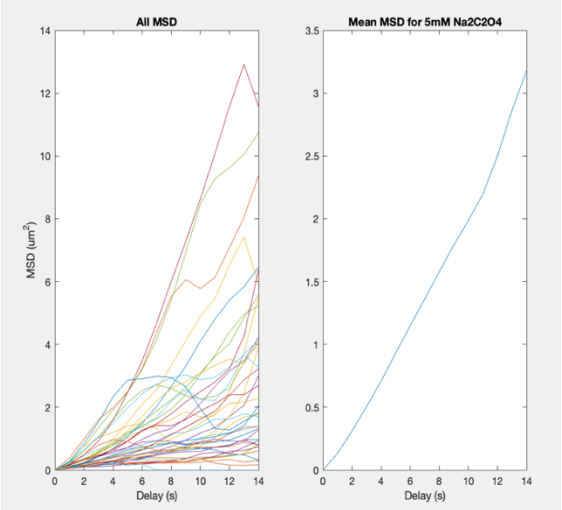


c. mean MSD for liposomes in 10mM $Na_2C_2O_4$

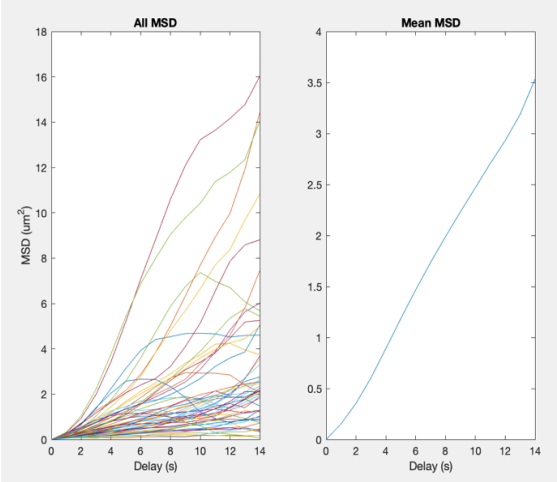


d. combined MSD for different concentration

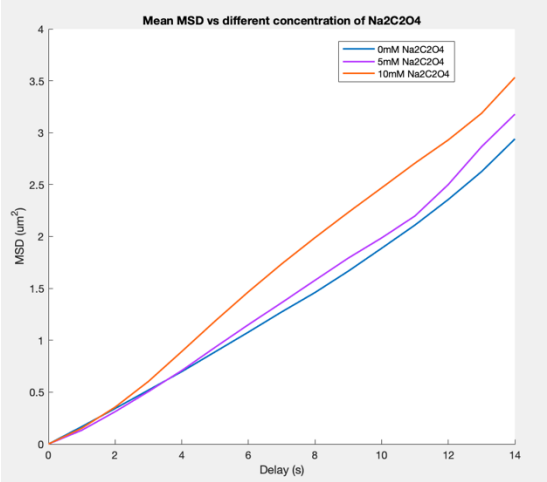

Figure 4.13 MSD characterization of motion behaviors of $Ru(bpy)_3^{2+}$ labeled Janus liposomes in $Na_2C_2O_4$ environment condition. a. Janus liposomes in DI water; b. Janus liposomes in 5mM $Na_2C_2O_4$; c. Janus liposomes in 10mM $Na_2C_2O_4$; d. combined MSD for different concentrations.

control group after 15s which indicated that most of these Janus liposomes undergo random diffusion motion in the presence of 5mM and 10mM $Na_2C_2O_4$ fuel. The expected photoelectrochemically-driven active motility of $Ru(bpy)_3^{2+}$ labeled liposomes haven't been observed at this moment possible due to the low efficiency of mass transfer between $Na_2C_2O_4$ and $Ru(bpy)_3^{2+}$ which was not enough to propel the liposomes. What's more, the $L_d$ domain of the membrane was disturbed during the quenching reaction between $Na_2C_2O_4$ and $Ru(bpy)_3^{2+}$ in which the chemical gradient has not formed at the separated semi-sphere of the liposomes. Besides, the laser light confinement to the liposomes also played an important role in reducing the motion behavior.

### 4.3.6 Other alternative candidates applied for photoelectrochemically driven active motion test of $Ru(bpy)_3^{2+}$ labeled liposomes

In order to realize the light-driven active motion of $Ru(bpy)_3^{2+}$ labeled liposomes, we continued to search out much more reactive fuel species during the electron transfer reaction with $Ru(bpy)_3^{2+}$. By holding this main goal, the methyl viologen/EDTA system provided a satisfactory chance to be tested in the following quenching experiment. In the early time, scientists have already found that EDTA could be scavenging the $Ru(bpy)_3^{3+}$ at a quick rate in an aqueous solution.[35]

$$Ru(bpy)_3^{2+} \xrightarrow{h\nu} {}^*Ru(bpy)_3^{2+} \quad (1)$$

$${}^*Ru(bpy)_3^{2+} \xrightarrow{k_0} Ru(bpy)_3^{2+} + h\nu' \quad (2)$$

$${}^*Ru(bpy)_3^{2+} + MV^{2+} \xrightarrow{k_q} Ru(bpy)_3^{3+} + MV^{\bullet+} \quad (3)$$

$$Ru(bpy)_3^{3+} + MV^{\bullet+} \xrightarrow{k_{et}} Ru(bpy)_3^{2+} + MV^{2+} \quad (4)$$

$$Ru(bpy)_3^{3+} + EDTA \xrightarrow{k_{sc}} Ru(bpy)_3^{2+} + EDTA_{ox}^{\bullet} \quad (5)$$

$$EDTA_{ox}^{\bullet} \xrightarrow{k_{tr}} EDTA_{red}^{\bullet} \quad (6)$$

Figure 4.14 The main mechanism of EDTA scavenging $Ru(bpy)_3^{2+}$/ $Ru(bpy)_3^{3+}$ in the presence of methyl viologen ($MV^{2+}$) under light exposure. (Copyright by *Inorg. Chem*)

Based on the previous research as Figure 3.12 displayed, in the presence of methyl viologen ($MV^{2+}$), the excited $Ru(bpy)_3^{2+*}$ has one electron transfer reaction with sacrificial electron donor $MV^{2+}$ to transform rapidly and irreversibly into oxidation state $Ru(bpy)_3^{3+}$. Then the latter $Ru(bpy)_3^{3+}$ molecules could be reduced by EDTA to reform $Ru(bpy)_3^{2+}$ species. In this total process, $Ru(bpy)_3^{2+}$ became a circulating utilization species even though a small part of them could be bleached under 450nm light exposure.

Upon this enduring electron transfer fuel model (EDTA/$MV^{2+}$) system, we further repeated the aforementioned quenching experiment protocol. To begin with, we tested the bleaching efficiency of $Ru(bpy)_3^{2+}$ (100uM) in the EDTA/$MV^{2+}$ (5mM) aqueous solution system upon blue LED light (450nm) exposure. As Figure 3.13 (a) demonstrated, once the mixture of EDTA/$MV^{2+}$ with $Ru(bpy)_3^{2+}$ was exposed to 450nm light for 30 seconds, the color of the solution mixture changed from orange to deep purple gradually and when extending the exposure time from half minutes to 2 minutes Figure 3.13 (b), the color of solution became deeper and deeper which means

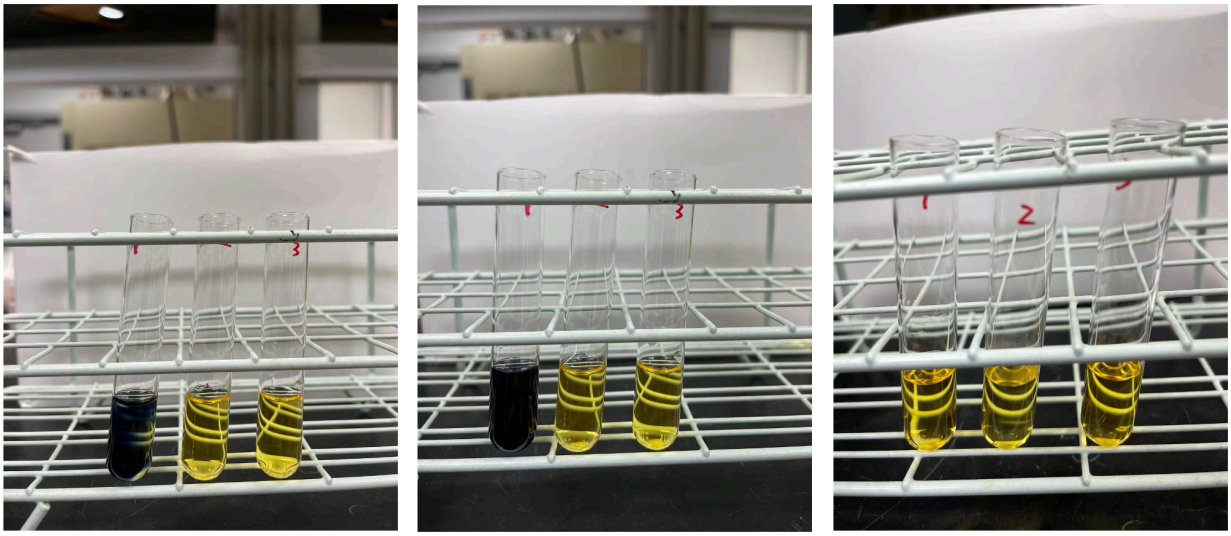

a. exposure at 450nm for 30s b. exposure at 450nm for 2mins c. shaking after 2mis exposure

Figure 4.15 Aqueous quenching test of 5mM EDTA/$MV^{2+}$ system to 100uM $Ru(bpy)_3^{2+}$ upon 450nm blue LED light. a. the mixture exposed at light for 30s; b. the mixture exposed at light for 2mins; c. the mixture solution was shaken after 2mins light exposure.1.$MV^{2+}$+ EDTA + $Ru(bpy)_3^{2+}$; 2. MV2+ +$Ru(bpy)_3^{2+}$ only; 3. EDTA + $Ru(bpy)_3^{2+}$ only;

the photoelectron transfer reaction between $Ru(bpy)_3^{2+}$ and $MV^{2+}$ proceeded at a higher efficiency. What needed to be mentioned here was the purple mixture solution could be recovered back to its orange color after shaking the test tube for several seconds which reversible this photoelectron transfer process from $Ru(bpy)_3^{2+}$ to EDTA/$MV^{2+}$ was reversible and reproducible. Furthermore, the quenching efficiency of the liposomes' bilayer membrane of $Ru(bpy)_3^{2+}$ by EDTA/$MV^{2+}$ system was also tested under a laser scanning confocal microscope. The sphere shape of most $Ru(bpy)_3^{2+}$ labeled Janus liposomes changed into snowman one in the presence of 5mM EDTA/$MV^{2+}$ solution upon external LED light exposure (images were not shown here). Even some of the liposome's bilayer structures were broken in this process. Considering the osmatic pressure issue outside and inside of the bilayer membrane, we further tried the well-prepared Janus liposomes hydrated in a 5 mM HEPES buffer solution to maintain the osmotic pressure. However,

these liposomes still have shape modification and $L_d$ domain redistribution in the presence of an EDTA/$MV^{2+}$ mixture as Figure 3.14 displayed. Besides, from the confocal images comparison in

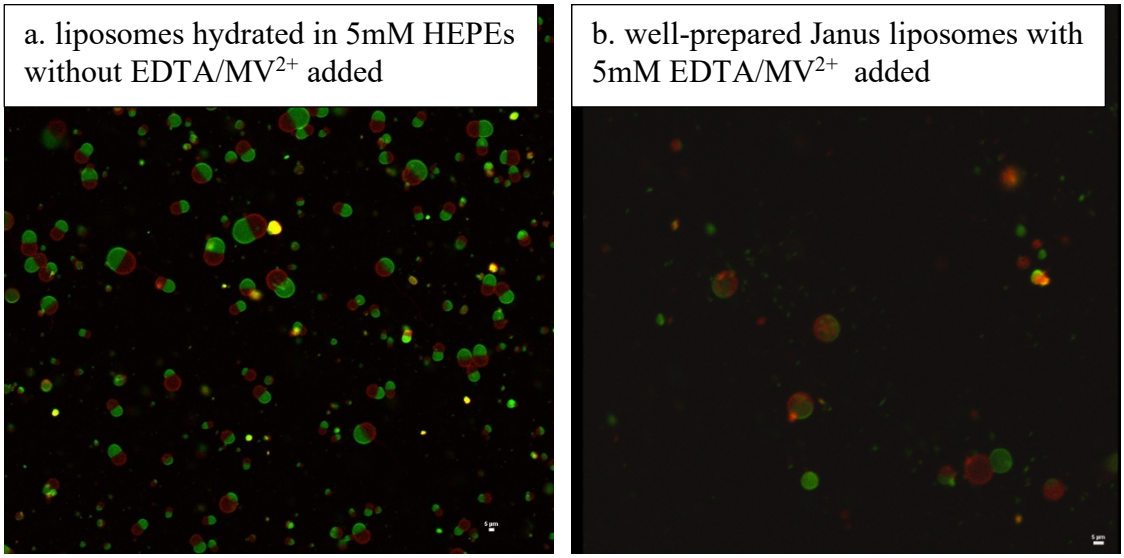


Figure 4.16. confocal images for buffer-based $Ru(bpy)_3^{2+}$ labeled Janus liposomes in the presence and absence of EDTA/$MV^{2+}$ system. (a) fresh well-prepared buffer hydrated Janus liposomes without EDTA/$MV^{2+}$; (b) well-prepared liposomes with EDTA/$MV^{2+}$ added.

the Figure 3.14, it is clearly evident that in the presence of a 5mM EDTA/$MV^{2+}$ fuel system, the $Ru(bpy)_3^{2+}$ molecules on the membrane still have a large amount of red residual even exposed under blue LED light for a few minutes which proved the photoelectron transfer process was recycled.

In order to further confirm if the EDTA/$MV^{2+}$ fuel system could propel the active motion of $Ru(bpy)_3^{2+}$ labeled Janus liposomes when exposed to the mixture under blue laser light of a confocal microscope, we repeated the same aforementioned liposomes' diffusion measurements procedure. After calculating and analyzing the mean square displacement (MSD) from the recorded trajectories of liposomes movement videos scanning, the active motion behavior of these

size-controlled $Ru(bpy)_3^{2+}$ labeled Janus liposomes hasn't been observed in our experiment (MSD curve not showed here). The results demonstrated light driven based active motion via the electron transfer mechanism of $Ru(bpy)_3^{2+}$ labeled Janus liposomes have serious challenge issues. Possible reasons that contributed to this challenge included light confinement for liposomes, low efficiency or mass transfer, and the low quantum yield $Ru(bpy)_3^{2+}$ molecules.

### 4.4. Conclusions

In summary, in this part, we fabricated a novel $Ru(bpy)_3^{2+}$ based Janus liposomes with the newly synthesized fluorescence metal-ligand sensitizer DOPE- $Ru(bpy)_3^{2+}$ successfully. To take full advantage of these well-prepared Janus liposomes, we further examined the enhanced diffusion behaviors of these size-controlled liposomes in different quenching fuel molecules including persulfate ions, oxalate ions, and methyl viologen combined EDTA system environment respectively through photoelectron transfer mechanism light-driven). Nonetheless, the light-driven enhanced diffusion of $Ru(bpy)_3^{2+}$ labeled Janus liposomes was not obvious in any of the environments of the previously mentioned fuel. This vesicle diffusion of the optimized one only increased about 40% in which the membrane extruded size controlled Janus liposomes were placed in 10mM persulfate ion solution. Compared with other light-driven micromotors [14-16] that the diffusion speed of particles generally enhanced ranging from a few folds to tens folds at least, our results demonstrated that $Ru(bpy)_3^{2+}$ labeled Janus liposomes have a great challenge to achieve light-driven enhanced diffusion only via mass transfer or forming chemical gradient on both sides of two semi-sphere of the liposome membrane. The most possible reason accounts for this challenge was the low quantum yield of $Ru(bpy)_3^{2+}$ molecules when exposed laser light made the

low mass transfer efficiency of fuel molecules to liposomes membrane. Other reasons including light confinement for liposomes, low quenching efficiency of fuel molecules to $Ru(bpy)_3^{2+,}$ and larger size of liposomes also could contribute to this challenge. To get rid of this specific challenge, more powerful chemical fuels need to be figured out such as special monomers that could achieve polymerization reactions induced by $Ru(bpy)_3^{2+}$ catalysis. Besides, the total experiment design also could be updated in the future.

# CHAPTER 5. Summary and Future Work

## 5.1 Summary of this dissertation

Inspired by the witnessing breathtaking advancement in artificial micro/nanomotors which are self-propelled microscopic objects capable of directional motion, we explored the possibility of active motion behavior of freshly prepared Janus liposomes in different environmental conditions. To begin with, the good quality of Janus liposome samples was the key step to moving forward. All through our active motion experiment, Janus liposomes were well-prepared with our modified PVA-gel assisted swelling hydration method, in which the lipids mixture precursor (ternary lipids system DPPC/DOPC/cholesterol) was deposited onto the dried and thin PVA gel to improve the detachment of lipids layer by layer during the liposome formation. In this specific process, individual liposome yields stable Janus particles with two distinctive liquid domains ($L_o$ and $L_d$). Though sharing several obvious advantages including high-efficiency giant liposomes formation, no organic solvent contamination, the low fraction of multilamellar liposomes, and employed in different kinds of lipids compared with other liposomes generation methods such as electroformation, our gel-assisted swelling hydration method generates wide size distribution of liposomes which hinders their further application. In order to get uniform liposomes, size controlling for these freshly prepared Giant Janus liposomes by gel assistance is an indispensable requirement. In our experimental study, the size-controlled liposomes were achieved by extruding the above-prepared hydration liposome samples through a plunger-based lipid extruder, furnished by polycarbonate filter membranes with 5-um diameter pores in both Chapter 2 and Chapter 3.

### 5.1.1 Enzyme-based active motion of Janus liposomes

In terms of further application of these well-prepared size-controlled Janus liposomes, directional/active motion behavior exploration has been an attractive research field because liposomes are desired drug delivery candidates in most pharmaceutical reports. In this dissertation, we systematically studied the enzyme-free based active motion behavior of Janus liposomes in Chapter 2 and the enzyme-based active motion behavior of Janus liposomes in Chapter 3, in detail respectively.

For the enzyme-based active motion of liposomes, we have taken full advantage of the biotin/avidin conjugation reaction in which incorporating the biotin-DOPE into the bilayer membrane and then horseradish peroxidase (HRP) with avidin conjugated was bound onto the half side of the sphere surface of liposomes. Later on, these HRP-bound Janus liposomes were placed into hydrogen peroxide solution and then the HRP enzyme catalysis reaction happened asymmetrically on the half-sphere side of the liposomes which induced the motion behavior of Janus liposomes. Various experimental parameters including hydrogen peroxide concentration, enzyme loading density on the liposome surface, and Janus ratio configuration of liposomes were systematically explored in Chapter 2. In order to investigate the enzyme efficiency effect of the aforementioned active motion behavior, later on, we further studied the active motion behavior of Janus liposomes conjugated with a higher turnover number of catalyzing hydrogen peroxide enzyme, catalase, on the semi-sphere surface. In the meanwhile, the catalase enzyme-bound Janus liposomes were placed into the hydrogen peroxide solution to record the motion activity. Then the motion behavior of liposomes was analyzed through the single particle tracking (SPT) method to acquire the trajectory of the single liposome. The mean square displacement (MSD) plot versus delay time was processed and displayed in the aforementioned figures. The motion speed of high-

efficiency catalase-bound Janus liposomes hadn't improved compared with HRP-bound ones. There are several possible reasons for this unexpected phenomenon, including longer space between the arm of the catalase to the surface, low enzyme density spread on the liposomes surface, and fast catalysis reaction that happen ahead of the recording in the channel.

### 5.1.2 Enzyme-free based active motion of Janus liposomes

In the enzyme-free active motion case, extracting agent cyclodextrins were added to the Janus liposomes system in which the cyclodextrins extract cholesterol from the bilayer membrane. This action triggers asymmetrical cholesterol efflux from the liposomes that propel the liposome's active motion. This work demonstrates liposome active motion through asymmetrical lipid efflux from Janus liposomes. Sustained by continuous Chol release from liposomes and inter-domain Chol transfer, the observed active motion exceeds the background diffusion by nearly two-fold. By exploiting intrinsic material properties of lipid assemblies, such as lipid phase separation and extraction, this work represents a significant departure from existing liposome-based motor design strategies.

### 5.1.3 photoelectrochemically-driven active motion of Janus liposomes

In light-driven active motion cases, we fabricated novel $Ru(bpy)_3^{2+}$ based Janus liposomes with the newly synthesized fluorescence metal-ligand sensitizer DOPE- $Ru(bpy)_3^{2+}$ successfully. To take full advantage of these well-prepared Janus liposomes, we further examined the enhanced diffusion behaviors of these size-controlled liposomes in different quenching fuel molecules including persulfate ions, oxalate ions, and methyl viologen combined EDTA system

environments, respectively, through photoelectron transfer mechanism (light-driven). Nonetheless, the light-driven enhanced diffusion of $Ru(bpy)_3^{2+}$ labeled Janus liposomes was not obvious in any of the previously mentioned fuel environments. This vesicle diffusion of the optimized one only increased about 40%, in which the membrane extruded size controlled Janus liposomes were placed in 10mM persulfate ion solution. Compared with other light-driven micromotors that the diffusion speed of particles generally enhanced ranging from a few fold to tens fold at least, our results demonstrated that $Ru(bpy)_3^{2+}$ labeled Janus liposomes had more difficulty achieving light-driven enhanced diffusion only via mass transfer or forming a chemical gradient on both sides of two semi-sphere of the liposome membrane. The most plausible reason accounts for this challenge was the low quantum yield of $Ru(bpy)_3^{2+}$ molecules when exposed laser light decreased the mass transfer efficiency of fuel molecules to liposome membrane. Other reasons including light confinement for liposomes, low quenching efficiency of fuel molecules to $Ru(bpy)_3^{2+,}$ and larger size of liposomes also could have contributed to this difficulty. To get rid of this specific challenge, more powerful chemical fuels need to be developed, such as special monomers that could achieve a polymerization reaction induced by $Ru(bpy)_3^{2+}$ catalysis.

## 5.2 Outlook

High yield and high-quality giant Janus liposomes formed with the common ternary lipids system (DPPC/DOPC/Cholesterol) were prepared successfully and reproducibly through a special equipment-free and easy-to-follow procedure, PVA-gel assisted swelling method, in our group. With this reliable preparation method in hand, there are various possible applications in which taking full advantage of these Janus liposomes could be explored and achieved in the future. Here in this dissertation, the investigation of active motion behavior of these generated Janus liposomes

including enzyme-free based, enzyme-based, and photoelectrochemically driven based was a great example of such applications. Thus, along this active motion direction, other applications involved in this new type of multifunctional, lipid-based asymmetrical colloidal particles could be appealing to researchers.

(1) **Encapsulation of enzyme in Janus liposomes**. Conjugation of different enzymes onto the surface of liposomes has been investigated in detail already in our group, while encapsulation of such kinds of enzymes into the liposomes to achieve active motion has been an interesting field to most researchers. What's more, enzyme encapsulation into liposomes is a super promising technique to stabilize and prevent denaturation and proteolysis.[1] Considering the bilayer membrane of liposomes has a semi-permeation function to some special solute molecules, the enzyme could only catalyze the substrate in the core center of those Janus liposomes. Encapsulation of such enzymes into the liposomes efficiently and removing the excess enzymes from outside environmental solutions is the key step for such application. Once encapsulated, the enzyme encountered another problem: the permeability barrier of the lipid membrane drastically diminished the activity of the enzyme entrapped in the liposome by reducing the entrance rate of the substrate molecules, thus reducing the substrate concentration inside the liposome. Catalase, which works efficiently for hydrogen peroxide, is a good candidate for this encapsulation because hydrogen peroxide is able to permeate through the bilayers of liposomes. Additionally, the permeation speed of hydrogen peroxide through the liquid-ordered phase ($L_o$) and liquid-disordered phase ($L_d$) is different and such difference could contribute to the motion behavior of Janus liposomes compared with homogeneous ones. The dialysis membrane setup could also be utilized to remove the excess enzyme in the outside solution during the hydration process.

(2) **Asymmetry-driven self-organization of Janus liposomes in a collective active state**. Nowadays, many forms of collective self-organization have been identified with active Janus particles because such Janus features provide a rich design space for particle-particle interaction. Generally, once these Janus particles have opposite charges on the two hemispheres and the two charges have the same sign and comparable magnitude, this particle will act similarly to an isotropic sphere, resulting in a random configuration.[2] An imbalance between two charges kicks in, and various Janus particle forms of self-organization could be achieved, including chains, swarms, and cluster structures. [3-4] In order to achieve the self-organization of liposomes in these aforementioned forms, dipolar Janus liposomes in which the liposomes contain opposite surface charges lipids decorating the two hemispheres of the same colloidal body [5] need to be prepared. The optimized experimental conditions to produce these liposomes in high yields, based on the gel-assisted hydration of ternary lipid systems (DPPC/DOPC/Cholesterol), have been explored already in our group. Considering locating these dipolar Janus liposomes on a sample container in which the alternating electric field is oriented perpendicular to the sample plane, we could try to control the collective active states by changing the frequency of the alternating current. In this regard, we could achieve the various active group structure, such as active chains, swarms as well as clusters with our dipolar Janus liposomes.

### 5.3 Contributions of this dissertation

The main contribution to experimental findings presented in this dissertation is the specific exploration of active motion behaviors for size-controlled Janus liposomes. In terms of active motion or self-propulsion for Janus particles, it is related to chemical fuels based driven, light-driven, thermal-driven, electrical-driven, and magnetic-driven. So far, the chemical fuel-based

self-propulsion of Janus particles was most widely investigated by researchers, especially for the enzyme catalysis-based-propulsion. In regards to this truth, we systematically studied the active motion behavior of uniform-size controlled Janus liposomes. In Chapter 2, we first examined the active motion behaviors of enzymes bound onto the hemisphere of Janus liposomes, including horseradish peroxide and catalase in detail in a common hydrogen peroxide solution. In this process, we first take full advantage of the single particle tracking method to acquire the trajectories of each particle and analyze the mean square displacement (MSD) of trajectories. By comparing the different MSD plots versus the time of these two enzymes (HRP and Catalase), we can learn the catalysis efficiency difference in comparison to hydrogen peroxide solution. Then in Chapter 3, we further demonstrated the active motion behaviors of Janus liposomes in an enzyme-free state in which the uniform size Janus liposomes were placed in β-CD, a cholesterol-extracting agent, at a low-mM level to the aqueous bulk which then triggers cholesterol released from these Janus liposomes. This work first reveals a uniquely distinctive experiment design principle based entirely on intrinsic physicochemical properties of lipid assemblies to achieve active motion. In Chapter 4, we inspected the light-driven active motion behavior of $Ru(bpy)_3^{2+}$ labeled Janus liposomes, combined with the photoelectrochemical reaction on the hemisphere surface of the membrane. In this case, size-controlled $Ru(bpy)_3^{2+}$ labeled Janus liposomes were placed into different photoelectrochemical fuel solutions to examine the light-induced electron transfer efficiency that occurred on the membrane surface. To summarize, this dissertation has introduced several reliable strategies and experimental setup possibilities to investigate the self-propelled active motion behavior of Janus liposomes, a promising drug delivery candidate. Our experimental findings could offer and open up a lot of possible applications for biocompatible multifunctional materials and drug delivery-related research.

## 5.4 References

1. Chaize B, Colletier J P, Winterhalter M, et al. Encapsulation of enzymes in liposomes: high encapsulation efficiency and control of substrate permeability. *Artificial Cells, Blood Substitutes, and Biotechnology*, **2004**, *32(1)*: 67-75.

2. Yan J, Han M, Zhang J, et al. Reconfiguring active particles by electrostatic imbalance. *Nature Materials*, **2016**, *15(10)*: 1095-1099.

3. Nishiguchi D, Sano M. Mesoscopic turbulence and local order in Janus particles self-propelling under an ac electric field. *Physical Review E*, **2015**, *92(5)*: 052309.

4. Bricard A, Caussin J B, Desreumaux N, et al. Emergence of macroscopic directed motion in populations of motile colloids. *Nature*, **2013**, *503(7474)*: 95-98.

5. Liu Z, Cui J, Zhan W. Dipolar Janus liposomes: formation, electrokinetic motion, and self-assembly. *Soft Matter*, **2020**, *16(9)*: 2177-2184.